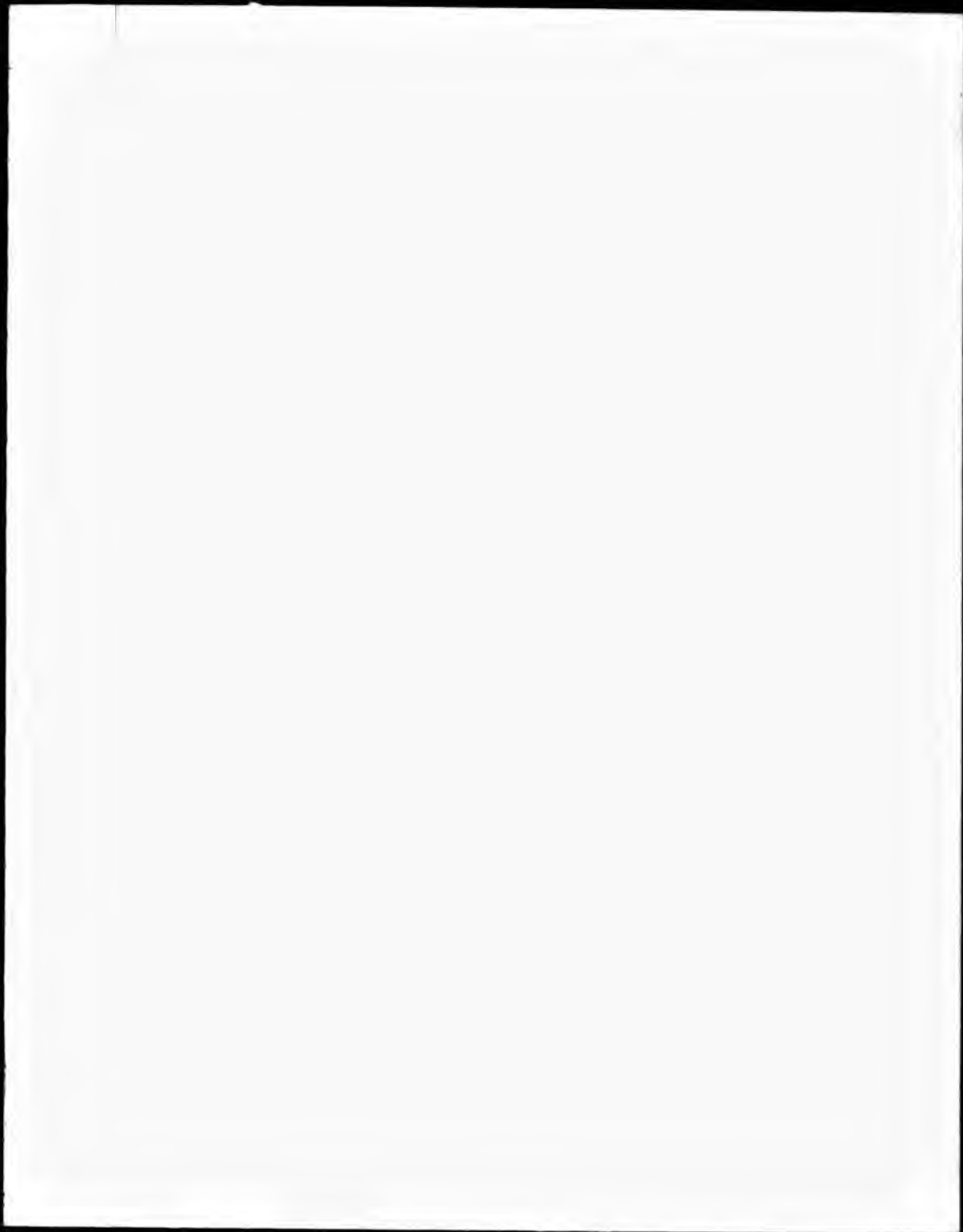


This PDF was created from the British Library's microfilm copy of the original thesis. As such the images are greyscale and no colour was captured.

Due to the scanning process, an area greater than the page area is recorded and extraneous details can be captured.

This is the best available copy

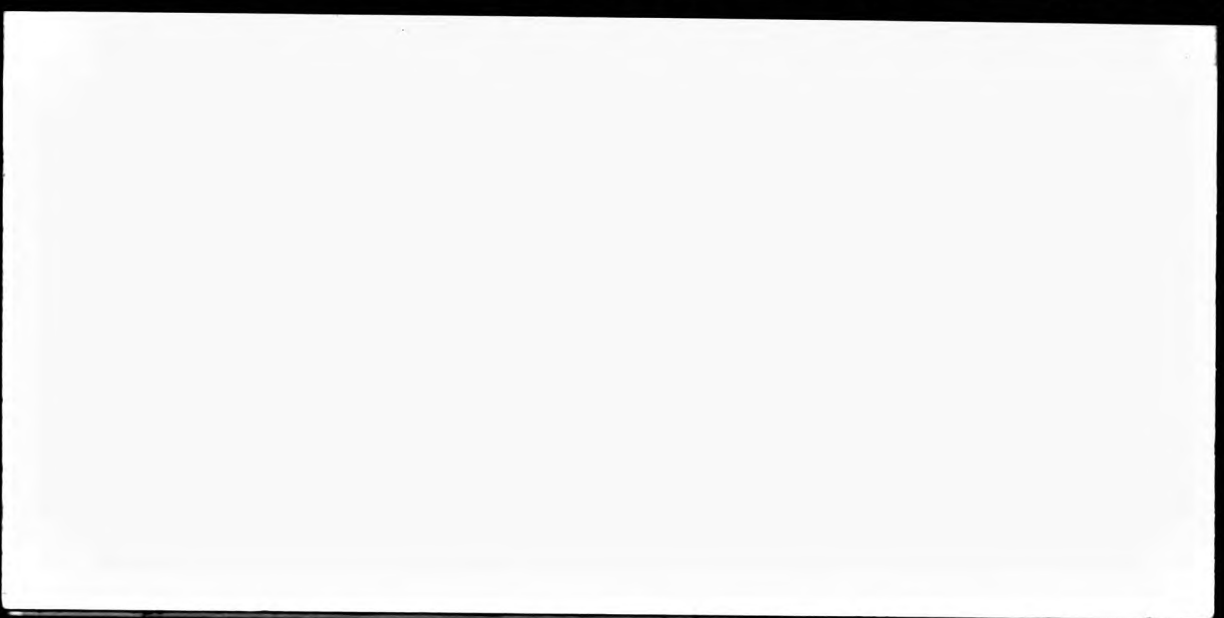


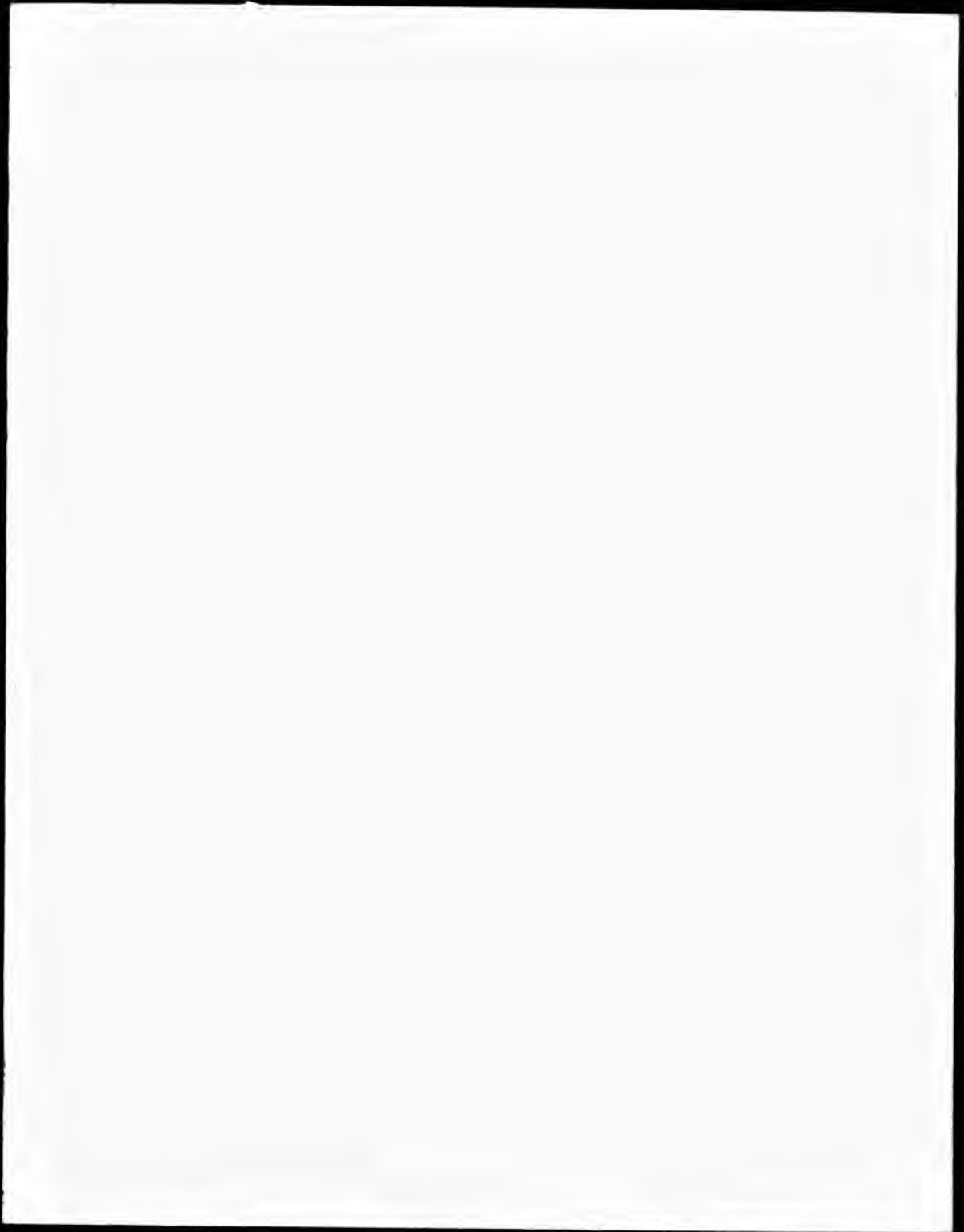


DX



89699





THE BRITISH LIBRARY DOCUMENT SUPPLY CENTRE

TITLE

ULTRASOUND PROPAGATION IN COLLOIDAL DISPERSIONS

AUTHOR

Nigel E. Sherman

INSTITUTION
and DATE

CITY OF LONDON POLYTECHNIC
1989 C.N.A.A.

Attention is drawn to the fact that the copyright of this thesis rests with its author.

This copy of the thesis has been supplied on condition that anyone who consults it is understood to recognise that its copyright rests with its author and that no information derived from it may be published without the author's prior written consent.

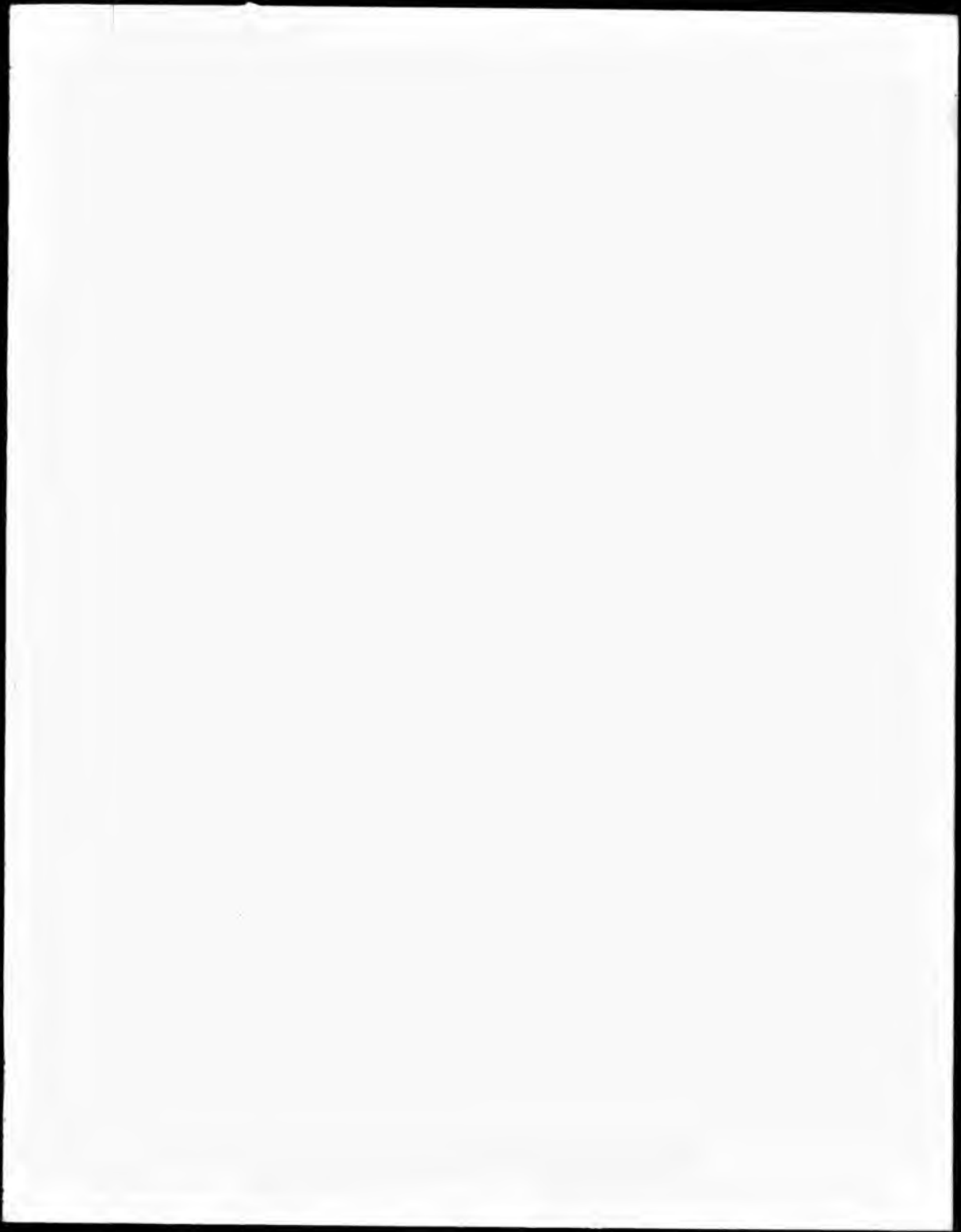


CAM. 9

THE BRITISH LIBRARY
DOCUMENT SUPPLY CENTRE
Boston Spa, Wetherby
West Yorkshire
United Kingdom

REDUCTION X

21



ULTRASOUND PROPAGATION IN COLLOIDAL DISPERSIONS

By Nigel E. Sherman

A thesis submitted for the degree of
Doctor of Philosophy in partial fulfilment
of the requirement of the Council for
National Academic Awards.

Department of Physics,
City of London Polytechnic,
31, Jewry Street,
London EC3N 2EY.

December 1989

ULTRASOUND PROPAGATION IN COLLOIDAL DISPERSIONS

Nigel E. Sherman

ABSTRACT

This thesis describes apparatus and techniques for making ultrasonic measurements in fluids and applications of them to measurements of ultrasonic parameters in colloidal dispersions.

A brief description of the properties and uses of ultrasound propagation in dispersions is followed by an extensive review of theories which relate the particulate properties of the dispersions to the measurable ultrasonic parameters, velocity (c) and attenuation (α).

Measurement principles are outlined related to the design of near-field measurement methods and the development of three techniques is described. These are shown to give results which are both highly self-consistent and in excellent agreement with a far-field method.

Measurements of α and c for model dispersions of glass spheres in Newtonian liquids are shown to be in good agreement with the relevant theory when particle polydispersity is taken into account. For structured fluids as the continuous phase, the α and c data for suspensions of spheres are used to obtain the continuous phase viscosity (η). The α data agree approximately with the macroscopic viscosity, but the velocity data requires the introduction of a shear elastic term and the revision of theory in order to obtain agreement.

Attenuation as a function of barite concentration in Newtonian liquids was investigated and the ultrasonic particle radius was found to be systematically larger than expected. This is attributed to particle rugosity.

Measurements of α and c using non-gelling aqueous kaolin~~ite~~ suspensions are shown to agree well with theory when the eccentricity and the interactions of particles are taken into account. For gelling aqueous bentonite suspensions, α and c were found to be time-dependent over a period of several days following initial dispersion. The observed increases in both α and c are interpreted in terms of a growth in gel fraction and shear modulus, respectively.

The effect of shear flow on α and c was investigated for the above dispersions. Changes were barely resolvable but consistent with shear-degradation of structure within the fluid.

Acknowledgements

There are a number of people who have helped make this thesis a reality and so I would like to say thankyou to;

- (i) my supervisor, Dr. G.H. Meeten for his help and endless enthusiasm throughout this work,
- (ii) Dr. C.M. Langton for many useful discussions,
- (iii) Dr. J.V. Champion whose dedication in his rôle as Director of Studies helped keep our research group together under difficult circumstances,
- (iv) Messrs Pat Driscoll, Vic Manning and Ray Hall for technical support and advice,
- (v) Schlumberger Cambridge Research for acting as the collaborating establishment,
- (vi) City of London Polytechnic for my Research Assistantship,
- (vii) my wife Jennie for doing the typing and being very patient.

Contents

1.INTRODUCTION	1
1.1 Review Of Ultrasound Propagation In Dispersions	1
1.2 Applications Of Ultrasound Propagation In Dispersions	5
1.3 Scope Of Work In This Thesis	8
2.ULTRASOUND PROPAGATION THEORY	11
2.1 Review Of Theory For Monodisperse Spheres	11
2.2 Polydisperse and Non-spherical Particles	19
3.ULTRASONIC APPARATUS AND TECHNIQUE	23
3.1 Ultrasonic Measurement Principles	23
3.2 Continuous Wave Interferometer	26
3.3 Tone Burst	37
3.4 Broadband Pulse	47
3.5 Technique Comparison	58
3.6 The Flow Cell	66
4.MATERIALS AND THEIR CHARACTERISATION	69
4.1 Materials	69
4.2 Sizing and Sieving Methods	77
5.EXPERIMENTAL RESULTS: Glass Spheres	83
5.1 Attenuation	83
5.2 Microscopic Rheology Measurements	86
5.3 Velocity	94
5.4 Summary	109
6.EXPERIMENTAL RESULTS: Barite	110
6.1 Attenuation	110
6.2 Summary	115
7.EXPERIMENTAL RESULTS: Clay Suspensions	116
7.1 Kaolinite	116
7.2 Bentonite	123
7.3 Summary	132
8.EXPERIMENTAL RESULTS: Flowing Systems	135
8.1 Velocity	135
8.2 Attenuation	137
8.3 Summary	138
9.CONCLUSION	140
10.REFERENCES	146
APPENDIX A	150
APPENDIX B	153

1. INTRODUCTION

1.1 Review Of Ultrasound Propagation In Dispersions

When a sinusoidal longitudinal ultrasonic wave is launched into a fluid (or any medium) it can be represented in the form

$$E = E_0 \exp i(kx - \omega t) \quad (\text{eqn. 1.1.1})$$

where E is the amplitude (displacement or pressure) and the propagation constant $k = \omega/c + i\alpha$ where ω is the ultrasonic pulsatance, c is the longitudinal velocity of propagation and α is the amplitude attenuation per unit distance. The presence of suspended particles within a fluid medium changes the ultrasonic propagation conditions from those of the pure fluid. In the most simple form, one might visualise a new material which is an ideal mixture of the two phases with volume averaged properties; e.g. the attenuation changes because a volume fraction (v) that was occupied by fluid, is now occupied by particles of a different ultrasonic attenuation. This is called an effective medium approach. However there are differences between the physical properties of the phases that introduce new mechanisms which affect both α and c :

(1) If there is a density difference between the phases, they will move relative to each other as they oscillate in the ultrasonic field. Thus any received signal will contain components out of phase with the incoming or primary beam. If the fluid is viscous, a frictional force will act opposing this net inertial force. This will damp the initial effect, introducing a loss mechanism which absorbs energy

from the primary beam.

(ii) As the ultrasonic pressure (or amplitude) varies sinusoidally the particles and surrounding fluid undergo a series of expansions and compressions, thus cooling and heating. If the thermal capacities of the phases are different, their temperatures will change by different amounts and a net irreversible heat flow will occur. This results in additional energy absorption from the sound wave.

(iii) Finally, energy will be scattered out of the primary beam by the suspended particles. This effect will depend on their shape, number density and size compared with the sound wavelength, and the degree to which the properties of the phases are mismatched.

The importance of these effects and their relative magnitudes for a given colloidal system will depend on the boundary conditions i.e. the relevant physical properties of the phases, their volume fractions and the wavelength of ultrasound relative to particle size. A number of authors have explored this propagation problem theoretically under various sets of boundary conditions. The rest of this section briefly describes the important cases that have been developed, with the specific expressions obtained for α and c being given in Chapter 2.

A suitable starting point is the work of Urick(1947) who took the simple effective medium approach and used volume averaged compressibility and density to predict sound velocity through a colloid in the absence of inertial, viscous or scattering effects. Later Urick(1948) considered compressible particles oscillating in a viscous suspending fluid using Stokes' expression for drag force. He showed

that for small spherical particles with radius $a \ll \lambda$, the dominant absorption mechanism was viscous drag between them and the fluid, in agreement with earlier findings from a scattering approach by Lamb(1945). A more rigorous approach based on conservation of mass, momentum and energy, and examination of a scattered wavefunction was used by Epstein and Carhart(1953) to introduce heat conduction between liquid phases. Further Chow(1964) used it to consider the effect of surface tension, which he found to be relevant only when bubbles were suspended in the fluid. Allegra and Hawley(1972) reviewed this procedure, extending it to include the attenuation in suspensions of solid particles. From their analysis it is clear that the importance of the various dispersion effects depends on the ratio of the particle radius to the characteristic wavelength associated with each mechanism. These ratios for solid particles suspended in fluids can be expressed as follows;

(i)Viscous effect. Here the ratio is aB_v ,

$$\text{where } B_v = \sqrt{(\pi f \rho) / \eta} \quad (\text{eqn.1.2})$$

f is the ultrasonic frequency, ρ and η are the density and viscosity of the fluid. B_v is the reciprocal of the characteristic wavelength known as the viscous skin depth.

The viscous effect is most important for frequencies such that $aB_v \sim 1$. At higher or lower frequencies there is less relative motion between the fluid and the particle.

(ii)Thermal effect. Here the ratio is aB_t

$$\text{where } B_t = \sqrt{(\pi f \rho C_p) / k} \quad (\text{eqn.1.3})$$

and where C_p and k are the specific heat capacity at constant pressure and thermal conductivity of the fluid.

This is also important only when $aB_c \sim 1$. When $aB_c \gg 1$ the wavelength of the thermal wave is small compared to the particle radius and heat fluxes are confined to a thin boundary layer around it. When $aB_c \ll 1$ the flow of heat is almost reversible and losses are small.

(iii) Scattering. Here the ratio is aB_s ,

$$\text{where } B_s = 2\pi/\lambda \quad (\text{eqn. 1.4})$$

and where λ is the ultrasound wavelength.

The radius to wavelength ratio determines the appropriate scattering regime. For example when $a < \lambda/10$ the particles can be considered as simple Rayleigh scatterers, where attenuation due to scattering is proportional to a^3/λ^4 .

The above statements are limited to dilute suspensions as they deal with scattering from isolated spheres, in other words the effects from increasing numbers of particles are assumed to be additive. In practice this holds closely only over a limited range of particle volume fraction beyond which multiple scattering increasingly occurs. The multiple scattering problem has been tackled by a number of authors including Waterman and Truell(1961), Davis(1979) and Schwartz and Johnson(1984). In their approach multiple scattering effects are represented by obtaining cross terms between the thermal and viscous scattering contributions of the individual particles. Perdigão et al.(1987), similarly to Franklin and Javanaud(1985), modelled attenuation using progressive loss of phase coherence during propagation, for concentrated suspensions of particles. They were able to predict values showing fair agreement (within 10%) with

experimental data, when acoustic impedance mismatch between the phases was negligible.

However, as the volume fraction of particles in a suspension increases, it can be considered more in terms of a fluid-saturated porous solid. This was done by Biot(1956a and 1956b) who considered the oscillatory losses due to (i) friction when relative motion occurs between a viscous liquid and a solid, (ii) stress-strain in the solid and (iii) fluid compression and dilation. This analysis has been experimentally validated by Salin and Schon(1981) from measurements of α and c for water saturated packed glass spheres. In order to adapt the Biot formulation to describe a concentrated suspension, the modulus of the porous frame has to be considered negligible. Under this condition, Hovem(1980a and 1980b) shows that the viscous loss mechanism dominates and that concentrated systems can be successfully modelled if an effective porosity is assumed. An equivalent result has been found more recently by Gibson and Toksöz(1989) from examination of energy loss due to viscous fluid flow around spherical particles. This approach is more rigorously applicable to a suspension problem as it does not require the adoption of a porosity constant (see section 2.1). However the authors found it no better fit than the modified Biot theory when applied to data from the literature.

1.2 Applications Of Ultrasound Propagation In Dispersions

Ultrasound is widely used as a non-destructive probe of colloidal suspensions, as the parameters α and c depend strongly on many physical properties of the constituent

materials and their relative volume fractions. Also, although an optical probe of dispersions has been developed by Molloy(1986), ultrasound lends itself to work with materials that can be opaque and abrasive in nature. The more common uses include velocimetry in fluid flow and floc break-up or dispersion of particles by high intensity ultrasound, however this section is intended to discuss ultrasonic measurements of material properties. Three main areas of application are the food industry, where on-line quality control is desired, marine particulate investigation and examination of gelling or structured fluids.

The application of ultrasound to food systems has recently been reviewed by Javanaud(1988) and it is clear that the most successful techniques have used measurements of group velocity of short pulses in the 1 to 10MHz frequency range. For example, Povey(1984) and Hussin and Povey(1984) correlated changes in ultrasonic velocity with solid fat content for solidifying fats and oils, as a function of sample temperature. Further, McClements and Povey(1987) have applied the pulse velocity technique to triglyceride in paraffin oil mixtures and obtained solid fat content values that show excellent correlation with data from an established pulsed NMR technique; the method was also sensitive to the triglyceride solubility and gel strength. Although most food industry applications are of this type e.g. aiming to establish the volume fraction of a particular phase, other examples include the measurement of velocity to monitor the crispness of biscuits and attenuation to determine the age of potatoes and eggs.

In marine acoustics the properties of suspensions are

of interest because sea bed sediments e.g. clays and floating particulates (like small marine organisms) will affect signals received by sonar equipment. Thus further understanding may allow sonar depth and range sounding to be made more accurate and yield more information. An early example in this field is the work of Urick(1947) using sound velocity to determine the compressibility of kaolin in aqueous suspension. Hampton(1967) investigated the dependence of α and c on solid concentration and sound frequency for sea bed sediments, results which Duykers(1970) used to validate empirically derived formulae that could be used to obtain values of physical properties, like sediment porosity, from acoustic data. More recently, the advances in signal processing electronics, used for the deconvolution of sonar signals, have resulted in sophisticated seabed analysis systems. For example Holliday(1987) has reported a profiling system capable of measuring the size distribution ($\approx 100\mu\text{m}$ to 10mm range) of pelagic biotic particles using a frequency range 100kHz to 10MHz.

Ultrasound has been applied as a low-strain probe of gelling or structured fluids as an alternative to conventional macroscopic mechanical measurements of rheology, which may destroy the very structure of interest. Bacri et al.(1980) found that the attenuation of high frequencies ($>100\text{MHz}$) was highly sensitive to (i) phase transition (sol to gel) in polyacrylamide solutions and (ii) gel volume fraction in gelatin. Further, Bourlion et al.(1986) correlated time dependent measurements of acoustic attenuation in drilling muds with gel strength data

obtained by measuring critical shear stress for gel breakdown at low shear rate ($\sim 2s^{-1}$). This correlation was purely an empirical comparison, but it gives an indication of a useful phenomenon that may eventually provide a non-destructive and robust quality control test for drilling fluids.

1.3 Scope Of Work In This Thesis.

The work with structured fluids mentioned in the previous section presents an interesting problem for a more fundamental examination. It requires an ability to measure ultrasonic propagation parameters accurately and to relate them to microscopic or particulate properties of suspensions using proven theoretical models. This theme underpins the work herein and the form of the investigation can be described in the following stages:

(i) Development of Techniques.

Here the objective was to measure absolute values of ultrasonic velocity (c) and attenuation (α), to a precision of a few percent, in attenuating colloidal dispersions with α in the range 1 to 10dB/cm. It was required that any system developed should use commercially available piezo-electric ceramic transducers, small sample volume (for economy and easy temperature control) and be suitably robust, for use with industrial and possibly aggressive fluids. A further consideration for apparatus was design to allow small changes in α and c to be measured, caused e.g. by gelation or flow.

(ii) Assessment of Theory

As mentioned in section 1.1, the applicability of the

effects to dominate over thermal effects as $aB_c \gg 1$, and for scattering to be of Rayleigh type.

(iii) Non-model Dispersions.

It was necessary that the effects of disperse phase size, polydispersity, shape and volume fraction on α and c should be investigated. This should be done by comparison of data obtained with previously assessed model theory, if necessary including suitable modifications, either novel or from the literature. Changes that may be caused by dispersion flow should be also examined to see if dynamic values of physical properties are detected, particularly in systems of non-spherical and gelling particles.

(iv) Application to Drilling Fluids.

Finally as a practical application of the work, the aim was to use the techniques developed for investigation of drilling muds. Interpretation of results should provide some measure of properties such as time-dependent gelation, gel strength, effective viscosity and densifier concentration. Even without a full interpretation the experimental results are relevant to the interaction of ultrasonic well-log tools with drilling muds.

2. ULTRASOUND PROPAGATION THEORY.

2.1 Review Of Theory For Monodisperse Spheres.

The theory of ultrasound propagation in suspensions of particles in fluids, has been recently reviewed by Harker and Temple(1987) and further, McClements and Povey(1987) have given a comprehensive survey and intercomparison of velocity theory. It therefore intended here only to bring out the salient features and equations of the theory applied in this thesis, which can conveniently be done by considering attenuation and velocity separately.

Attenuation

A theoretical equation for the excess attenuation of sound by colloidal particles was published by Urick in 1948, valid for rigid spheres, small compared to the sound wavelength and free to move in the sound field, subject only to viscous and inertial forces. He obtained an expression representing viscous absorption, by theoretically investigating the effect of viscosity on the period of a pendulum, swinging in a viscous fluid. This, together with treatment of the spheres as simple Rayleigh scatterers, gave an equation of the form:

$$\alpha = v \left\{ (k^4 a^3 / 6) + [k/2 (r - 1)^2 s] / [s^2 + (r + T)^2] \right\} \text{ (eqn.2.1)}$$

where v is the volume fraction of suspended particles, $k=2\pi/\lambda$, a = particle radius, r = ratio of particle to fluid density. s, T are defined by $s= 9(1+1/Ba)/4Ba$ and $T=1/2+9/4Ba$, where $B=\sqrt{\kappa f \rho/\eta}$; η, ρ are the viscosity and density of the fluid respectively. $1/B$ is called the

viscous skin depth, which is the characteristic thickness of the fluid layer around the sphere over which viscous coupling of the phases occurs.

This equation can be simplified by expanding in powers of $1/Ba$ and assuming $Ba \gg 1$ to give:

$$\alpha = \nu \left[\frac{1}{6} k^4 a^3 + \frac{2k}{2a} \left(\frac{\rho' - \rho}{2\rho' + \rho} \right)^2 \sqrt{\frac{\eta}{\rho}} \right] \quad (\text{eqn.2.2})$$

where ρ' is the density of the solid. The assumption that $Ba \gg 1$ requires that the viscous skin depth should be less than the particle radius. Taking an example typical for this work; for glass beads suspended in polypropylene glycol with $a=25\mu\text{m}$, $\eta=0.4\text{Pas}$, $\rho=1000\text{kg/m}^3$ and $f=5\text{MHz}$, then $Ba \sim 5$ indicating that eqn.2.2 is likely to be appropriate.

This form compares favourably with expressions obtained in the long wavelength limit from more rigorous approaches by (i) Allegra and Hawley(1972) who studied sound absorption in dilute suspensions of spherical particles, by expanding a scattered wave function in complex form as a series of spherical harmonics, attenuation being obtained from the real coefficients. (ii) Hay and Mercer(1989) who derived an expression for viscous attenuation by considering phase shifts of waves scattered by a solid elastic sphere. Hay and Mercer's expression in lowest order of $1/Ba$ is identical to the viscous term in eqn.2.2. Sherwood(1988) has shown that this is also true for the absorption part of the Allegra and Hawley expression in the long wavelength limit (i.e. $ka \ll 1$) and where thermal transport effects are negligible. Thus under these

conditions only the scattering term differs from that in eqn.2.2 and this is given by:

$$\alpha_{\text{scatt.}} = v \frac{k^4 a^3}{2} \left[\frac{1}{3} \left(\frac{K-K'}{K} \right)^2 + \left(\frac{\rho' - \rho}{2\rho' + \rho} \right)^2 \right] \quad (\text{eqn.2.3})$$

where K, K' are the compressibilities of the liquid and solid respectively. As the expressions 2.2 and 2.3 are valid only for $ka \ll 1$, the scattering part should not be dominant for dispersions where the equations are applicable. However they will be compared by application to experimental data in Chapter 5.

The above expressions have been derived for dilute suspensions where a linear dependence of α on solid volume fraction exists, indicating that the particles act independently. Urick's (1948) data for aqueous kaolin dispersions showed that this assumption was only valid for volume fractions less than about 0.1 and in general the experimental data reported in Chapter 5 has been acquired within the linear regime. However, for use with work at higher concentrations, it is useful to quote the expression given by Hovem(1980) and shown to compare favourably with Urick's data over the volume fraction range 0 to 0.4. To obtain this equation, earlier work by Biot(1956a and 1956b) for a fluid-saturated porous frame was adapted, by allowing the modulus of the frame to become negligible and therefore more representative of solid particles free to move in the sound field. However, application of the expression requires that a permeability be assigned to the dispersion, as shown in the equation below Hovem's expression is

$\alpha = \text{Im} [k]$, where

$$k^2 = \omega^2 \rho^* K^* \left[\frac{v/(1-v)(\rho \rho' / \rho^*) - 1 \eta [F(f)/\omega B_0]}{v/(1-v)\rho^* - 1 \eta [F(f)/\omega B_0]} \right] \quad (\text{eqn. 2.4})$$

and k is the complex wavenumber for propagation in the colloid, $\rho^* = v\rho + (1-v)\rho'$, $\rho = v\rho + (1-v)\rho'$, $K^* = vK + (1-v)K$ and $F(f)$ is a frequency correction function for viscosity given by complex Kelvin functions, where $F(f) \rightarrow 1$ for conditions of Poiseuille fluid flow at low frequencies. B_0 is the permeability given by the Kozeny-Carman equation [Carman 1956] as,

$$B_0 = (1-v)a_p^2 / 4K_0$$

where $a_p = 2a(1-v)/3v$ is a pore size parameter related to particle radius. K_0 is the Kozeny-Carman constant which is obtained empirically by measuring permeability as a function of $a^2(1-v)^3/v^2$ for a given material. Although the assignment of an effective permeability to a dispersion may cast doubt on the applicability of eqn. 2.4, a result of similar form, developed from the Stokes drag force on a sphere oscillating in a viscous liquid, has recently been reported by Gibson and Toksöz (1989). Their expression for the complex wavenumber is;

$$k^2 = \omega^2 \rho^* K^* \left[\frac{\rho \rho' / (1-v)\rho^* - 1(9\eta \xi / 2a^2\omega)}{\rho^* / (1-v) - 1(9\eta \xi / 2a^2\omega)} \right] \quad (\text{eqn. 2.5})$$

where $\alpha = \text{Im} [k]$ and ξ is an analytically derived factor, due to Hasimoto (1959), to account for the effects of multiple spheres on the viscous drag coefficient, where $1/\xi = 1 - 1.791v^{3/2} + v - 0.329v^2$. Gibson and Toksöz also comment

that a frequency correction function, which scales the drag coefficient with $(1+Ba)$, is important when the viscous skin depth becomes small compared with particle size.

The applicability of eqn.2.5 appears more rigorous than that of 2.4 for suspensions as no arbitrary constants or permeability values need to be applied. Further, frequency correction factors are more readily calculated for eqn.2.5. In order to compare the two, the non frequency corrected forms have been applied to data for aqueous kaolin suspensions in Chapter 7, and then the frequency corrected Gibson and Toksöz expression used to improve agreement. For the purposes of the relevant calculations we may write the expressions in the form

$$k^2 = A \left[\frac{M - iN}{P - iN} \right]$$

thus $\text{Im} [k] = (Y^2 + Z^2)^{1/2} \sin[(\arctan Z/Y)/2]$

and $\text{Re} [k] = (Y^2 + Z^2)^{1/2} \cos[(\arctan Z/Y)/2]$

with $Y = \frac{A(MP + N^2)}{\rho^2 + \eta^2}$ and $Z = \frac{A(NM - NP)}{\rho^2 + \eta^2}$.

In eqn.2.4 $A = \omega^2 \rho^* K^*$, $M = v \rho \rho^* / (1-v) \rho^*$, $N = \eta / \omega B_0$, $P = v \rho^* / (1-v)$ and for eqn.2.5 $A = \omega^2 \rho^* K^*$, $M = \rho \rho^* / (1-v) \rho^*$, $P = \rho^* / (1-v)$ and $N = 9 \eta \xi / 2a^2 \omega$ or $N = [9 \eta \xi (1+Ba)] / 2a^2 \omega$ if frequency correction is applied. The velocity can also be obtained from the wavenumber where $c = \omega / \text{Re} [k]$. For the kaolin dispersion mentioned above, velocity values were also calculated from eqn.2.5 as a further test of applicability.

Visco-elasticity

In order that eqn.2.5 might be useful when visco-elastic bentonite muds are used instead of viscous liquids, one can replace the simple viscosity with a complex viscosity $\eta = \eta' + i\eta''$. η' is equivalent to the simple viscosity and the term $\eta'' = G/\omega$ and so some representation of the shear modulus (G) is included. The result is simply to introduce a factor such that in the above notation M becomes $M + 9\eta'' \xi / 2a^2\omega$ and P becomes $P + 9\eta'' \xi / 2a^2\omega$. With these modifications eqn.2.5 has been used to predict α , from $\text{Im}[k]$ and c, from $\omega/\text{Re}[k]$ for glass spheres suspended in bentonite, and the effect of the shear modulus G is found to be important (see Section 5.3).

Velocity.

A simple and widely used equation for predicting velocity of sound in suspensions and emulsions was derived by Urlick(1947). He assumed an ideal homogeneous mixture of the two phases where the suspended particles were infinitesimally small compared to the sound wavelength, in order that scattering could be neglected. In this case density and compressibility of the mixture are additive properties of the two materials depending upon their proportion in the mixture giving,

$$\rho_s = \rho'v + \rho(1-v) \quad \text{and} \quad K_s = K'v + K(1-v)$$

where ρ_s , ρ' , ρ are densities of suspension, disperse and continuous phase respectively, and K_s , K' , K are compressibilities of suspension, disperse and continuous

phase respectively.

Using the well known Wood(1941) equation for velocity of sound in a homogeneous material, Urick gave his expression

$$c = \sqrt{\frac{1}{K^* \rho^*}} \quad (\text{eqn.2.6})$$

Urick successfully applied this equation to measurements of sound velocity in aqueous kaolin~~ic~~ suspensions and xylene-water emulsions, reporting that greater accuracy was obtained in predicting the compressibility of the disperse phase, when K and K^* were of the same order of magnitude.

The main limitations of Urick's expression are the assumption of infinitesimally small particles compared with the sound wavelength i.e. $\lambda \gg a$, and that no account is taken of inertial and viscous effects (see section 1.1). Sherwood(1988) has shown that Allegra and Hawley's analysis, as described earlier, reduces to give a velocity result equivalent to that of simple effective medium theory when Ba , the ratio of particle radius to viscous skin depth, is small. When $Ba \gg 1$ the effective density changes from the

simple $\rho^* = \rho^*v + \rho(1-v)$ to

$$\rho^* = \rho \left[1 + v \frac{3(\rho^* - \rho)}{(2\rho^* + \rho)} \right] \quad (\text{eqn.2.7})$$

which is equivalent to that predicted using the classical theory of inviscid fluids, assuming that the particles are unable to follow the motion of the surrounding fluid. The

resulting expression for suspension velocity is

$$c = \sqrt{1/K\rho} (1 + v/2[1 - K'/K - 3(\rho' - \rho)/(2\rho' + \rho)]) \quad (\text{eqn.2.8})$$

The assumption that the particles are unable to follow the fluid motion means that eqn.2.8 represents the high frequency limit (i.e. $Ba \gg 1$) and eqn.2.7 represents the low frequency limit, as it is obtained when $Ba \ll 1$.

A number of other equations have been developed that attempt to overcome the Urlick limitations, but only that of Ament(1953) will be included here for comparison, as this was found to be most useful by McClements and Povey(1987) in their review. Further, it provides a link between the high and low frequency extremes as it is valid when $Ba \sim 1$, provided that the viscous skin depth (i.e. $1/B$) is less than interparticle distances and that $a \ll \lambda$. Ament's equation, derived from considering the resistance of a fluid to oscillation of a rigid sphere, contains a density difference term (representing the inertial effect) and a term that includes Ba (the viscous effect). The form of the equation is;

$$c = \sqrt{1/(K\# \rho_{eff})} \quad (\text{eqn.2.9})$$

where $\rho_{eff} = \rho\# + z$,
 $z = -[2v(\rho' - \rho)^2(1-v)A]/[A^2 + C^2]$,
 $A = 2(\rho' - \rho)(1-v) + 2\rho(1+T)$
 and $C = 2\rho s$. (s and T are as defined in eqn.2.1,
 with $\rho\#$ as in eqn.2.6)

Here the effective density of the system is modified as viscous coupling between the phases takes place. This means that a layer of fluid becomes associated with the particle, changing its effective density and altering the conditions of relative motion between the phases. So, the strength of the correction term z depends on the particle to fluid density ratio (or density difference) and the magnitude of Ba . For the dispersions investigated in this thesis, density differences are relatively high, also Ba is not negligible i.e. kaolin ($a \sim 0.5 \mu\text{m}$ $\rho \sim 2600 \text{kg/m}^3$) and water ($\eta \sim 1 \text{mPa s}$ $\rho \sim 1000 \text{kg/m}^3$) $\rho'/\rho \sim 2.6$ and at 5MHz $Ba \sim 1.9$; glass beads ($a \sim 16 \mu\text{m}$ $\rho \sim 2900 \text{kg/m}^3$) and glycerol ($\eta \sim 1.4 \text{Pa s}$ $\rho \sim 1252 \text{kg/m}^3$) $\rho'/\rho \sim 2.3$ and at 5MHz $Ba \sim 1.8$.

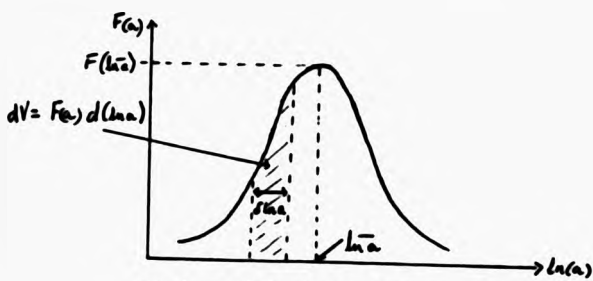
It is not immediately obvious to what extent the viscous and inertial effects will operate and so the Urick, Ament and inviscid fluid equations have been compared by application to experimental results in Chapter 5.

2.2. Polydisperse and Non-spherical Particles.

Attenuation.

Eqn.2.2 predicts the excess attenuation developed when monodisperse spherical particles are added to a suspending fluid. Any irregular particles used in this work have an equivalent spherical radius associated with them. The effect of polydispersity can readily be incorporated into the equation as follows;

assume the particle size distribution is of the Gaussian log-normal form,



$$F(a) = F(\ln \bar{a}) \exp\left[-\frac{(\ln a - \ln \bar{a})^2}{2\sigma^2}\right] \quad (i)$$

where σ is the standard deviation, and $\ln \bar{a}$ is the mean logarithmic radius.

Differentiating eqn. 2.2 w.r.t. volume fraction one obtains

$$d\alpha = f(a) dV \quad (ii)$$

where $f(a) = Aa^3 + C/a$, (iii)

$$A = k^4/6, C = \frac{9k}{2} \left[\frac{\rho' - \rho}{2\rho' \rho} \right]^2 \sqrt{\frac{2}{\pi}} \rho$$

substituting for dV in (ii) and integrating to get the average attenuation value over the distribution gives

$$\bar{\alpha} = \int_0^{\infty} \alpha / \int_0^{\infty} dV = \int_{\ln a = -\infty}^{\infty} f(a) F(a) d(\ln a) / \int_{-\infty}^{\infty} F(a) d(\ln a) \quad (iv)$$

Putting $\ln(a) = x$ and using (i) and (iii), (iv) becomes

$$\bar{\alpha} = \frac{A \int_{-\infty}^{\infty} \exp[3x - ((x - \bar{x})/2\sigma)^2] dx + B \int_{-\infty}^{\infty} \exp[-x + ((x - \bar{x})/2\sigma)^2] dx}{\int_{-\infty}^{\infty} \exp[-((x - \bar{x})/2\sigma)^2] dx} \quad (v)$$

This can be solved using the standard integrals

$$\int_0^{\infty} \exp(-at^2 + 2bt + c) dt = \int_{-\infty}^0 \exp(-at^2 - 2bt + c) dt$$

$$= 0.5 \sqrt{\pi/a} \exp((b^2-ac)/a) \operatorname{erfc}(b/\sqrt{a})$$

where $\operatorname{erfc}(y) = 1 - \operatorname{erf}(y)$ and erf is the error function

$$\operatorname{erf}(y) = \frac{2}{\sqrt{\pi}} \int_0^y \exp(-t^2) dt.$$

Equation (v) becomes

$$\bar{\alpha} = \frac{A}{2} \exp(9\sigma^2 + 3x) [\operatorname{erfc}(-3\sigma - \bar{x}/2\sigma) + \operatorname{erfc}(3\sigma + \bar{x}/2\sigma)] \quad (vi)$$

$$+ \frac{B}{2} \exp(\sigma^2 - \bar{x}) [\operatorname{erfc}(\sigma - \bar{x}/2\sigma) + \operatorname{erfc}(-\sigma + \bar{x}/2\sigma)].$$

Using $\operatorname{erfc}(y) = 1 - \operatorname{erf}(y)$ and $\operatorname{erf}(-y) = -\operatorname{erf}(y)$ (vi) becomes

$$\bar{\alpha} = A \exp((3\sigma)^2 + 3\bar{x}) + B \exp(\sigma^2 - \bar{x}) \quad (vii)$$

Substituting for A, B and $x = \ln(a)$ we obtain

$$\bar{\alpha} = \frac{k^4 a^3}{6} \exp(3\sigma)^2 + \frac{9k \left(\frac{\rho' - \rho}{2\rho' + \rho} \right)^2 \sqrt{2}}{2a \sqrt{\pi} \rho} \exp(\sigma)^2 \quad (\text{eqn. 2.10})$$

Thus values of excess attenuation can be calculated for a log-normal distribution of spheres, whose mean radius and standard deviation are known. In chapter 4 it will be shown that this information was obtainable for the particles investigated and that a log-normal distribution was a good approximation to the experimental one.

Velocity.

In order to allow for the non-spherical nature of kaolin particles examined in this thesis a modified form of equation 2.7 was used to compare with the standard Urick, Ament and Gibson and Toksöz (i.e. $c = \omega/Re[k]$) in eqn. 2.5) expressions. This incorporated shape factors due to Ahuja and Hendee (1978). By considering mass and momentum balances for circular discs moving in a viscous liquid, they made

corrections to the inertial and viscous terms T and s being,

$$T = L + 9M^2/4Bb \quad \text{(eqn.2.11)}$$

$$s = 9M^2/4Bb(1+(1/MBa)) \quad \text{(eqn.2.12)}$$

where L , M are inertia and shape coefficients respectively; a is the radius, and b the thickness, of a circular disc.

For a disc of aspect ratio $a/b \sim 100$, Ahuja and Hender predict $L=0.627$ and $M=0.849$ for broadside orientation to the acoustic field and $L=0.008$ and $M=0.571$ for edgewise orientation. Both configurations have been applied to the relevant data in chapter 7.

3. ULTRASONIC APPARATUS AND TECHNIQUE

3.1 ULTRASONIC MEASUREMENT PRINCIPLES

In commercially available ultrasonic transducers, a lead-zirconate-titanate (PZT) ceramic is generally used in the form of a disk arranged to radiate or receive energy at its front flat surface, the rear being highly damped (usually by a tungsten-loaded epoxy backing) to avoid rear face reflection and hence interference. Such a disk can be theoretically treated as a cophasally vibrating piston, producing a picture of the ultrasonic field normal to the plane of the disc which agrees remarkably well with experimental data (Wells 1969). Using this analysis, it has been shown (Kinsler and Frey 1962, Goberman 1968) that for steady state conditions (continuous wave, constant amplitude drive) the intensity distribution along the beam's central axis is given by:

$$I_x = I_0 \sin^2 \left\{ \frac{\pi}{\lambda} (\sqrt{r^2 + x^2} - x) \right\} \quad \text{(eqn. 3.1)}$$

where I_0 = the principal intensity maximum, ultrasonic intensity I being defined as the power transmitted normally through unit area,

I_x = intensity at distance x from piston

r = radius of piston

and λ = wavelength of propagated ultrasound.

Equation 3.1 can be solved to give the position of the axial maxima and minima as:

$$X_{max} = (4r^2 - \lambda^2(2m+1)^2) / 4\lambda(2m+1) \quad \text{(eqn.3.2)}$$

where X_{max} = position of max. intensity along axis normal to transducer, and $m = 0, 1, 2, \dots$

AND

$$X_{min} = (r^2 - \lambda^2 m^2) / 2m\lambda \quad \text{(eqn.3.3)}$$

where X_{min} = position of min. intensity along axis normal to transducer, and $m = 1, 2, 3, \dots$

Putting $m=0$ into eqn.3.2 gives the distance of the last axial maximum from the transducer as:

$$X'_{max} = (4r^2 - \lambda^2) / 4\lambda \quad \text{(eqn.3.4)}$$

Now if the radius of the transducer is much greater than the ultrasonic wavelength i.e. $r^2 \gg \lambda^2$, eqn.3.4 becomes:

$$X'_{max} = r^2 / \lambda \quad \text{(eqn.3.5)}$$

The position of the last axial maximum marks the transition between the Fresnel and Fraunhofer diffraction zones or the near and far field. In the near field, energy is mainly confined within a cylinder of radius r , but the distribution across the beam diameter at any distance x from the transducer is non uniform (which is apparent from

eqn.3.1); whereas in the far field, the beam diverges (intensity distribution being described by a first order Bessel function) and intensity falls off in accordance with the inverse square law. In view of these considerations, the techniques used in this investigation were restricted to near field measurements (to minimise diffraction effects) with identical receiver and transmitter transducers being used to effectively integrate any detected signal over the beam diameter (negating non-uniform intensity distribution effects). To ensure near field operation, the following constraints were observed:

- (i) radius of transducer \gg ultrasonic wavelength
- (ii) path length (L) for ultrasound in any sample limited by:

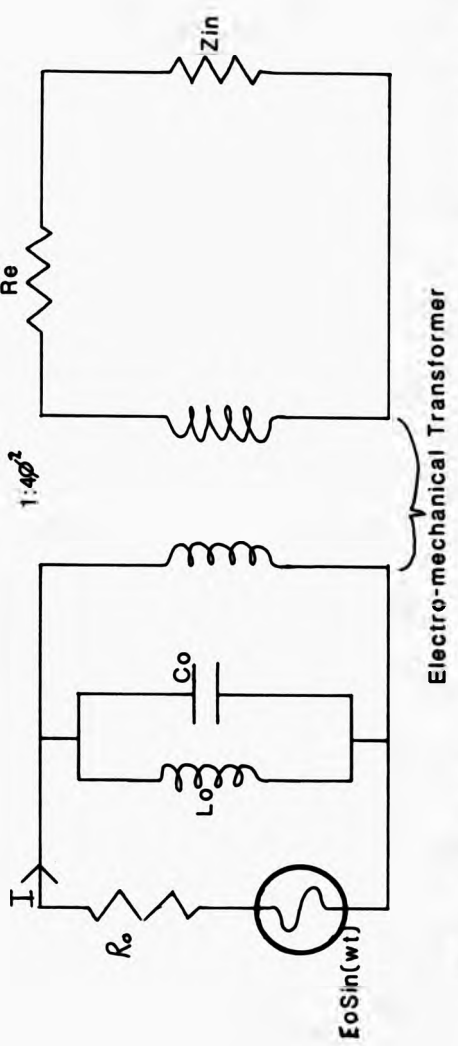
$$L < r^2/\lambda \quad (\text{eqn.3.6})$$

Adhering to the above criteria, the following three distinct forms of transducer excitation were used to produce the ultrasonic field, and although the latter two do not strictly comply with the theoretical steady state boundary condition, their practical validity was tested by means of intercomparison.

Units Of Attenuation.

In this work the amplitude of a wave is assumed to decay with distance x as $\exp(-\alpha x)$ (see eqn.1.1), so the natural units of α are m^{-1} sometimes called neper m^{-1} . However, the units of dB/cm are also widely used where $1 m^{-1}$ or 1 neper $m^{-1} = 0.21 \log_{10} e$ dB/cm. For this thesis α in

FIGURE 3.1 Equivalent Circuit Of An Ultrasonic Interferometer



Electro-mechanical Transformer

- KEY E_0 - Peak amplitude of supply voltage R_0 - Internal resistance of source
 I - Current drawn by transducer at resonance
 L_0, C_0 - Transducer inductance and capacitance at resonance
 ϕ - Applied voltage to force transfer function for the transducer crystal
 Z_{in} - Effective input resistance impedance of liquid-reflector system
 R_e - Resistance in crystal at resonance

For a transducer run at its resonant frequency so that its impedance is predominantly resistive, R_e , Mason shows that the electrical impedance Z of the transducer-sample-reflector combination is given by

$$Z = \left[\frac{R_e + Z'_{in}}{4\phi^2} \right] \quad \text{(eqn.3.8)}$$

where ϕ is the voltage to force transfer function of the transducer element.

From this result, an expression for the current (I) drawn by the transducer as a function of L can be obtained giving:

$$I = \left[\frac{E_0}{R_0 + (R_e + Z'_{in})/4\phi^2} \right] \quad \text{(eqn.3.9)}$$

The maximum in $\coth \Gamma L$ occurs when $\beta L = n\pi$, making I a minimum for L -any integral number of half wavelengths. Similarly, maxima occur in I for L -odd quarter wavelengths. The resulting equations describing I_{max} and I_{min} are:

$$I_{max} = \left[\frac{E_0}{R_0 + R_e/4\phi^2 + Z'_{in}/4\phi^2} \right] \quad \text{(eqn.3.10)}$$

$$\text{where } Z'_{in} = Z_0 \left[\frac{\tanh(\alpha L) + Z_0/Z_r}{1 + Z_0/Z_r \tanh(\alpha L)} \right]$$

and

$$I_{min} = \left[\frac{E_0}{R_0 + R_e/4\phi^2 + Z'_{in}/4\phi^2} \right] \quad \text{(eqn.3.11)}$$

$$\text{where } Z_{in} = Z_0 \left[\frac{1 + Z_0/Z_r \tanh(\alpha L)}{\tanh(\alpha L) + Z_0/Z_r} \right]$$

The resulting prediction for the variation of I with L agrees remarkably well with earlier experimental data (Mason 1950); hence from interferometric data where I is measured as a function of L, one can obtain attenuation (α) for a given liquid from eqns. 3.10 & 3.11. Further, as the maxima (or minima) are separated by a whole number of half wavelengths, the velocity of propagation can be found from the separation ΔL between successive extrema of the interferogram by;

$$c = 2\Delta L \cdot f \quad (\text{eqn. 3.12})$$

where f is the resonant frequency of the transducer.

The above theoretical treatment was used to interpret data obtained from the interferometer now described.

The Ultrasonic Interferometer.

Continuous wave measurements of α and c were made for liquids and colloids using an interferometer constructed as shown in Figure 3.2. For a description of design considerations the system may be split into two sections as follows:

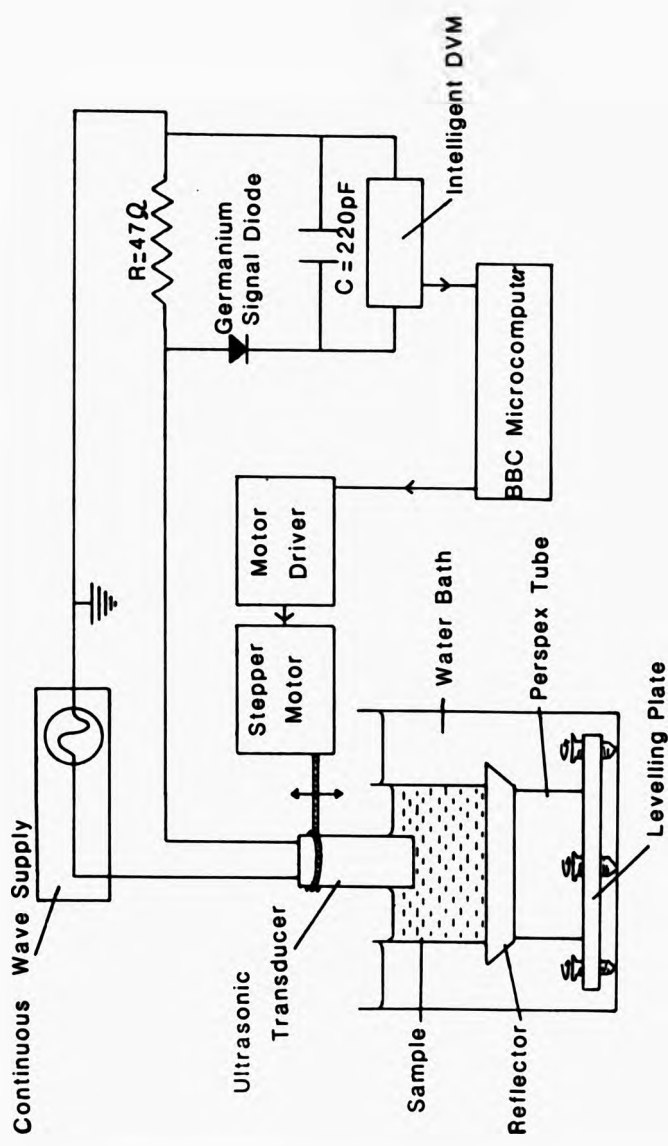


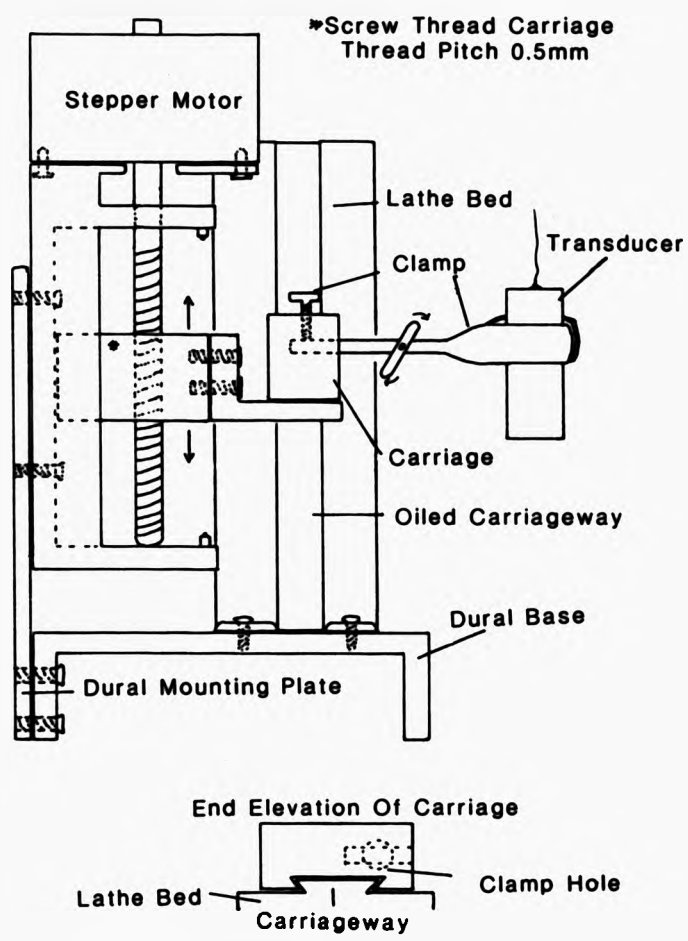
FIGURE 3.2 Ultrasonic Interferometer

(1) Transducer Drive Circuit And Data Collection.

It was required that the current drawn by the transducer, whilst driven continuously at resonance, should be monitored as a function of increasing sample column length. In practice, measurement was made of the voltage across a known resistance, R , in series with the transducer. R was chosen as the nearest standard value to transducer resonance resistance in order that optimum voltage variation resolution could be obtained. This signal was half-wave rectified using a germanium signal diode (offering high stability with low turn on voltage, $\approx 0.65V$, for optimum dynamic range), smoothed by a 220pF capacitor and then recorded using a digital voltmeter. The transducer was moved by 2.5 μ m steps through the sample by a stepper motor via a micrometer screw thread (detail shown in Figure 3.3). This step size gave adequate spatial resolution of amplitude maxima and minima offered by its 2.5 μ m step size. For example, taking velocity $c = 1500m/s$ and the maximum resonant frequency of transducers to be 10MHz, then using eqn.3.12 the maxima and minima in signal are separated by 75 μ m. Thus at least 30 data points could be obtained between any successive maximum and minimum.

To interlink and automate the current and position measurements, both the DVM and stepper motor drive were interfaced with a microcomputer (B.B.C.model B). Data from the DVM was collected via the RS423 serial port at a rate of three readings per second (the fastest possible with the DVM used) and on receipt of each, a stepping signal was sent to the motor driver via the BBC user port to move the

FIGURE 3.3 Transducer Translation Mechanism

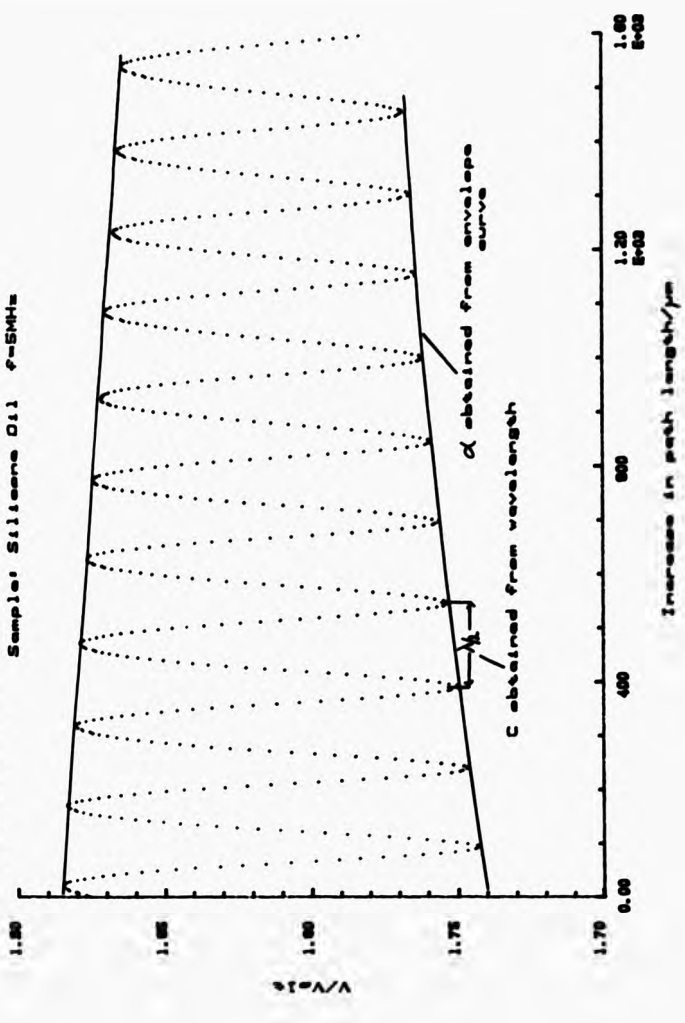


transducer up. Care was taken to check that this collection rate allowed the motor and transducer time to equilibrate after each step. In fact, comparison of the steady state DVM signal sent to the BBC with that following a single step revealed no significant difference in noise levels with time. In both cases, fluctuations of around 0.1% about the mean existed.

Thus, a continuous set of data points, in this case limited to ~1200 for VDU screen-plotting resolution, could be obtained as a function of increasing transducer-reflector separation from an arbitrary origin (see Figure 3.4). In practice this origin had to comply with the constraint of eqn.3.6, which for the radius range of transducers used meant a lower limit to the value L_{max} of 6cm. Also the maximum usable distance from the reflector was ≈ 0.5 cm if good voltage variation resolution was to be obtained when highly attenuating samples were used. The computer software developed for data collection and stepper motor drive control is described in Appendix A. Facilities were available to:

- (a) instantaneously plot the interferogram (i.e. the voltage vs. distance graph) during data collection in order that satisfactory progress of the experiment could be monitored,
- (b) save data onto floppy disc for later analysis or hardcopy plotting
- (c) move the transducer either up or down by a known number of steps in order that a starting position could be easily set and returned to.

FIGURE 3.4 Voltage vs. Increase in Path Length
 Sample: Silicone Oil ρ -SMHs



Further processing of an interferogram was required in order to obtain α and c . This was achieved by extracting the maxima and minima coordinates and fitting them simultaneously to eqns. of the form:

$$V_{\max}(L) = \left[B + C \left\{ \frac{E + \tanh(DL + F)}{1 + E \tanh(DL + F)} \right\} \right]^{-1} \quad (\text{eqn. 3.12})$$

$$V_{\min}(L) = \left[B + C \left\{ \frac{1 + E \tanh(DL + F)}{E + \tanh(DL + F)} \right\} \right]^{-1} \quad (\text{eqn. 3.13})$$

where, from eqn. 3.10 and eqn. 3.11, $B = R/E_0(R_0 + R_e/4\theta^2)$, $C = RZ_0/4E_0\theta^2$, $D = \alpha$, $E = Z_0/Z_r$ and F is a constant to allow for arbitrary phase origin.

It can be seen that the use of voltage across a constant resistance instead of current drawn (as per eqns. 3.10 and 3.11) is permissible as they differ only by a constant of proportionality which is the resistance R . This leaves α extractable from fitting parameter D . The average separation of maxima and minima was also computed giving velocity c from eqn. 3.12. Both these fitting routines were performed on the VAX mainframe computer using software developed by Nandi (1987).

(11)The Ultrasonic Cell.

The major consideration for the cell was the reflector material. Stainless steel was chosen for a strong acoustic impedance mis-match with typical liquids for strong reflection (See Table 1 Appendix B). The reflector thickness t was chosen such that extra contributions to total reflected intensity, due to the existence of a second steel face, were much less than those from the first. The relevant analysis used is given in Appendix B. The ideal t would be infinite but a value of $t=2.5\text{cm}$ was adopted as a useful working figure. Using e.g. a castor oil sample at 5MHz, second face contributions to total reflected intensity then represented 0.5%. The reflector was polished to near optical flatness and mounted on a height-adjustable plate in order that parallelism with the transducer could be attained, both factors being necessary to avoid assymetry and secondary peaks in the interferogram as reported by McMillan and Langerman(1947), and Hubbard(1940). The ultrasonic cell was completed by mounting a stainless steel ring onto the reflector of 6cm diameter, chosen to be greater than the diameter of the transducers used (max. 2cm). This reduced the possibility of detecting surface wave propagation in the cell walls and made r.f. pick-up between transducer and cell negligible. Using a sample volume of 20ml, for this reflector area a liquid height of approximately 7mm was obtained thus restricting L ; in practice a working figure of $L_{\text{max}} \approx 5\text{mm}$ was adhered to.

With the interferometer as described above, sample measurements were conducted as follows:

Experimental Procedure 1

The transducer, shown in Figure 3.2, was lowered into the sample using the stepper motor and repeatedly excited with a 150V, 100ns pulse whose reflection was monitored using an oscilloscope. This enabled transducer position and reflector tilt to be adjusted, optimising pulse amplitude and shape to ensure transducer-reflector parallelism. Now driven continuously by a 5V peak to peak signal at its resonant frequency, the transducer was moved upward from the reflector in 2.5 μ m increments, and the resulting variation of voltage across R (see Figure 3.2) was recorded under microcomputer control.

Finally, with the interferogram collected, the maxima and minima coordinates were extracted and fitting procedures performed to obtain attenuation and velocity. For intercomparison purposes a test liquid, Dow Corning 710 silicone fluid, was measured at 5MHz, 23 $^{\circ}$ C giving results $c=(1377\pm 7)$ m/s and $\alpha=(9.6\pm 0.3)$ dB/cm (errors discussed in section 3.5).

3.3 Tone Burst

A tone burst is a harmonic signal of finite length. If this signal has a mean frequency equal to that of the transducer at resonance, it has been shown by Matsuzawa et al.(1987) that after traversal of a liquid sample, the signal detected at a second (receiver) transducer can be predicted mathematically subject to certain boundary conditions. Consider the ultrasonic cell shown in Figure 3.5.

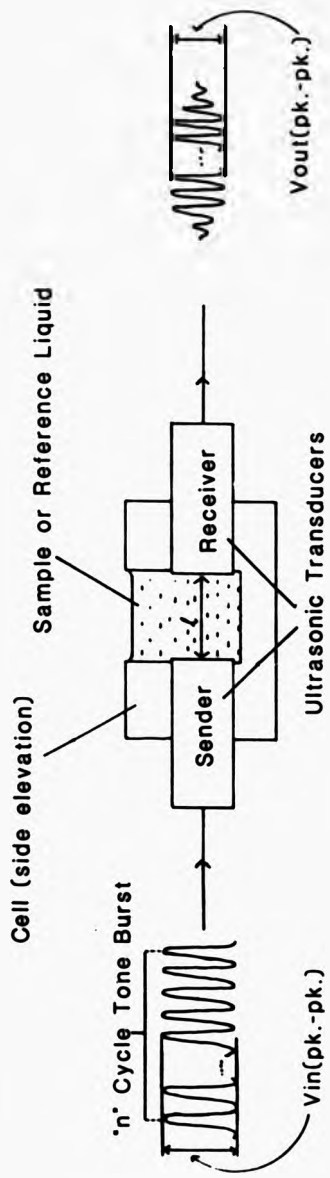
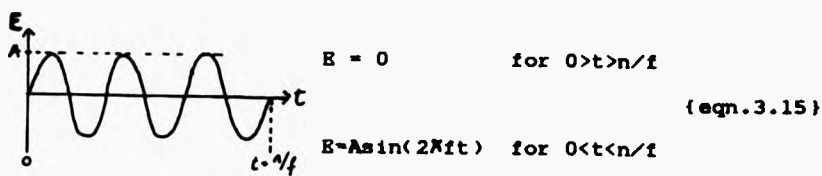


FIGURE 3.5 Tone Burst Cell

If the transmitter is driven by a voltage such that:



where n is the number of periods in the tone burst and A is the voltage amplitude, then if n is large such that a single period is $\ll n/f$, the form of the received waveform is described by:

$$E_r \approx (2\pi ft)^2 - 3 \sin(2\pi ft) + 6\pi ft \cos(2\pi ft) \quad (\text{eqn.3.16})$$

Equation 3.16 predicts that the first received cycle (corresponding to the first one transmitted) is negative, making it easy to identify. Further if the number of transmitted cycles is increased from n to $n+1$, only cycles after the n th received will increase in amplitude as the additional contribution to the n th is negative. This has been verified experimentally by Matsuzawa (1987). Thus, if the time delay between transmission and receipt of corresponding cycles is measured, the velocity of ultrasound propagation in the liquid can be obtained from:

$$c = L/\Delta t \quad (\text{eqn.3.17})$$

where L = path length in liquid
and Δt = average time delay

For measurements made using transducers fitted with quarter wave matching plates, Δt includes time for travel through

the plate on the sender and receiver i.e. extra time of $1/4f$ at each, where f is the transducer resonance frequency. This was verified for the transducers used in this work using distilled water as a test liquid, by measuring Δt_1 for one way transmission and Δt_2 from successive received reflections. Effectively, Δt_2 does not include time travel through the plates as reflections take place at the liquid-plate interface, and thus comparison of Δt_1 and Δt_2 allows the extra delay to be assessed. The results for the 5MHz (PAR Scientific) transducers were:

$(T \pm 0.1)/^{\circ}\text{C}$	$(c_1 \pm 3)/\text{m/s}$	$(c_2 \pm 3)/\text{m/s}$	$(c \pm 0.5)/\text{m/s}$
18.0	1460	1476	1476
18.9	1464	1480	1479
20.8	1471	1487	1485
22.7	1473	1490	1490
23.1	1479	1494	1491
24.5	1480	1496	1495
25.8	1484	1502	1499

Here, c_1 and c_2 are the velocities calculated using Δt_1 and Δt_2 respectively, with c being reference data from Kaye and Laby(1973). Further, the mean difference between the transit times was 0.12 μs . The excellent agreement between c_2 and the expected velocity, together with the low values of c_1 , indicates that a quarter wave plate correction is necessary for one way transmission times. Also the mean delay of 0.12 μs agrees well with that expected at 5MHz, i.e. 0.1 μs , from the expression $1/2f$. Thus this correction was applied to one way transit times measured in this work.

In order to find the attenuation of the liquid, one can compare the peak received amplitude with that obtained for a known or reference liquid. For the configuration shown in Figure 3.5, if the equilibrium pk-pk output voltage is assumed to be of the form:

$$V_{out}(pk-pk) \propto V_{in}(pk-pk) \exp(-\alpha L) \quad \text{(eqn.3.18)}$$

and V_{in} is constant assuming identical transmission coefficients at the liquid-transducer interfaces for both sample and reference liquid, the ratio of output voltages can be written such that:

$$\frac{V_{out}(\text{sample})}{V_{out}(\text{ref.})} = \frac{\exp(-\alpha_s L_s)}{\exp(-\alpha_r L_r)} \quad \text{(eqn.3.19)}$$

Solving for α of sample liquid, if $L_s = L_r = L$ eqn.3.18 gives:

$$\alpha = \alpha_{ref} + \{\ln(V_{o.ref}/V_{o.sample})\}/L \quad \text{(eqn.3.20)}$$

Hence measurement of output voltage ratio and path length in the cell enables sample attenuation to be calculated provided a reference liquid is used whose properties are known. The above treatment was employed to process data obtained from tone burst experiments now described, using water as the reference liquid.

The Tone Burst System.

The design of this system is set out in Figure 3.6. Two identical transducers were mounted in a non-conducting Tufnol laminate cell (to eliminate r.f. pick up) separated by a fixed distance $L \approx 2\text{cm}$ for frequencies except 1MHz, where $L \approx 3\text{cm}$. This value of L was used to satisfy constraints of tone burst duration (see next paragraph) and eqn.3.6 i.e. $L < r^2/\lambda$, and keep sample volume low (max vol. 8.6ml- 1MHz cell). For the transducers used in this project, assuming an ultrasonic velocity in the sample of the order 1500m/s, the L_{max} values from eqn.3.6 were as follows:

<u>Frequency/MHz</u>	<u>Manufacturer</u>	<u>Radius/cm</u>	<u>($L_{\text{max}} 0.5$)/cm</u>
1	Panametrics	0.95	6
2.25	"	0.64	6
5	"	0.64	13
5	PAR Scientific	0.50	8
10	Panametrics	0.64	27

Thus $L=2\text{cm}$ (3cm in the 1MHz case) was an adequate choice. The transducer connections were protected by silicone rubber sealant in order to allow immersion of the cell in the water bath.

A relatively simple drive and data collection circuit was employed, using a variable duration tone burst generator, impedance matched to the transducers, to excite the sender with an up to 30V pk-pk, 15 cycle burst (set at

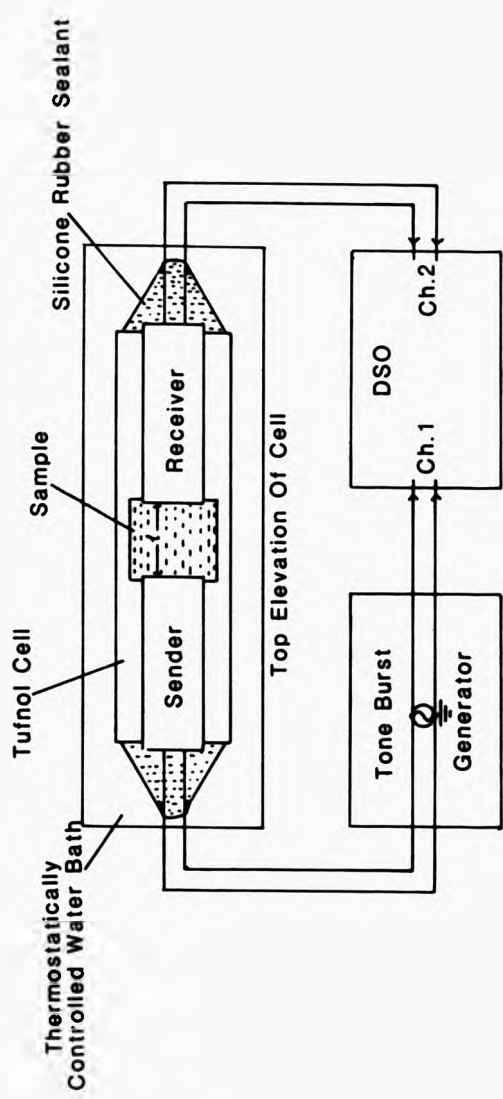


FIGURE 3.6 Tone Burst System

or near to transducer resonance frequency) and a 40MHz digital storage oscilloscope (DSO) to record the sent and received bursts up to 5MHz. Above this frequency, measurements were made using the normal oscilloscope mode, as the digitisation rate became unsatisfactory e.g. at 10MHz only four points per cycle. The working value of $n=15$ cycles was selected on two principles:

- (i) that the signal duration should be less than cell transit time in order that successive bursts could be resolved i.e.

$$n/f < t \quad \text{(eqn.3.21)}$$

(e.g. with the lowest f in this work, 1MHz, cell length $L=3\text{cm}$, ultrasonic velocity in the sample $c \approx 1500\text{m/s}$, eqn.3.21 dictates that $n < 20$).

- (ii) that n should be large to satisfy the theoretical boundary condition that a single period must be much shorter than n/f (although values as low as $n=8$ were found adequate by Matsuzawa et al.(1987)). The length of the tone burst has consequences for amplitude distribution with frequency and for bandwidth. This can be examined using Fourier analysis on a simple sinusoidal tone burst as follows:

$$\begin{aligned} \text{Let } F(t) &= E_0 \exp(-2\pi i f_0 t) & \text{for } 0 < t < n/2f_0 \\ \text{and } F(t) &= 0 & \text{for } 0 > t > n/2f_0 \end{aligned}$$

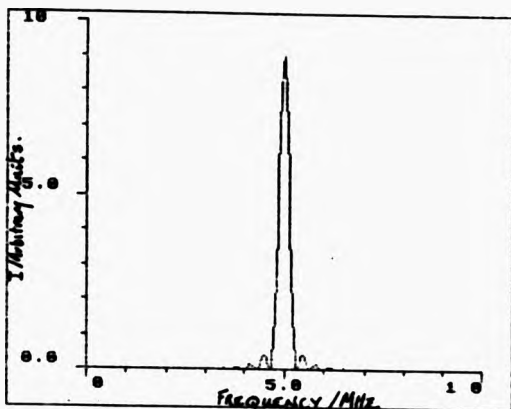
then the distribution of F in frequency space is given by:

$$F(f) = \frac{1}{\sqrt{2\pi}} \int_{-\infty}^{\infty} F(t) \exp(2\pi i f t) dt$$

hence
$$F(f) = E_0 / \sqrt{2\pi} \left[\frac{\sin(n\pi(f-f_0)/t_0)}{\pi(f-f_0)} \right]$$

If, for example, $f = 5\text{MHz}$ and $n=15$, the intensity function $[F(f)]^2$ has the form shown in Figure 3.7.

Figure 3.7 Intensity Vs. Frequency: $f_0 = 5\text{MHz}$, $n=15$



This indicates that the greatest peak in power occurs at $f=5\text{MHz}$ and the half peak height value of $f \approx 0.2\text{MHz}$. It can be shown that over 90% of the power in such a tone burst falls in the frequency range $f_0(1 \pm 1/n)$. The consequences of this impure f signal for experimental accuracy could be modelled analytically but are investigated in this work by comparing experimental results with a pure f technique (see Section 3.5). Further, although the excitation signal used was not a perfect sinusoid, the sender transducer output was found to be so. Thus the assumption in the above analysis that the transmitted burst is sinusoidal appears reasonable when applied to the tone burst experiment.

A working figure of $n=15$ was used, satisfying (i) and (ii) above whilst being easy to employ in practice and providing a workable equilibrium region for pk-pk voltage measurements on the received burst.

Experimental Procedure 2

With transducers of the required frequency selected, their wear plate separation was accurately measured using a telescoping gauge and a micrometer, prior to introduction of the sample into the cell. The sender was then excited by a 15 cycle tone burst, of pk-pk voltage up to 30V according to the attenuation of the sample, to give a convenient received voltage level for measurements on the DSO screen. Both sent and received bursts were monitored on the oscilloscope and recorded using the storage facility. Employing the x and y axis cursors, the time delay Δt between five successive corresponding sent and received cycles, and the steady state pk-pk received voltage (see Figure 3.5) were measured. An average signal, constructed by the oscilloscope from 256 bursts, was used for f up to 5MHz. Higher f measurements were made using the DSO in the normal mode. The experiment was then repeated using distilled water as a reference liquid, or using the pure sample liquid if only changes due to the addition of colloidal particles were to be monitored. Values of Δt and the output voltage ratio thus obtained were then used to calculate c and α in accordance with eqns.3.17 and 3.20 respectively. Measurements on the aforementioned silicone fluid gave $c=(1373\pm 6)\text{m/s}$, $\alpha=(9.5\pm 0.2)\text{dB/cm}$.

3.4 Broadband Pulse.

Under this category, two distinct techniques have been developed in this work and it is therefore useful to describe two sets of measurement principles.

(1) Pulse-Echo Overlap

Consider the system shown in Figure 3.6. Here the transducer is excited by a voltage pulse of short duration, and an ultrasonic pulse is sent through the sample and reflected between the sample boundaries (i.e. at the transducer-liquid and liquid-reflector interfaces) until it decays away. If the pulse length is much less than the round trip transit time for the cell, a simple pulse-echo decay pattern develops, from which the time delay t between each successive reflection is measured. The pulse velocity c can be calculated, provided that a correction to t is made for propagation time Δt through the front wearplate which protects the piezoelectric disc [Vincent1987]. Δt can be obtained by measuring the time delay t' for a liquid of known velocity c' and calculating Δt from

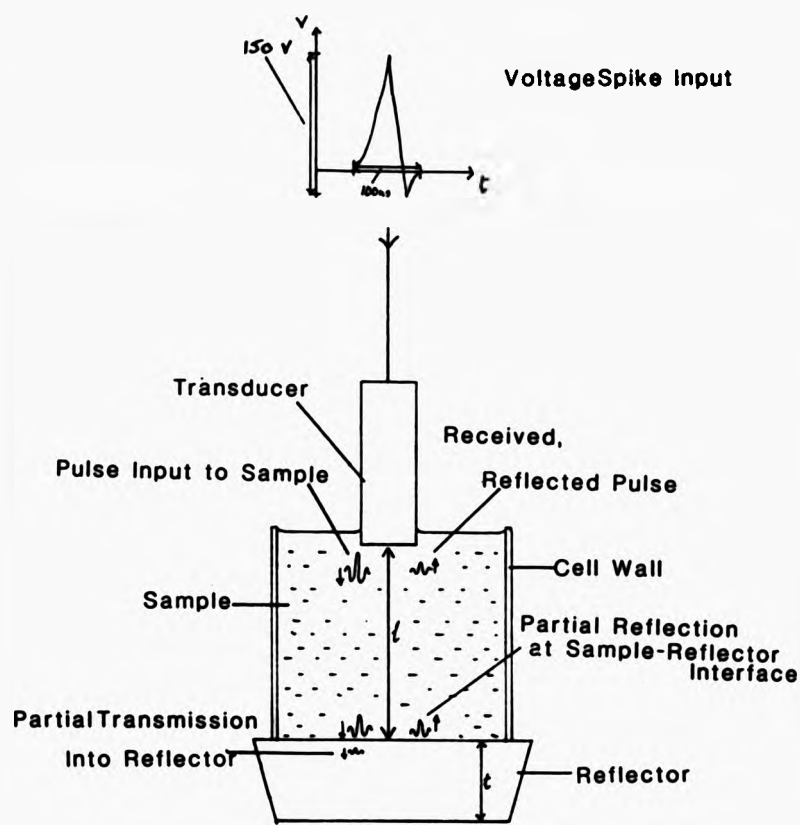
$$c' = 2L / (t' + \Delta t) \quad (\text{eqn.3.22})$$

where L is the geometric path length

A more refined method for obtaining c is to vary the pulse repetition period (PRP) of pulses entering the sample until it is equal to the time for traversal of the cell. This is the Pulse Echo Overlap (PEO) technique described by Breazeale et al.(1981). The velocity is found from:

$$c = 2L / \text{PRP} \quad (\text{eqn.3.23})$$

FIGURE 3.8 Pulse Cell



If a similar wearplate correction is made, in this case by finding the change in PRP introduced by a known increase in path length, then:

$$c = 2 \Delta L / (PRP_2 - PRP_1) \quad \text{(eqn.3.24)}$$

where PRP_1 and PRP_2 are the pulse repetition periods for $l=L$ and $l=L+\Delta L$ respectively.

(ii) Spectrum Analysis Of A Broadband Pulse.

Measurements of ultrasonic attenuation were made on a sample by a through-transmission technique where the signal from the receiving transducer was processed by a commercial spectrum analyser, as described by Langton^{et al.} (1984). Using a cell identical in geometry to that in Figure 3.5, the transmitter was fired with a voltage pulse (as in (i) above) and the resulting received voltage was analysed as a function of frequency, the sample attenuation in dB/cm at a given frequency was obtained from:

$$\alpha = [20 \log_{10} (V(f)_s / V(f)_w)] / L \quad \text{(eqn.3.25)}$$

where $V(f)_s$ is the component of output voltage at frequency f for the sample and $V(f)_w$ is the value of the same parameter using distilled water as the transmission liquid. This assumed that attenuation due to water was negligible compared to that of the sample which appears reasonable when, for example, at $T=25^\circ\text{C}$, $f=5\text{MHz}$, $\alpha(\text{water}) \approx 0.046\text{dB/cm}$ and $\alpha(\text{castor oil}) \approx 13\text{dB/cm}$ (Mason 1950). This represents an error of approximately 0.3% in α from eqn.3.25 which is well within experimental error. However, if eqn.3.25 is to be

generally applicable one must correct for the finite attenuation of water ($\alpha_w/\text{dBcm}^{-1}$) and replace $V(f)_w$ with V_{in} where:

$$V_{in} = V(f)_w / \log_{10}(\alpha_w L / 20) \quad \text{(eqn. 3.26)}$$

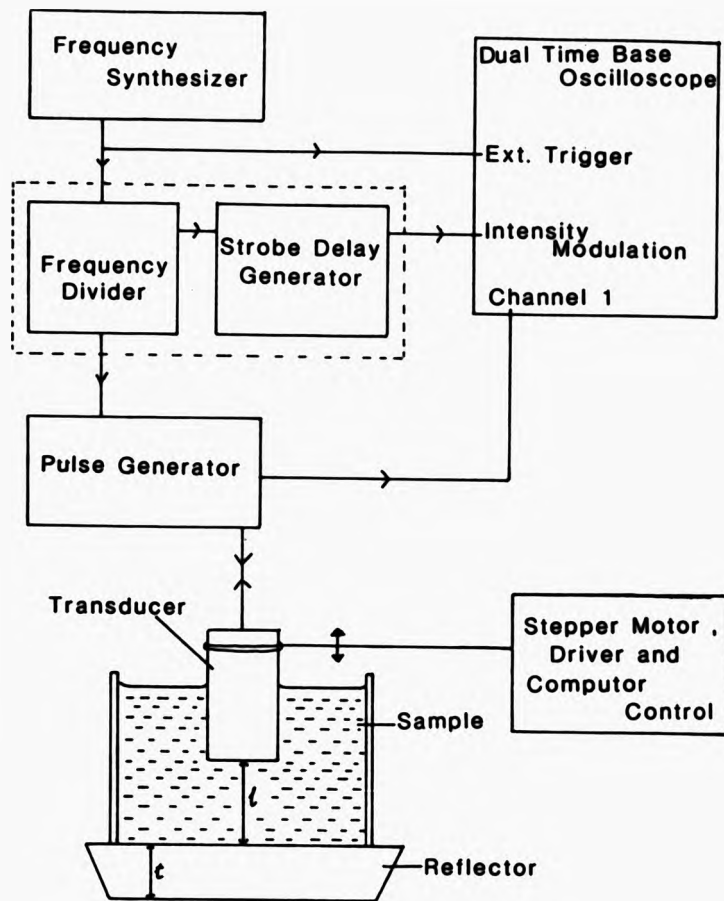
The Broadband Pulse Techniques.

(i) Pulse Echo Overlap (velocity measurements).

For this work, the equipment used was set out as shown schematically in Figure 3.9. A frequency synthesizer was used to generate a c.w. signal of frequency equal to an approximate reciprocal transit time for the cell (estimated from pulse transit time measurements recorded from an oscilloscope trace). A submultiple of this frequency (selected by a frequency divider) was then fed to a pulse generator and double strobe delay generator. The signal to the pulse generator triggered it to fire a 150V, 100ns spike to the transducer at a repetition rate set by the submultiple frequency ($f/10$ was routinely used). The response of the transducer to each spike was to ring at its resonant frequency for about four cycles (amplitude and no. of cycles depending on attenuation; four cycles was typical), thus producing a pulse of duration $4/f_{res}$, e.g. 0.8 μ s for 5MHz transducers.

An oscilloscope having an intensity modulation provision was used to monitor the resulting sequences of decaying amplitude pulses, caused by successive reflections, received by the transducer. Signals from the

FIGURE 3.9 Pulse-Echo Overlap System



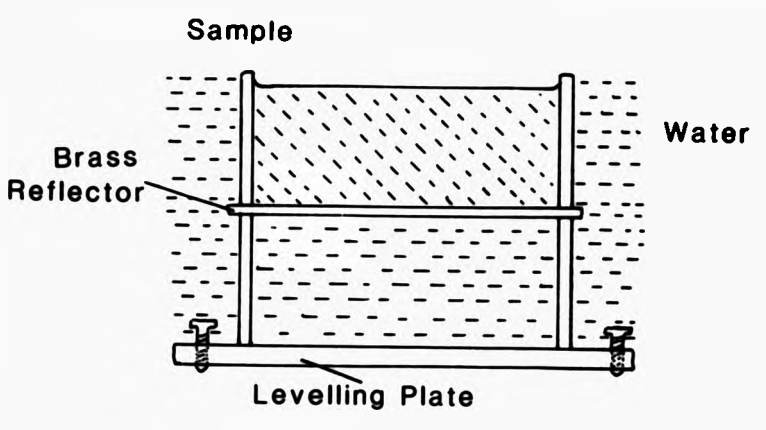


strobe generator were then used to increase the intensity of two sections of the oscilloscope trace, and as their triggering points, duration and interdelay could be varied, two pulses in each sequence could be selected for viewing. This function produces an enormous advantage in that the original excitation pulse, being of far greater amplitude and more complex in shape than those ensuing, is electronically blanked out; thus the two pulses to be overlapped are easily seen and accurate overlap is more readily obtained. This overlap was performed by fine tuning of the frequency output of the synthesizer to the required PRF. The fact that the actual PRF in the cell is only $f/10$ presents no major problem because the oscilloscope is triggered by the frequency synthesizer thus electronically recreating the required PRF. However, this does mean that an approximate knowledge of this PRF (and therefore c in the sample) is required as overlap can be obtained at any submultiple thereof: a rough value can be found from simple measurements of transit time for the cell (see Experimental Procedure 3(1)).

The complex nature of the pulse pattern from the transducer has consequences for cell design. Any pulses from the second surface of a reflector would be received at a rate $\neq PRF/n$ due to the difference between ultrasonic velocity in the sample and reflector, thus providing pulses for overlap which may be indistinguishable from the others and deliver incorrect results if used. To overcome this a cell was developed with a thin brass reflector having $t=0.3mm$ (see Figure 3.10).



FIGURE 3.10



It was found that any second surface reflection was small compared with the first (approx. by a factor of 10) and appeared to occur within the decaying portion or tail end of the main pulse. This left a less complex set of pulses, each with a very clear initial 2-4 cycles for overlap.

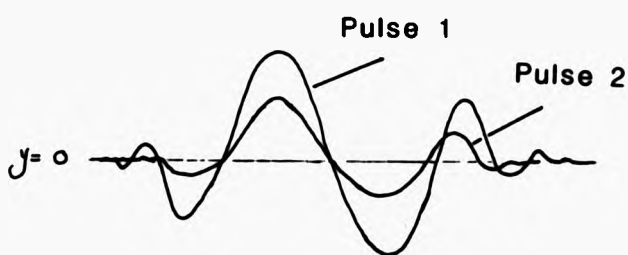
Experimental Procedure 3(1).

Using the apparatus shown in Figure 3.9, the transducer was initially excited by the pulse generator only with 150V, 100ns pulses at a repetition rate of 5kHz, chosen such that $1/PRF \gg$ the transit time for the cell, allowing one sequence of pulses to decay away before the next excitation. The resulting received signal was monitored on an oscilloscope, from which the time delay t between successive pulses was measured and hence a rough value of $PRF \approx 1/t$ for the occurrence of pulse-echo overlap obtained. The output of the frequency synthesizer, set to

this value, was then used to trigger transducer excitation pulses via the frequency divider. With two pulses selected for viewing, fine adjustment of the synthesizer output frequency was carried out until the pulses coincided on the oscilloscope screen, thus giving PRF_1 . The transducer was then moved upward a known distance ΔL by the stepper motor system, $\Delta L=2mm$ was found convenient and routinely used, overlap being regained by synthesizer output fine adjustment to provide PRF_2 .

Accurate and repeatable overlap was obtained by employing the B time base oscilloscope function to expand the time axis in the region of the pulses, together with the adoption of a simple criterion for overlap as displayed in Figure 3.11.

FIGURE 3.11



overlap criterion: that 1st resolvable cycle on each pulse should overlap such that the falling edges coincide at $y=0$.

This criterion could be easily adhered to, giving rise to reproducible PRFs. Thus with overlap PRFs acquired for two sample path lengths whose difference ΔL was accurately

known, the ultrasonic velocity in the sample was calculated using eqn.3.24. Changes in velocity e.g. due to flow, were found by monitoring the PRF and using,

$$c = 2*L(PRf_1 - PRf_2), \quad (\text{eqn.3.27})$$

where L was measured ultrasonically using distilled water at a fixed temperature to calibrate the cell. As the frequency synthesizer output could be set to a few parts in 100,000 changes of a fraction of 1m/s were detectable. Measurements on the test liquid Dow Corning 710 silicone fluid gave $c=(1370\pm 2)\text{m/s}$.

(ii) Spectrum Analysis (Attenuation Measurement).

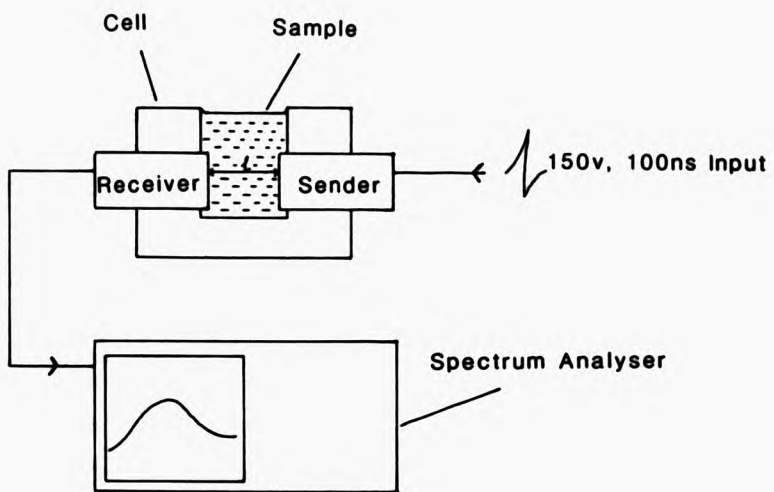
No extra development was required here as: (i) the tone burst cells were used, (ii) transducer excitation was provided by the pulse generator employed in all aforementioned pulse measurements and (iii) deconvolution of received pulse data was performed using a Hewlett Packard spectrum analyser.

Experimental Procedure 3(ii).

Using the apparatus set out schematically in Figure 3.12, having measured L using a telescoping gauge and micrometer, water was placed in the cell and the sender transducer excited by a 150V, 100ns spike. The signal obtained at the receiver, after transmission through the water, was fed directly to the spectrum analyser. By performing Fourier analysis on this pulse, the analyser produced a distribution of amplitude as a function of frequency and this trace was stored using a memory function. The experiment was then repeated with the sample in the cell

and the resulting amplitude vs. frequency trace divided by that obtained for water. A cursor facility available on the instrument was used to select the required frequency component, whereby a digital readout of the relative attenuation was displayed. Using this data and length L, the sample attenuation was calculated using eqns. 3.25 and 3.26. Measurements made on the 710 silicone fluid gave $\alpha = (9.3 \pm 2) \text{ dB/cm}$.

FIGURE 3.12 Spectrum Analysis System



3.5 Technique Comparison.

It is necessary to appraise the applicability of eqn.3.6 (defining the near field) to the latter two methods, both using a non-steady-state drive, particularly with a view to assessing the necessity or otherwise of diffraction corrections, together with general accuracy and repeatability of the techniques. Also, account has to be taken of the different velocities that are measured i.e. phase velocity c_p from continuous wave methods and group velocity c_g from pulse transit time measurements. The difference between the two is determined by the dispersion relationship,

$$c_g = c_p + f dc_p/df, \quad (\text{eqn.3.28})$$

where f is the frequency.

However, little reference data exists in the literature for highly attenuating liquids or dispersions and as a consequence, the most effective means of appraisal was intercomparison between results. Thus data was obtained for a standard sample under constant conditions using each technique, to compare them with each other and with comparable data from an external source using a far field technique. For the purposes of this intercomparison, Dow Corning 710 Silicone Oil at 5MHz, 23°C, was chosen as the standard sample and collaboration was undertaken with Dr. Bajram Zeqiri at The National Physical Laboratory, who provided the far-field data. All measurements were made on liquid taken from the same bottle. The results are shown in Table 3.1.

TABLE 3.1

Sample: Dow Corning 710 Silicone Fluid $f=5\text{MHz}$ $T=(23\pm 0.1)^\circ\text{C}$

Method	c/ms^{-1}	α/dBcm^{-1}
+Interferometry	1377 \pm 7	9.6 \pm 0.3
+ Tone Burst	1373 \pm 6	9.5 \pm 0.2
+Broadband Pulse	1370 \pm 2	9.3 \pm 0.2
* Far Field	1372 \pm 2	9.5 \pm 0.4

In Table 3.1, uncertainties of data marked + represent standard deviation from the mean for 10 determinations. The far field result was supplied by Zeqiri(1987) and obtained using the National Physical Laboratory transmission method in the far field, i.e. $L \gg r^2/\lambda$. The uncertainty in this data is not purely statistical and incorporates uncertainties in experimentally determined quantities.

The data in Table 3.1 show a remarkable agreement between the various techniques for measurements of attenuation and velocity on Dow Corning 710 silicone oil at 5MHz, 23°C, with a spread of approximately 3% in α and approximately 0.5% in c . This would appear to suggest that any diffraction or reflection effects in the tone burst and broadband pulse techniques, cause errors of less than 3% error in α and 0.5% in c . These figures compare well with other, published reproducibilities. For attenuation one has $\pm 3\%$ in $\alpha \approx 3\text{dB/cm}$ at 14MHz (Musa 1958), $\pm 5\%$ in $\alpha \approx 10\text{dB/cm}$ at 5MHz (Rahalkar et al.1986) and $\pm 7\%$ in $\alpha \approx 10\text{dB/cm}$ at 4MHz (Dumas ^{et al.} 1983). Velocity errors also appear to be of the same order as those found in this work, for example, $\pm 0.3\%$ in $c \approx 1500\text{m/s}$ at 2MHz (Rahalkar et al.1986) and $\pm 0.3\%$ in $c \approx 1300\text{m/s}$ at 1-200MHz (Kessler et

al.1971). Table 3.1 shows that the continuous wave interferometry measurements give a phase velocity, which was higher than the group velocity of the other methods. Although all the velocity measurements agree within experimental error, further investigation of the frequency dependence of c_p would be necessary, to determine the extent of dispersion in the range 1 to 10 MHz. However some indication of dc/df in silicone fluids is given by the data in Tables 3.2 and 3.3. The tone burst measurements show that velocity decreases with frequency, so we expect $dc_p/df < 0$ and hence from eqn.3.28 $c_p > c_g$, in accord with the data in Table 3.1.

In view of the good agreements, the applicability of the various techniques to different measurement conditions needs to be assessed. This may best be done by looking at each method in turn.

Although the interferometer is soundly based in theory, with the near-field boundary conditions strictly applicable, the reproducibility was, marginally, the poorest of the three and the fact that the transducer moves during the experiment may make it unsuitable for monitoring a stable gel or gelation process as any short-range structure may be broken down. Further, the transducer-reflector parallelism needed to ensure an accurate interferogram, may be difficult to obtain in flowing dispersions owing to drag on the transducer. Also it would be difficult to introduce a moving transducer to a pipe flow system. Comparison with similar data obtained from other techniques would provide some quantification of the extent of these problems, but will not be dealt with in this work.

The close agreement, for both α and c , between the tone burst and the far field methods (obtained under conditions where very careful diffraction corrections are essential), together with the ease and speed with which the experiment can be conducted, makes the tone burst technique very attractive. The simple, rigid cell geometry also makes it easy to introduce flow perpendicular to the plane of the transducer faces, and the good reproducibility in α makes it sensitive to changes greater than a few %; this is important in studying gel-formation and flow effects. However the sensitivity in c is not as great as that found in PEO, making the latter more attractive as a velocity monitor.

The spectrum analysis method for attenuation measurement has similar attractions as those for the tone burst, but no velocity data is obtained and the complicated nature of the analyser makes it more expensive and certainly less portable at present although this should be improved by rapid developments in microelectronics. In fact an equivalent apparatus for bone analysis, made by Ultrasonic Innovation Ltd., is already available in portable form. These are important considerations when eventual adaptation to an industrial context is desirable. However, for the sake of this work it provides a quick method whereby attenuation values at a number of frequencies (depending on attenuation level and transducer bandwidth) can be made simultaneously and this is its attractive feature. Velocity measurements from broadband pulse, using PEO, gave a very encouraging $\pm 0.2\%$ reproducibility which approaches that predicted by

Papadakis(1972) using quantitative error analysis, where a transit time resolution of $\pm 0.015/f_{res}$ (equivalent to $\pm 0.15\%$ in c for $L=2\text{mm}$, $f=5\text{MHz}$) is quoted. This indicates that it would be a useful monitor of small changes in c that might occur during gel formation, flow or changes in disperse phase concentration. In any of these cases, the problem of disturbance caused by movement of the transducer could be overcome by monitoring only changes in c (i.e. PRF) with the transducer in a static position, and not repeatedly measuring the absolute value which requires a path length change. This seems sensible as Papadakis indicates that for broadband pulse PEO, the accuracy of absolute measurements is nearer $\pm 0.1/f_{ref}$.

In summary, it may be said that the general experimental reproducibility i.e. $<3\%$ in α and $<0.5\%$ in c , is quite acceptable in the context of this investigation with the tone burst appearing most useful as it is robust, adaptable and fairly portable. However the theoretically sound interferometer sets a useful benchmark and further, the velocity sensitivity of PEO and ease with which frequency dependent information can be obtained from spectrum analysis are also attractive.

In view of these points, the tone burst system was adopted as the routine method for attenuation and velocity measurement, with PEO used for small velocity change detection, and interferometry referred to occasionally for comparison.

Further measurements were made on silicone fluids and the results are presented in tables 3.2 and 3.3; the tone burst method was chosen to assess its suitability over

the the frequency range 1-10MHz. (Interferometric velocity results have been included for comparison). The figures in brackets are from pulse transit time measurements by Ali and Langton (1989). The tone burst attenuation data has been fitted, using a least squares routine, to the form $\alpha = \text{constant } f^n$ where for the 710 fluid $n=1.80 \pm 0.05$ and for the 200/350 fluid $n=1.77 \pm 0.05$.

TABLE 3.2

Sample: Dow Corning 710 silicone fluid $T=(20 \pm 0.2)^\circ\text{C}$

Method	f/MHz	$(\alpha \pm 3\%)/\text{m}^{-1}$	$(c \pm 0.5\%)/\text{ms}^{-1}$	
Tone Burst	1	6.3 (5.7 \pm 12%)	1386 (1378 \pm 0.5%)	
	2.25	30		
	5	125 (125 \pm 2%)	1381 (1389 \pm 1%)	
	6	170 (170 \pm 1%)		
	7	226		
	8	262		
	9	332		
	Interferometer	5		1380

TABLE 3.3

Sample Dow Corning 200/350 Silicone Fluid $T=(20 \pm 0.2)^\circ\text{C}$

Method	f/MHz	$(\alpha \pm 3\%)/\text{m}^{-1}$	$(c \pm 1\%)/\text{ms}^{-1}$	
Tone Burst	1	1.6	1013 (1020 \pm 0.5%)	
	2.25	8.9		
	4	19.6 (25 \pm 7%)		
	5	27.6 (35 \pm 5%)	1007 (1024 \pm 1%)	
	6	39.1		
	8	71.4		
	9	84.0		
	10	105	- (1027 \pm 1%)	
	Interferometer	5		1016 \pm 0.5%

The data for the 710 fluid compares favourably with that reported by Dunn and Breyer(1962) who also found attenuation to be a function of $f^{-0.6}$ over the range 1-10MHz. This is consistent with a decrease in α/f^2 (a constant for classical or Stokes liquids) with increasing frequency, characteristic of associated and highly viscous liquids where structural relaxation can occur (Hertzfeld and Litovitz 1965). Dunn and Breyer report that their data, obtained at 26°C, fits a single relaxation process centred at approximately 40MHz. The data in table 3.2 also fits a single relaxation expression of the form given by Hertzfeld and Litovitz i.e.

$$\alpha = A \left[\frac{\omega^2/\omega'}{1 + (\omega^2/\omega'^2)} \right] \quad \text{(eqn.3.29)}$$

where A is a constant and $\omega' = 2\pi F_r$ is the relaxation pulsatance; using a least squares fitting routine, $F_r \approx 3$ (16+/-2)MHz.

In general, Hertzfeld and Litovitz show that structural relaxation frequencies are found to be inversely proportional to viscosity (η) and for 710 silicone fluid, the manufacturer's data sheet indicates a drop of approximately a factor of two in viscosity from that at 20°C to 26°C. Therefore it would be expected that $F_r(26)/F_r(20) \sim 2$. In fact from the above data $F_r(26)/F_r(20) \sim 2.5$, which is in fair agreement as no estimation of uncertainty is given by Dunn and Breyer.

The data for 200/350 silicone fluid (Table 3.3) also indicates that it is not a classical liquid as attenuation is found to be proportional to $f^{-1.77 \pm 0.05}$. Using eqn. 3.29,

the relaxation frequency is found to be $2(28 \pm 4)$ MHz.

If $F_r \propto 1/\eta$ then,

$$\frac{F_r 710}{F_r 200/350} = \frac{\eta_{200/350}}{\eta_{710}}$$

From the manufacture's data sheet $\eta_{710} \approx 0.65$ Pa s and $\eta_{200/350} \approx 0.36$ Pa s, giving a ratio of 1.8, where that given by the experimental F_r values is 1.75 ± 0.53 . Again there is good agreement within the experimental uncertainties. Further, over the frequency range 1 to 5 MHz for both liquids, the results compare favourably with those found by *Ali and Langton* (1989). In attenuation, for the 710 fluid there is excellent agreement within the experimental error and for the 200/350 fluid the results agree within about 10%. For both liquids, the tone burst and pulse measurements of c show good agreement within 1%.

All the comparisons so far have been for molecular samples. As it was intended to use the technique for colloidal dispersions, the frequency dependent attenuation of a 20% by volume kaolinite solution was measured and the results are given in Table 3.4.

TABLE 3.4

Sample: 20% by volume aqueous kaolinite solution

$T = (22 \pm 0.2)^\circ\text{C}$

f/MHz	$(K \pm 3\%)/\text{dB cm}^{-1}$
1	1.4
3.5	6.9
4	8.1
5	11.6
7	18.2
8.25	21.6
10	28.2

A least squares fit of the data to the form $\alpha = Kf^n$ gives $n=1.3 \pm 0.02$. Again there is excellent agreement with data in the literature as Hampton (1967) found an $f^{-1.3}$ relationship for dispersed kaolinite in a volume concentration range 12 to 30% and frequency range 0.1 to 1 MHz. He also reported an $f^{-0.7}$ frequency dependence for attenuation in undispersed kaolinite solutions. Hence the slightly lower value of $n=1.3 \pm 0.02$ found in this work could be explained by incomplete dispersion of the kaolin, although an optimum deflocculation preparation was used, described in Chapter 4.

From the evidence of the data in Tables 3.2, 3.3 and 3.4, it may be concluded that the tone burst method is suitable for measurements in the frequency range 1 to 10 MHz.

3.6 The Flow Cell.

Having adopted the tone burst technique for routine measurements, with PEO employed for velocity change detection, a suitable flow cell and pumping system was developed as shown in Figure 3.13. The flow bore between the transducers was a thin slot (1 cm wide, 7.5 cm long with ~ 3 mm transducer separation) chosen to increase the shear rate, compared with that in the supply pipe, for a given flow rate. A long slot was selected in preference to a restriction purely between the transducer faces, to reduce turbulence effects caused by sudden pipe diameter changes. For non-turbulent slot flow it is then possible to derive an expression for average shear rate in a slot of height a and width b assuming (i) a velocity profile $V(x)$ (where dimension x is in the x -direction), (ii) a pressure drop

ΔP along the length of the slot, (iii) a fluid viscosity η and (iv) that $b \gg a$ (hence only consider $dV(x)/dx$).

Equating the pressure and viscous drag forces gives-

$$\Delta P 2bx = 2bL \eta \frac{dV(x)}{dx}$$

Writing shear rate $dV(x)/dx = \dot{\gamma}$ and assuming that each element of volume contributes equally then,

$$\bar{\dot{\gamma}} = \frac{\int_0^a \dot{\gamma} dx}{\int_0^a dx} = \frac{1}{a} \int_0^a (3Q/2ba^3)x dx$$

$$\Rightarrow \bar{\dot{\gamma}} = 3Q/4ba^2, \quad \text{(eqn.3.30)}$$

where Q is the volume flow rate.

Equation 3.30 was therefore used to calculate the shear rates quoted in the results section Chapter 5.

The other essential features of the cell are (i) that flow, at a constant rate, can be introduced perpendicular to the ultrasound propagation direction, (ii) a thermocouple is placed at the entrance to ensure that sample temperature is not significantly increased by viscous dissipation, (iii) the transducers are placed coaxially, being suitable for tone burst transmission and PEO, where the second transducer is employed as a reflector. The flow was induced by a variable speed peristaltic pump, operating with 8mm internal bore silicone rubber tube. The variable speed allowed adjustment to avoid significant warming effects, detection of critical flow rates for inducing α and c changes, and maintenance of solid particles in suspension. Flow rates for a given pump speed were found by measuring the time taken for 100ml to be pumped out of the cell.

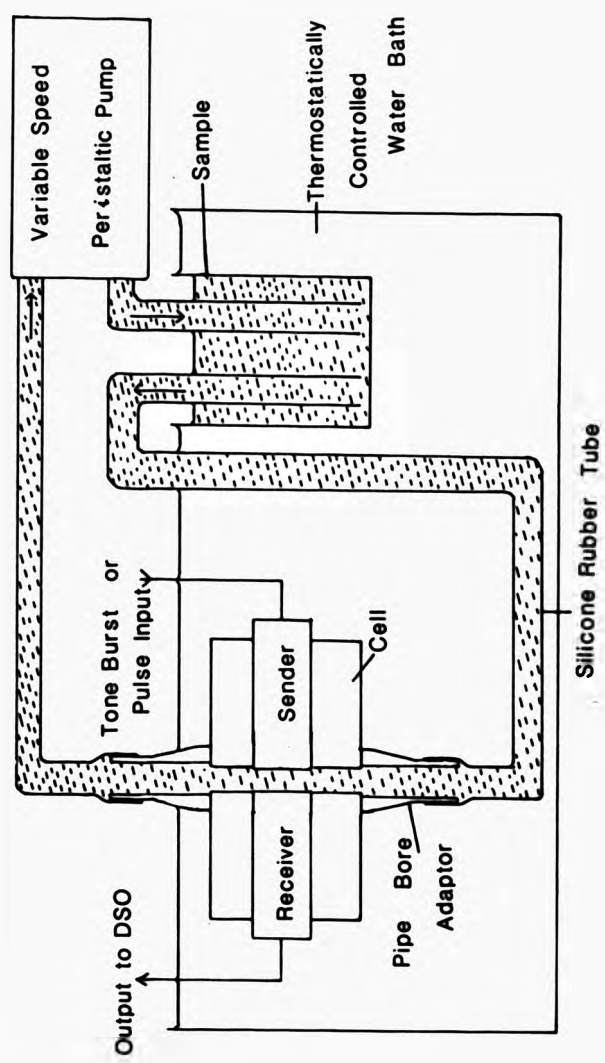


FIGURE 3.13 The Flow Cell

4. MATERIALS AND THEIR CHARACTERISATION.

4.1 Materials.

The Model Colloidal System.

In order to assess the applicability of the modified Urick theory (see section 2.2), a model colloidal system was desirable. The essential features required were (i) a large density mismatch between solid and suspending phase, giving suspended phase concentration sensitivity in velocity and viscous attenuation, (ii) sphericity of suspended phase with well-characterised size distribution, having mean radius $a < \lambda$ as assumed in the Urick theory, (iii) stability of the dispersion for the duration of a measurement and (iv) ready availability and inexpensive as relatively large volumes were required, e.g. 200ml for the flow cell. A system of lead-glass spheres in glycerol, or polypropylene glycol 2025, at around 20°C was found to match the above criteria. The relevant physical properties are given in Table 4.1. The density data was obtained by weighing a known volume using the density bottle method. In section A the data marked + was taken from the manufacturer's data sheet. For section B the viscosities marked + were measured at the collaborating establishment (Alderman 1989) and those marked * were obtained using a Haake concentric cup and rotor viscometer system. The symbol \$ denotes data taken from Kaye and Laby (1973).

TABLE 4.1

A. Jencons No.18 Ballotini lead glass spheres.

<u>Particle Diameter/μm</u>	<u>Density/kg m^{-3}</u>
80% in the range	
40-75 +	2900+/-20 *

B. Suspending Phases.

<u>Description</u>	<u>T/$^{\circ}\text{C}$</u>	<u>Viscosity/mPa s</u>	<u>Density/kg m^{-3}</u>
Polypropylene	17+/-0.3	481 +	
Glycol (PPG)	20+/-0.3	415 +	1000+/-10 #
Mol. Wt.2025	23+/-0.3	342 +	
Analytical	20+/-0.1	1330+/-30 *	1260+/-10 #
reagent grade	22+/-0.1	1210+/-10 *	
glycerol			
Standard grade	20	1495 #	1252+/-10 #
glycerol			

From the data in table 4.1, it can be seen that a high density mismatch was achieved with a solid to liquid density ratio of 2.9 for PPG and 2.3 for glycerol. Further, the liquid viscosities are high, of the order 500 to 1000 mPa s, as suitable for producing a system stable to sedimentation with the size distribution of glass available, e.g. assuming isolated spheres (~1% volume concentration) using Stokes' equation for the drag force on a sphere falling in a viscous

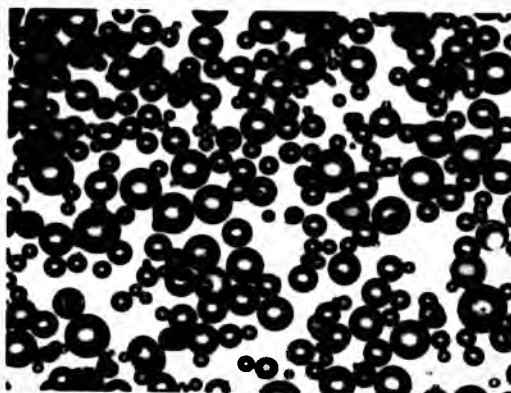
liquid, equilibrium velocity, $v = [2a^2g(\rho' - \rho)/9\eta]$, gives for particles of $a \approx 30\mu\text{m}$, $v \approx 2\mu\text{m/s}$ for glycerol at 20°C and $v \approx 8\mu\text{m/s}$ for PPG at 20°C . Hence in a 2cm depth cell, approximately 10% settling would occur in the time taken to travel 2mm i.e. 17mins for glycerol and 5mins for PPG. Although higher stability is desirable, this appears acceptable as once apparatus and sample are prepared, tone burst data collection takes under a minute to perform. Further, in experiments where settling was found to be a problem (section 5.1) the flow cell, described in section 3.6, was employed to maintain even dispersion of the solid phase.

The choice of Jencons no.18 Ballotini for the disperse phase was made as the sphericity appeared good, see Figure 4.1, and they were readily available by the kilogram, in a radius range an order of magnitude down on the ultrasonic wavelength i.e. say $f=5\text{MHz}$, $c \approx 1500\text{m/s}$ then $\lambda \approx 300\mu\text{m}$; from Table 4.1 $a \approx 20-40\mu\text{m}$. Further, they were non-aggregating if stored in dry conditions, and hence lent themselves to sieving, sizing and freely dispersing in colloidal preparation.

Finally, in addition to providing a model colloid, the glass and liquids were suitable to model more complex systems, like non-spherical barite (barium sulphate) particles in a bentonite gel (drilling mud). This was possible by using glass in bentonite gel, as a probe of suspending phase rigidity effects, and then studying barite in the liquids to determine the importance of non-sphericity.



FIGURE 4.1 Ballotini Sample: Magnification X80



NON SPHERICAL PARTICLES

Within the scope of this thesis, investigation of commercially available colloidal systems containing non-spherical particles was carried out using ultrasound as a probe. These were a deflocculated aqueous suspension of kaolinite, a platelet-like clay used in high quality paper coating, and barite suspended in an aqueous bentonite gel, used as an oil field drilling fluid. These materials are described in more detail below.

The Clays

Both kaolinite and bentonite are naturally occurring mineral clays, made up from two-dimensional arrays of silicon-oxygen tetrahedra (the silica sheet) and two-dimensional arrays of aluminium-oxygen-hydroxyl

octahedra (the alumina sheet), in a layered structure. Crystallites are formed by the sharing of oxygen atoms between these sheets and may occur between one silica and one alumina sheet, giving a two-layer clay e.g. kaolinite, or between one alumina and two silica sheets (one either side), producing a three-layer clay e.g. bentonite. The distance between corresponding planes in one crystallite to the next is called the basal spacing, being 7.2Å and 9.6Å for crystalline kaolinite and bentonite respectively. The cohesive force between layers is primarily electrostatic, augmented by van der Waals attraction, so cleavage parallel to the layers is relatively easy, creating flakes. Kaolin forms platelet-like particles with lateral dimension $\sim 1\mu\text{m}$ and having thickness $\sim 0.1\mu\text{m}$ with bentonite platelets being thinner, having length $\sim 1\mu\text{m}$ and thickness $\sim 10\text{\AA}$ to 10nm , depending on the degree of face to face (F-F) and edge to edge (E-E) aggregation. Thus the latter has an aspect ratio about a thousand times that of the former, both considered as unaggregated platelets.

In both kaolinite and to a greater extent bentonite, some replacement of the trivalent Al by divalent atoms, often Mg, occurs in the octahedral layer, a process called isomorphous substitution. This results in an excess negative charge which is compensated by the adsorption of a face layer of cations. Also, at the crystallite edges, the silica and alumina sheets are disrupted and primary bonds are broken. When the clays are dispersed in deionised water, the compensating face cations have a tendency to diffuse away from the surface, since their concentration is negligible in

the bulk solution. However, they are also attracted electrostatically to the charged faces and therefore form a diffuse electrical double layer on the exterior layer surfaces of the clay particles. The edge double layer is pH-determined with the edge being net positive in acid and neutral solutions (Al acting as the potential-determining ions), and net negative in alkaline solutions (hydroxyl acting as the potential-determining ions). In the presence of water, the compensating cations on the layer surfaces may be easily exchanged for other cations available in solution or the positive edge of another crystallite. The latter process of electrostatic edge to face attraction, along with E-E attraction, is called flocculation and the former is likely to predominate because of the surface charge considerations. As the clay concentration is increased, floc size grows until a linked, card-house like structure is formed producing a gel. Although this relatively simple description is adequate for the purposes of this work, more detail is given by van Olphen (1963) and Mitchell (1976), it should be noted that experimental evidence reported by Avery and Ramsay (1985), for measurements on a synthetic swelling clay called laponite, suggests that gelation is also due to electrostatic repulsion of like-charged faces.

There are two fundamental differences between kaolinite and bentonite which make the latter form a gel at much lower volume concentrations. Firstly, as detailed earlier, bentonite has a much larger aspect ratio. Making the assumption that the clays are regular flat plates with kaolin dimensions $1\mu\text{m} \times 1\mu\text{m} \times 0.1\mu\text{m}$ and bentonite $1\mu\text{m} \times 1\mu\text{m} \times 1\text{nm}$, the the volume of clay required to occupy $1\mu\text{m}^3$ of

dispersion in edge to face association is roughly,

$$\begin{aligned} \text{kaolin } 3*(1*1*0.1) &= 0.3\mu\text{m}^3 \\ \text{bentonite } 3*(1*1*0.001) &= 0.003\mu\text{m}^3. \end{aligned}$$

So, the required volume of bentonite is ~ 100 times less than that of kaolin and may be even less as flakes down to 10\AA thick can occur. Further, bentonite unlike kaolinite is a member of the montmorillonite or swelling three layer clay group. When montmorillonites are contacted with water, water molecules penetrate between the crystallite layers, a process called intra-crystalline swelling. This causes an initial increase in the basal spacing from 9.6\AA to $12.5\text{-}20\text{\AA}$ and thus increases the effective volume of the clay. If the clay is dispersed in water, the weak inter-layer bonding is broken down and individual swollen particles are produced that can begin to flocculate as described above. Both these factors then indicate that, ceteris paribus, a lower volume of bentonite than kaolinite is required to form a linked network. In fact a measurable shear modulus in concentrations as low as ~ 1% wt/wt Na montmorillonite with water, have been reported by Goodwin et al.(1980).

For the purposes of this work, the difference between the the clays was exploited to provide gelling and non-gelling samples at similar volume concentrations, in order to explore the possibility of structure detection using the ultrasonic parameters α and c . Sample preparation was undertaken as described overleaf.

Preparation Of Clay Dispersions.

The required weight of clay, measured to a precision of around 0.5% using a microbalance, was gradually added to a known volume of water. This was continuously agitated by a rotary stirrer to ensure even dispersion. In order to produce a stable, deflocculated kaolinite sample, a commercial surfactant Dispex N90 was added in the proportion 0.3mg per gram dry weight clay. Dispex is an aqueous solution containing a long chain molecule Na polyacrylate where the acrylate ionises to give negatively charged COO groups on a carbon backbone. These can attach themselves to the positive particle edge and reduce inter-particle electrostatic interaction.

The main bentonite type used was an industrial grade material (mostly sodium montmorillonite), often employed for its thixotropic and other rheological properties in drilling muds. A similar material of pharmaceutical grade called Bentopharm (supplied by Bromhead and Denison Ltd.) was also used. In mixing the muds the presence of air bubbles, introduced by vigorous stirring and trapped upon gellation, caused excessive attenuation in some experimental work. To reduce this problem dispersions were routinely de-gassed in a bell jar, pumped down to about -1bar compared with atmospheric pressure, for about an hour. The addition of glass beads or barite was achieved without adding air using a magnetic stirrer to agitate the prepared mud whilst the particles were gradually added. In order to produce high concentration samples i.e. $v > 0.03$, samples having $v \sim 0.02$ were dewatered by contact with filter paper, the final

volume fraction being determined by weighing the wet and dried product.

Oil-Based Bentonite Suspension

Measurements have also been made on an as-received oil-based mud, supplied by the collaborating establishment, for comparison with rheological data and the water-based samples. The components are a clay called Carbogel, in a continuous phase of Milclean oil (mainly hexadecane) both produced by Milchem Ltd.. The material densities are $\rho' = 1700 \text{ kg/m}^3$ and $\rho = 798 \text{ kg/m}^3$ respectively.

Barite

Barite is a highly fractured mineral, which forms granular shaped particles of average equivalent spherical diameter about $30 \mu\text{m}$. The material used in the dispersions was again of industrial grade, employed as a densifier in drilling muds. Its effectiveness is apparent when one compares the density of barite, 4200 kg/m^3 , with that of bentonite (and kaolinite) i.e. 2600 kg/m^3 .

4.2 SIZING AND SIEVING METHODS.

In order to calculate theoretical values of excess attenuation and velocity (when effective medium theory is not appropriate) for the colloids, it is necessary to know the suspended particle radius or mean radius and standard deviation. Therefore some assessment of size and degree of polydispersity must be made. Further it is desirable to reduce polydispersity, in order that the dependence of α on particle radius can be examined. For example, although the ballotini glass spheres are nominally $20\text{--}38 \mu\text{m}$ radius, brief

inspection under a microscope shows that radii as low as $\sim 15\mu\text{m}$ and as high as $\sim 50\mu\text{m}$ occur. Using equation 2.2, for a glass in glycerol dispersion at 20°C with $f=5\text{MHz}$, moving from radius $15\mu\text{m}$ to $50\mu\text{m}$ changes the dominant attenuation mechanism from viscous loss to scattering, i.e. using data from Table 4.1,

at $15\mu\text{m}$ $\alpha_{\text{scat.}} / \alpha_{\text{visc.}} \sim 0.03$

at $50\mu\text{m}$ $\alpha_{\text{scat.}} / \alpha_{\text{visc.}} \sim 3.9$.

It is apparent then that size characterisation and sub-division of existing distributions are essential, in order that the applicability of equations 2.2 and 2.10 can be assessed. The methods used are now described.

Sieving

A nest of Endecotts bronze mesh sieves was employed, with nominal apertures 38,45,53,63,75,90 and $125\mu\text{m}$. After drying in an oven at 35°C for 30 minutes, to reduce sticking that dampness may cause, the particles were poured into the most coarse grade sieve and allowed to fall through the nest, settling at the appropriate mesh. To aid the grading process, the sieves were shaken and tapped by hand. Before extraction from the sieve, the particles were gently brushed across the mesh to ensure that smaller particles fell through to the next grade. In practice, to avoid clogging up the sieves it was found best to work with 2-3g batches, and to clear the meshes by brushing the underside each time. This method was used to produce size fractions of the glass spheres from the polydisperse supply and a barite sample of nominal diameter 45-53 μm . Once fractionated the particles were characterised in terms of their size distribution.

Sizing

Size distribution data for the particles was obtained using a Leeds and Northrop Microtrac particle analyser. This machine employed a laser light scattering method, requiring a mass of only one tenth the specific gravity in grams of the material, dispersed in distilled water. Mean diameter, standard deviation and size distribution data were automatic outputs from this method. The distribution data was not continuous with diameter but split into fixed diameter ranges; the relative volume of spheres within each range was given.

To test the reliability of this method, a comparison was undertaken with a SEESCAN Image Analysis system, where a monochrome photomicrograph (e.g. Figure 4.1) was digitised in terms of image intensity. This work was done at the collaborating establishment by Roussel (1988). As-received No.18 Jencons ballotini was used and the results for both the light scattering and image analysis methods are plotted out in Figure 4.2. The relative volume values have been plotted against the mid-value of the diameter range to which they correspond. The data have been fitted to an equation of the form

$$y = \text{constant} \cdot \exp\left(-\left(\ln d - \ln \bar{d}\right)/2\sigma\right)^2 \quad (\text{eqn.4.1})$$

where d is diameter, $\ln \bar{d}$ is the natural logarithmic mean of the distribution and σ is the standard deviation.

From Figure 4.2 it can be seen that both sets of data display the log-normal type of distribution (eqn 4.1), with the light scattering results having a broader form. Using

the values of $1/\bar{r}^2$ to find a mean radius \bar{r} , the fitting results give;

Image analysis $\bar{r} = (30.5 \pm 0.5) \mu\text{m}$ $\sigma = 0.35 \pm 0.02$

Light scattering $\bar{r} = (31.5 \pm 0.5) \mu\text{m}$ $\sigma = 0.41 \pm 0.01$

The agreement for mean particle radius is very good, within the fitting error, and the standard deviations are close being equivalent to a distribution half-width at half peak height of $15 \mu\text{m}$ for image analysis and $19 \mu\text{m}$ for the light scattering.

In view of this favourable comparison the Microtrac was used to characterize fractionated glass spheres and two barite samples; the results are given in Table 4.2.

Although as previously discussed the barite particles are granular in shape, the Microtrac provides an equivalent spherical radius which may account for the discrepancy between nominal sieve size and mean radius. This will be discussed further in chapter 6.

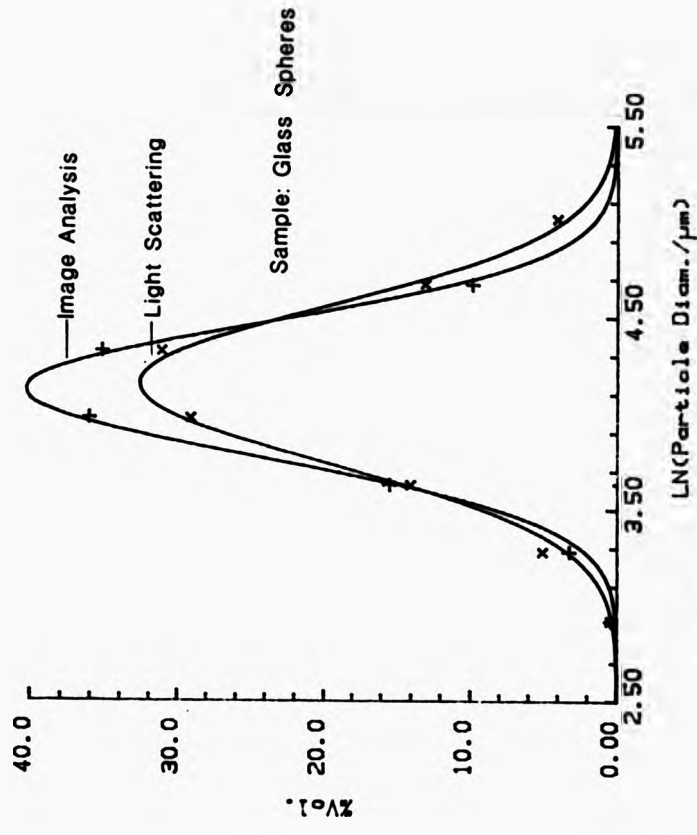


FIGURE 4.2 Relative Volume vs. Ln(Diameter/ μm)

TABLE 4.2

<u>Material</u>	<u>Sieved Radius/μm</u>	<u>Mean Radius/μm</u>	<u>σ</u>
Glass Spheres	<19	15.8	0.31
	19-22.5	19.9	0.25
	22.5-26.5	25.0	0.24
	26.5-31.5	28.1	0.24
	31.5-37.5	31.3	0.27
	37.5-45.0	40.4	0.29
	45.0-62.5	44.3	0.33
Barite	22.5-26.5	15.2	0.5
	As received	20 +	0.32+

+log normal fitting results for data supplied as typical for barite.

5. EXPERIMENTAL RESULTS: Glass Spheres.

5.1 Attenuation.

In order to establish an upper disperse phase volume fraction (v) above which the spheres ceased to act individually, attenuation measurements at 5MHz were made for Jencons No.18 Ballotini suspended in glycerol. The results are displayed in Fig.5.1. The linear relation between α and v indicates that for glass volume concentrations up to 3%, the spheres are non-interacting and there is negligible multiple scattering. Thus all further attenuation measurements for glass suspended in glycerol or polypropyleneglycol (PPG) were restricted to samples in this concentration range.

Figure 5.2 shows the excess attenuation measured for the addition of 1% by volume glass spheres to standard grade glycerol, as a function of mean sphere radius (as given in Table 4.2). For the maximum and minimum sizes used, $Ba_{min} = 1.9$, $Ba_{max} = 5.3$, $(\lambda/a)_{max} = 24$ and $(\lambda/a)_{min} = 9$, indicating that the Urick expression for attenuation, valid for $Ba \gg 1$, $\lambda/a \gg 1$, should be applicable. Curves 1, 2 and 3 refer to eqns. 2.2, 2.3 and 2.10 respectively which have been plotted out using the material property values given in Tables 4.1 and 4.2. Thus the inclusion of a polydispersity factor in eqn.2.10 improves the agreement between theory and data over that achieved by the Urick expression or that from Allegra and Hawley in the long wavelength limit. In order to get a best fit to the data, the measured physical properties have been fixed and the standard deviation σ allowed to vary. The

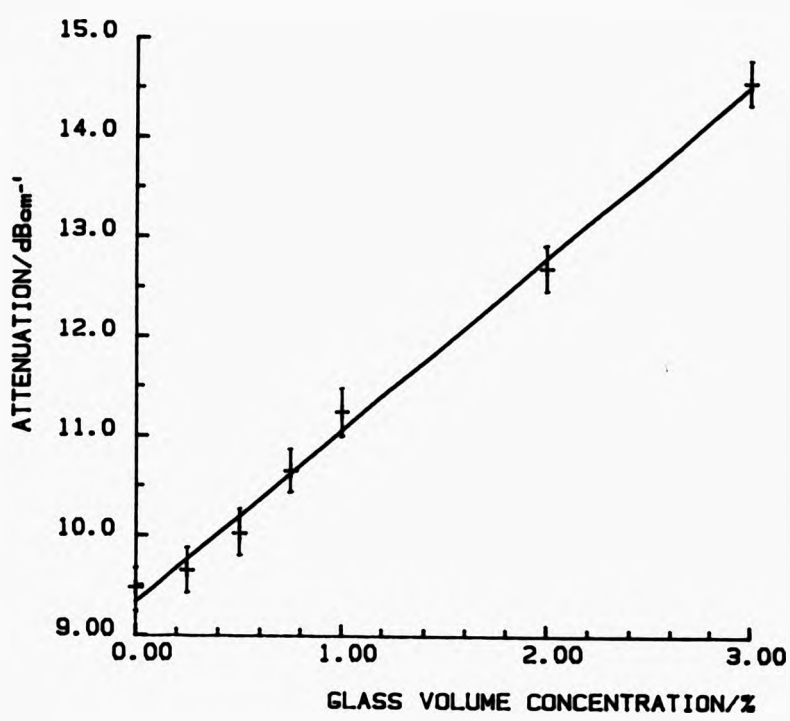


FIGURE 5.1 Attenuation vs. Glass Volume Concentration

Jencons No.18 Ballotini inGlycerol $f=5\text{MHz}$ $T=20^\circ\text{C}$

KEY +, data —, best fit

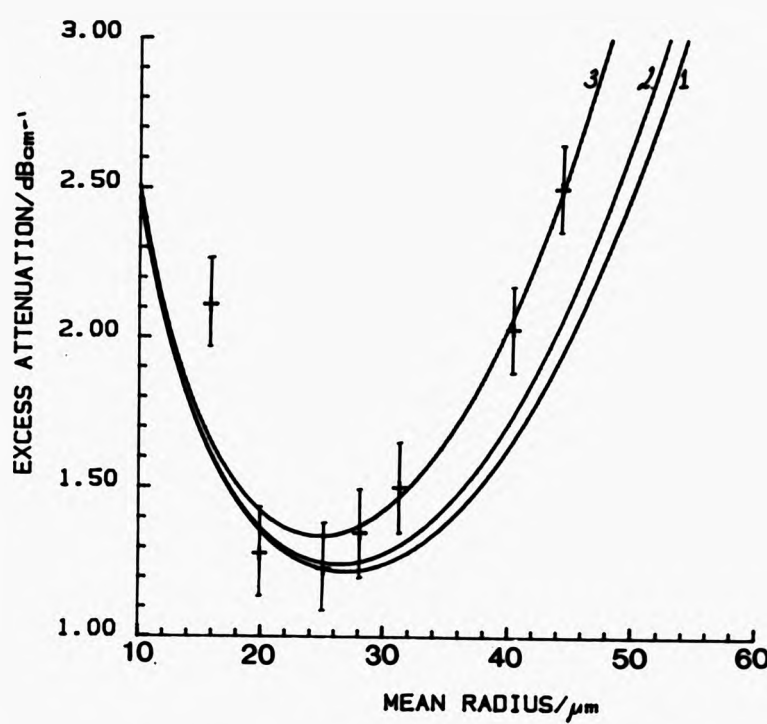


FIGURE 5.2 Excess Attenuation vs. Mean Radius

Sieved ballotini in 95% glycerol aqueous soln.

$\nu = 0.0124$ $f = 5\text{MHz}$ $T = 20^\circ\text{C}$

Ba range 1.9 to 5.3 λ/a range 9 to 24

KEY: 1,2,3 from eqns. 2.2.2.3, 2.10

+ , data

result $\sigma = (0.21 \pm 0.04)$ shows good agreement with values obtained from the Microtrac particle sizer (see Table 4.2). In Figure 5.3 excess attenuation at 5MHz is plotted as a function of mean radius for glass spheres (1% by volume) in PPG where $Ba_{max} = 8.8$, $Ba_{min} = 3.2$, $(\lambda/a)_{max} = 17$ and $(\lambda/a)_{min} = 6.2$. The plotted curve is from eqn.2.10 using the value $\sigma = 0.21$ as found earlier. Agreement with the data breaks down around $a = 30\mu m$ where $\lambda/a \sim 9$. This is not surprising considering that the theory treats the spheres as simple Rayleigh scatterers where $a \ll \lambda$ and Allegra and Hawley (1972) comment that this is limited in practice to $a < \lambda/10$. In Figure 5.4 the frequency has been reduced to 2.25MHz making $Ba_{max} = 6$, $Ba_{min} = 2.1$, $(\lambda/a)_{max} = 39$ and $(\lambda/a)_{min} = 14$; it can be seen that eqn.2.10 gives excellent agreement with the data when the Rayleigh limit is not exceeded.

Microscopic Rheology Measurements.

Having established the applicability of eqn.2.10 it is possible, that by measuring attenuation as a function of disperse phase volume fraction, that the continuous phase viscosity can be derived when the densities and disperse phase size distribution are known. An example is shown in Figure 5.5 for as-received Ballotini in PPG at 2.25MHz. For these particles Microtrac measurements give $a = 31.5\mu m$, $\sigma = 0.4$. The gradient gives $d\sigma/dv = (1220 \pm 23)m^{-1}$ giving a derived viscosity of $(450 \pm 20)mPa s$, which compares well with that directly measured by viscometry i.e. $415mPa s$ at $20^\circ C$. A number of other materials have been measured in the same manner and the results are given in Table 5.1. All the data was obtained at 2.25MHz except that marked * which was

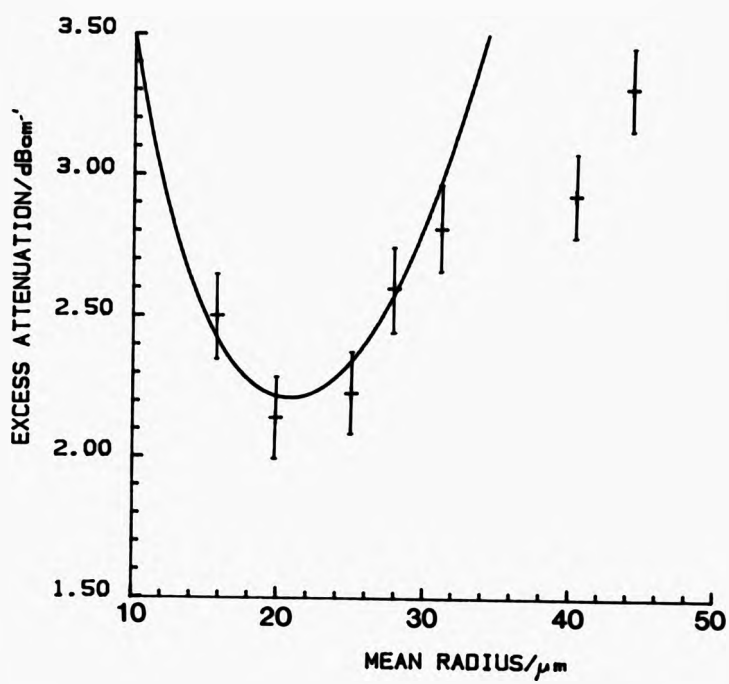


FIGURE 5.3 Excess Attenuation vs. Mean Radius

ballotini in PPG2025 $\nu = 0.01$

$T = 20^\circ\text{C}$ $f = 5\text{MHz}$

Ba range 3.2 to 8.8 λa range 6.2 to 17

KEY +, data — eqn. 2.10

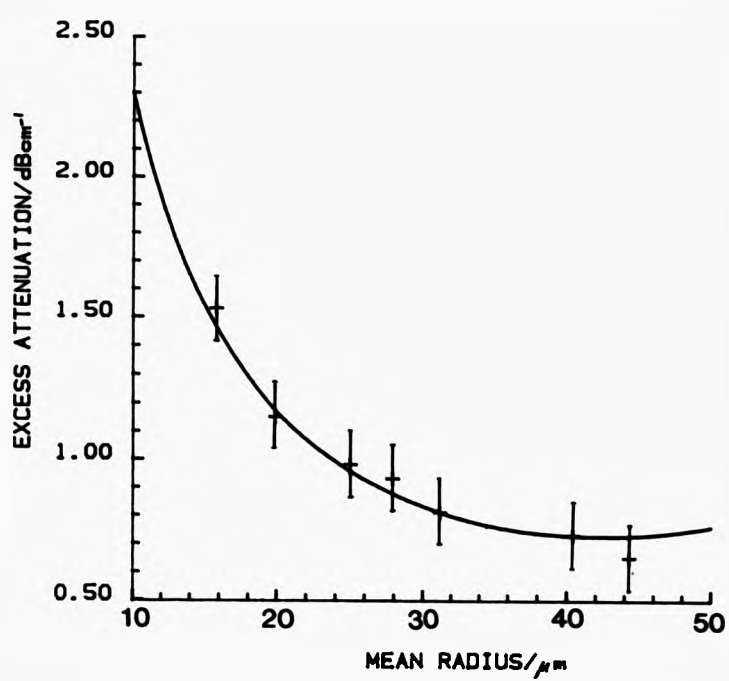


FIGURE 5.4 Excess Attenuation vs. Mean Radius

ballotini in PPG 2025 $\nu = 0.01$

$T = 20^\circ\text{C}$ $f = 2.25\text{MHz}$

B_a range 2.1 to 6 λ_a range 14 to 39

KEY +, data —, eqn.2.10

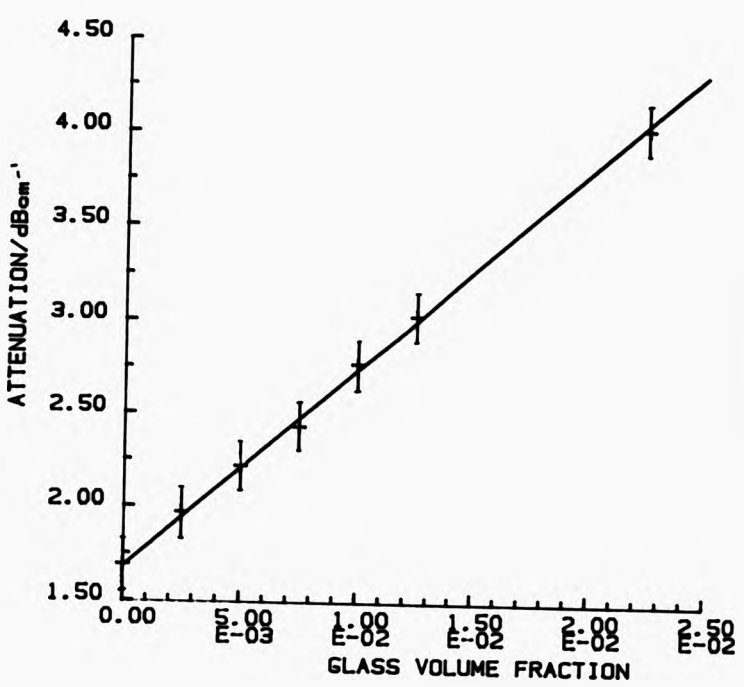


FIGURE 5.5 Attenuation vs. Glass Volume Fraction

ballotini ($\bar{a} = 31.5\mu\text{m}$) in PPG 2025

$T = 20^\circ\text{C}$ $f = 2.25\text{MHz}$

$Ba = 4.2$ $\lambda\bar{a} = 21$

KEY +, data

—, best fit to data

Material	v	a/ μ m	σ	T/ $^{\circ}$ C	(d^2/dv)/ m^{-1}	η /mPa s	η /mPa s
Glass in PPG2025	0-0.03	31.5	0.4	20	1220+/-23	360+/-20	
	0-0.03	+ 30.5	0.35	20	1220+/-23	450+/-20	415
Glass in Glycerol	0-0.03	20.05	0.21	22	1508+/-70	1230+/-130	1210+/-10
	0-0.03	31.5	0.4	22	875+/-80	1200+/-200	"
	0-0.03	+ 30.5	0.35	22	875+/-80	1300+/-200	"
Bentopharm in Water	0.01	19.9	0.21	23	66+/-11	0.6+/-0.6	3.3
	0.015	-	-	25	-	-	7.7
	0.02	19.9	0.21	23	164+/-30	2.4+/-0.6	-
	0.023	-	-	25	-	-	13.8
	0.0275	19.9	0.21	23	143+/-16	4.2+/-0.8	-
	0.031	-	-	25	-	-	26.7
	0.035	19.9	0.21	23	148+/-16	4.6+/-1	-
	0.0375	-	-	23	157+/-18	5.5+/-1	-
	0.04	-	-	"	200+/-17	9.5+/-1.2	-
	0.05	-	-	"	341+/-18	35+/-5	-
	0.06	-	-	"	1594+/-60	796+/-50	-
0.1	-	-	"	1298+/-60	667+/-60	-	
Carbogel in Oil	0.025	25	0.24	23	229+/-19	5.5+/-1	8.2
	0.03	-	-	"	268+/-22	8.1+/-1	8.6
	0.033	-	-	"	294+/-15	10+/-1.3	11.0
	0.037	-	-	"	294+/-15	10.5+/-1.3	12.6

TABLE 5.1

measured at 5MHz. For the mean glass sphere radii data, the symbol + refers to image analysis results, otherwise Microtrac measurements are used. The column marked § refers to viscometry values which, for the bentonite samples, were measured at SCR using a Carrimed viscometer. The viscosity value was obtained by measuring shear stress as a function of shear rate, with a good fit to the data being given by the semi-empirical Casson (1959) model i.e.

$$\tau^{1/2} = \tau_y^{1/2} + \eta_p^{1/2} \dot{\gamma}^{1/2} \quad (\text{Eqn.5.1})$$

where τ is the shear stress, τ_y is the yield stress, $\dot{\gamma}$ is the shear rate and η_p is the plastic viscosity. It is η_p that is given in Table 5.1.

From the table it can be seen that good agreement is obtained between viscosities derived from ultrasound experiments and the directly measured values for the Newtonian liquids, fair agreement for the Carbogel fluids and poor agreement for Bentopharm. In the case of the thixotropic drilling muds it is not obvious how the structured nature of the fluid will affect the ultrasonically measured viscosity. In practice the only data available for comparison is that for plastic viscosity i.e. the viscosity of the material measured above yield stress. However the ultrasonic technique is non-destructive and the material remains in the gel state during measurement. This is apparent if one considers that for PZT the piezo-electric constant relating applied field to mechanical strain ($\Delta l/l$) is about 80 to 320 $\cdot 10^{-12}$ m/V (Blitz 1967) so for the maximum amplitude used in the tone burst technique, $V \sim 15V$, $\Delta l \sim 5nm$. This means that the amplitude of the ultrasonic wave is very small compared to the unit length making up the structure

(i.e. the $\sim 1\mu\text{m}$ clay particles) and so is likely to be non-destructive; therefore the gel will retain any elasticity it may have. Nevertheless, the ultrasonic viscosities are not far removed from the plastic viscosity values. In the case of the oil-based mud where both sets of measurements were made on the same samples, the agreement is excellent. For the water-based mud, samples were prepared independently and although the direct agreement is not so good, Figure 5.6 shows that both methods detect a rapid rise in viscosity as clay volume fraction is increased. The rheological data gives a best fit when η is allowed to vary as a function of v^2 , whereas for the ultrasonic values a cubic form is better. Although different sample preparations may explain the discrepancy, there is also the possibility of elastic effects. A measure of the elasticity is given by τ_y from the Casson fit and this data is given in Table 5.2.

TABLE 5.2

Clay Suspension	v	τ_y /Pa
Bentopharm	0.008	0.000
	0.015	0.007
	0.023	0.25
	0.031	1.60
Carbogel	0.025	0.1
	0.030	0.8
	0.033	1.4
	0.037	1.0

From Table 5.2, it would appear that the water-based mud has a higher yield stress for a given clay volume

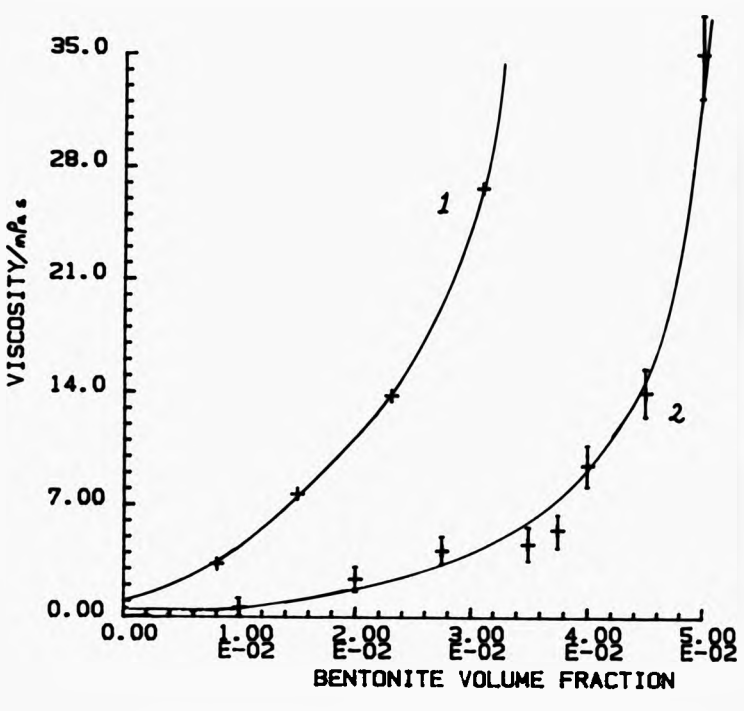


FIGURE 5.6 Viscosity vs. Bentonite Volume Fraction
 Bentopharm in water
 KEY: 1.rheological data 2.ultrasonic data

fraction when one compares $\zeta=0.25\text{Pa}$ at $v=0.023$ and $\zeta=1.8\text{Pa}$ at $v=0.031$ for Bentopharm, with $\zeta=0.1\text{Pa}$ at $v=0.025$ and $\zeta=0.8$ at $v=0.03$ for Carbogel. So, it is conceivable that elasticity accounts for the departure of ultrasonic measurements from the rheometric data, causing a decrease in the effective viscosity. Qualitatively this would appear to be reasonable, as one might expect the existence of some elasticity to reduce the relative motion of the spheres and the mud, thus reducing the energy loss from the incoming beam and giving a smaller attenuation than if the same viscosity alone were present. One returns to this effect in detail in section 5.3 where the theory of attenuation in viscoelastic fluids developed in Chapter 2 is applied.

5.3 Velocity.

In order to establish the applicability of the various expressions for velocity in Chapter 2, the glass phase volume fraction dependence of velocity has been measured for a number of samples, as shown in Figures 5.7 to 5.12.

Glycerol.

For the glycerol samples the smallest sieved fraction $a=15.8\mu\text{m}$ was used together with temperature control at 20°C , in order to produce stable samples i.e. reduce the settling rate. The results in Figure 5.7 were obtained at 1MHz where $Ba\sim 0.8$ and $\lambda/a\sim 115$ indicating that the Urick expression eqn.2.6 may be valid as $\lambda \gg a$, but the fact that $Ba \rightarrow 1$ suggests that the skin depth correction factor in effective density (Ament eqn.2.9) may be necessary. Curve 1 represents a least squares fit to the data using eqn.2.6 with the measured density values given earlier and allowing K and K' (continuous and disperse phase compressibilities

respectively) to vary. The result $K'=(5.7\pm 0.2)\times 10^{-12}\text{ Pa}^{-1}$ is not good when compared to the value in Kaye and Laby (1973), $K'=1\times 10^{-10}\text{ Pa}^{-1}$, but that for $K=(2.24\pm 0.05)\times 10^{-10}\text{ Pa}^{-1}$ is close to the literature value for glycerol i.e. $K=2.3\times 10^{-10}\text{ Pa}^{-1}$. Curve 2 was plotted using the compressibility values from Kaye and Laby, showing that the Urick expression does not follow the data closely.

In Figure 5.8 the same data is compared with the predictions of the Ament eqn. 2.9. For curve 1 the Kaye and Laby values for compressibilities have been used together with the measured physical properties i.e. $\rho=1252\text{ kg/m}^3$, $\rho'=2900\text{ kg/m}^3$ and $\eta=1.33\text{ Pa s}$. In curve 2 viscosity has been allowed to vary to obtain a best fit to the data giving $\eta=(3.6\pm 0.1)\text{ Pa s}$, much higher than expected. However, a number of authors including Einstein (1906), Batchelor (1974) and Dimitrov^{and Lakov} (1989) have found that the viscosity of a dispersion is modified by the disperse phase and have formed expressions for the effective viscosity. These expressions are;

(a) Einstein: $\eta_{eff} = \eta_0(1+2.5v+14v^2\dots)$

(b) Batchelor: $\eta_{eff} = \eta_0(1+2.5v+7.6v^2)$

(c) Dimitrov: $\eta_{eff} = \eta_0[1+2.5v/(1-v)]$

where η_0 is the continuous phase viscosity.

Using these expressions in the Ament equation a good fit to the data (as in curve 2 Figure 5.8) was obtained when in (a) $\eta_0=(1.9\pm 0.1)\text{ Pa s}$ in (b) $\eta_0=(2.1\pm 0.1)\text{ Pa s}$ and in (c) $\eta_0=(3\pm 0.2)\text{ Pa s}$. Thus the predicted values for viscosity are nearer the measured value (1.33 Pa s) when some account is taken of the presence of the disperse phase. However the values are still larger than expected, with the Einstein and

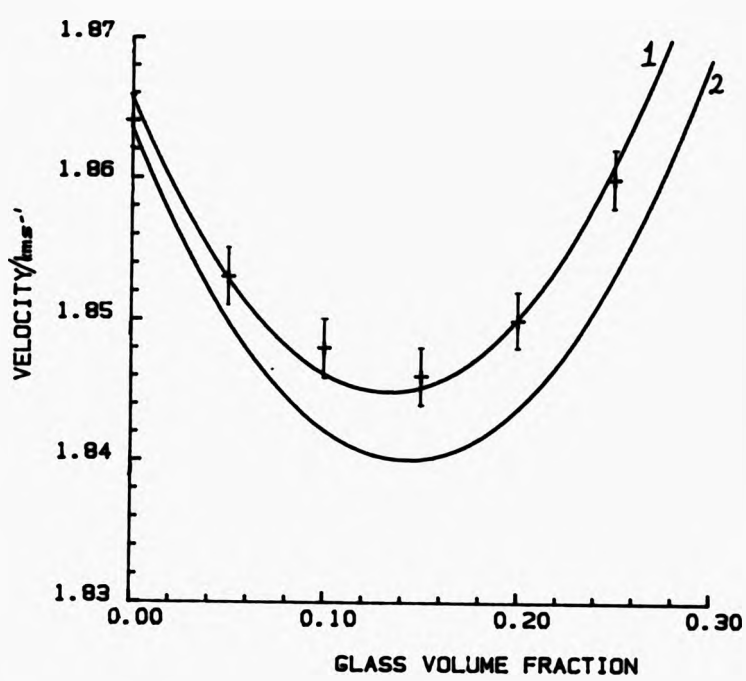


FIGURE 5.7 Velocity vs. Glass Volume Fraction
ballotini ($\bar{a} = 15.8\mu\text{m}$) in glycerol

$T = 20^\circ\text{C}$ $f = 1\text{MHz}$ $Ba = 0.8$ $\lambda_a = 115$

KEY: 1. eqn.2.6, $K' = 5.7 \times 10^{-13} \text{Pa}^{-1}$, $K = 2.25 \times 10^{-10} \text{Pa}^{-1}$

2. eqn.2.6 $K' = 1 \times 10^{-14} \text{Pa}^{-1}$, $K = 2.3 \times 10^{-10} \text{Pa}^{-1}$

+ ,data

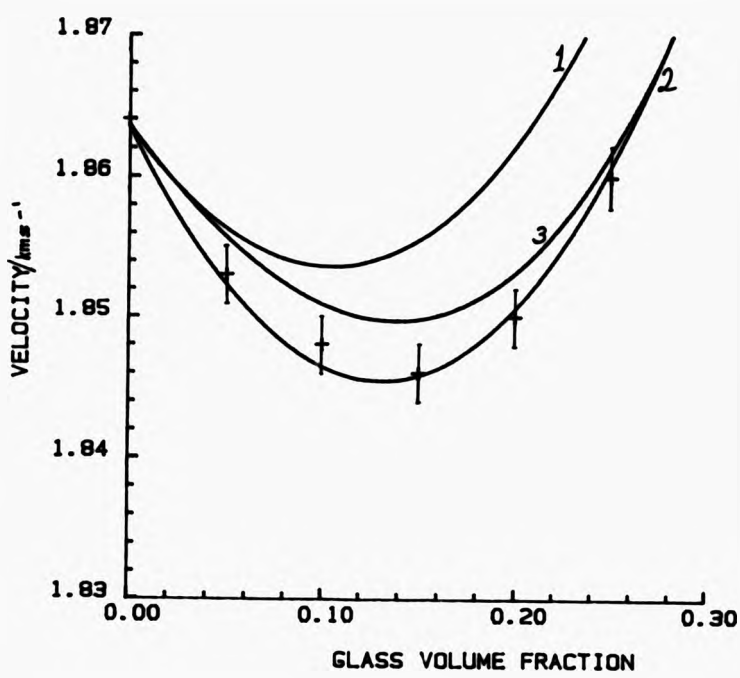


FIGURE 5.8 Velocity vs. Glass Volume Fraction

ballotini ($\bar{a} = 15.8\mu\text{m}$) in glycerol

$T = 20^\circ\text{C}$ $f = 1\text{MHz}$ $Ba = 0.8$ $\lambda_a = 115$

KEY: using eqn. 2.9 1. $\eta = 1.33\text{Pa s}$
 2. $\eta = 3.6\text{Pa s}$
 3. $\eta = \eta_{\text{eff}}$
 +, data

Batchelor formulae, which agree within the error, appearing the most useful. The result for the Dimitrov expression is disappointing, although it should be noted that it was found by applying special conditions to analysis aimed primarily at emulsions. Both the Einstein and Batchelor expressions are strictly infinite series but the closed form of Batchelor's equation is the most suitable for further application. It has been used with η_0 set at 1.33 Pa s (as found for the glycerol from viscometry) to produce curve 3 in Figure 5.8. On balance it is probably most useful to compare curve 2 Figure 5.7 with curve 3 Figure 5.8, as they were both obtained using values of the relevant physical properties that were measured for the actual samples used. Thus it would appear that the Ament equation gives the best agreement with the data, provided that a suitable correction is made to the Ba term by using an effective viscosity, which takes into account the presence of a disperse phase.

To test this further, measurements were also made at other frequencies in order to vary the value of Ba and λ/a . Figure 5.9 shows the velocity data obtained as a function of glass volume fraction at 5MHz where Ba=1.8 and $\lambda/a=24$. Although $a \ll \lambda$ the boundary conditions for the Urick equation are not satisfied because the size of the Ba term indicates that viscous interaction effects are not insignificant; curve 1 shows that the agreement with the data is poor. Curve 2 shows the improved situation when the Ament formula is used and in curve 3, where the Batchelor and Einstein equations have been used with $\eta_0 = 1.33$ Pa s (the two are indistinguishable) the agreement is excellent. The expression for velocity in the inviscid fluid case,

eqn.2.8, produced curve 4 which shows poor agreement with the data. In Figure 5.10 the data was obtained at 2.25MHz so $Ba=1.2$ and $\lambda/a=52$. Again the Ament formula (curve 2) shows closer agreement than the Urick (curve 1) or inviscid fluid (curve 5) expressions. Curves 3 and 4 show the improvement made by inclusion of the Batchelor and Einstein formulae respectively.

From Figures 5.7 to 5.10 it can be seen that when $Ba > 1$ the Ament formula (eqn.2.9) provides the best model for the velocity data and that an improvement can be made by the introduction of a modified viscosity which includes disperse phase effects. It is interesting to note that Ament's equation is limited in applicability to disperse phase concentrations such that the viscous skin depth is small compared with the inter-particle distance. If viscous coupling occurs over distances commensurate with inter-particle separation, then one would expect that any one sphere would experience an ambient viscosity which is affected by the presence of others; this is what the Batchelor and Einstein expressions introduce. For the three frequencies used i.e. 1MHz, 2.2MHz and 5MHz the skin depth $1/B$ is $20\mu\text{m}$, $13\mu\text{m}$ and $9\mu\text{m}$ indicating that the lower the frequency, the smaller the glass volume fraction range over which the Ament equation is applicable. Assuming uniformly spaced spheres, the above mentioned skin depths dictate that volume fraction should be less than 0.12, 0.19 and 0.25 respectively. From the Figures it can be seen that the agreement between the Ament expression and the data breaks down before these volume fractions are reached, as expected.

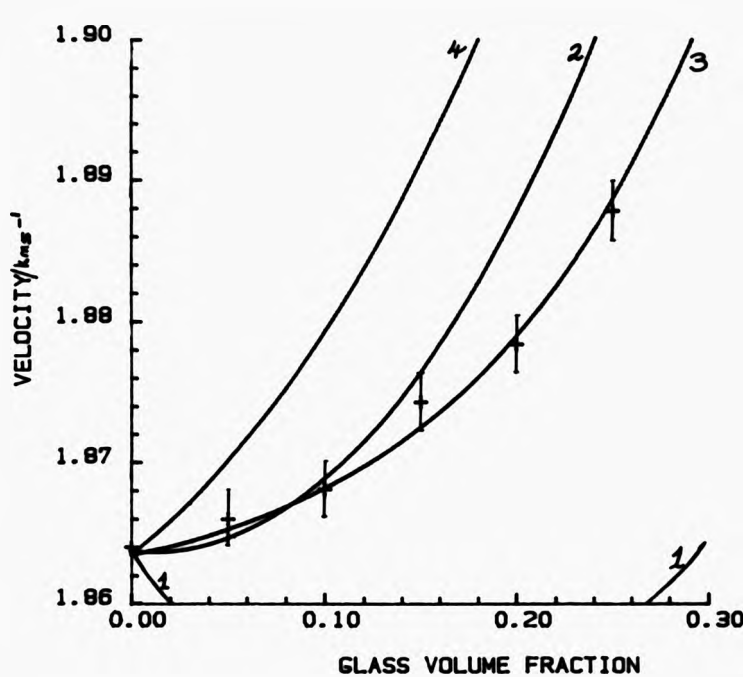


FIGURE 5.9 Velocity vs. Glass Volume Fraction
ballotini in ($\bar{a} = 15.8\mu\text{m}$) in glycerol

$T = 20^\circ\text{C}$ $f = 5\text{MHz}$ $Ba = 1.8$ $N_a = 24$

KEY: 1. eqn.2.6 2. eqn.2.9 3. eqn.2.9, $\eta = \eta_{eff}$
4. eqn.2.8 +, data

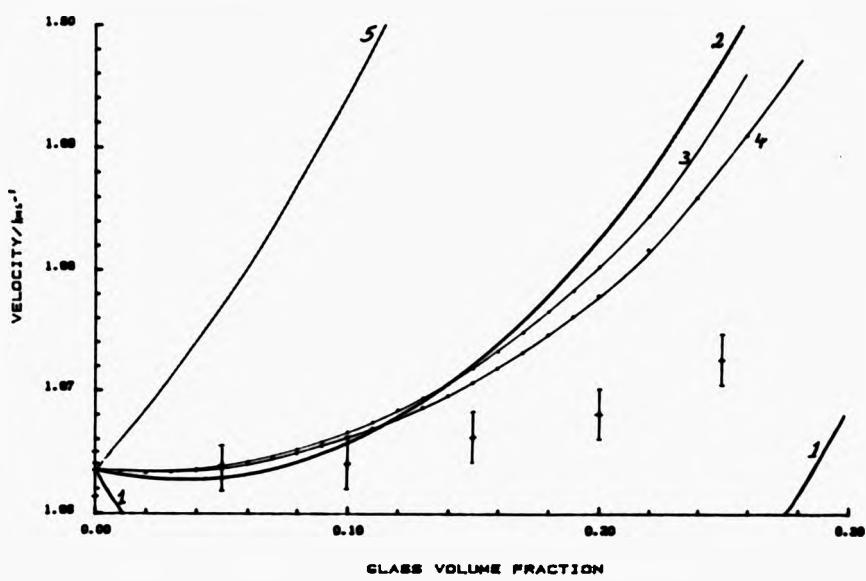


FIGURE 5.10 Velocity vs. Glass Volume Fraction

ballotini ($\delta = 15.8\mu\text{m}$) in glycerol

$T = 20^\circ\text{C}$ $f = 2.25\text{MHz}$ $Ba = 1.2$ $\lambda/a = 52$

KEY: 1. eqn.2.6 2. eqn.2.9 3. eqn.2.9 and Batchelor η

4. eqn.2.9 and Einstein η 5. eqn.2.8 +, data

Drilling Muds.

Measurements were made at 5MHz on the water-based mud Bentopharm (at clay volume fraction 0.025) and the oil-based mud Carbogel (at clay volume fraction 0.037), with the results being shown in Figures 5.11 and 5.12 respectively. Having successfully applied the modified Ament theory to samples where the glass was suspended in a Newtonian liquid, it was hoped that the theory could be fitted to the data for thixotropic muds to provide an effective viscosity value. In Figure 5.11, curves 1 and 2 represent the Ament and modified Ament forms respectively. A least squares fitting routine was used to find the best fit when viscosity was allowed to vary and the results were for curve 1 $\eta = (260 \pm 15) \text{ mPa s}$ and for curve 2 $\eta_0 = (188 \pm 5) \text{ mPa s}$. Similarly in Figure 5.12 for curve 1 $\eta = (200 \pm 10) \text{ mPa s}$ and curve 2 $\eta_0 = (125 \pm 5) \text{ mPa s}$. It is evident that for both the oil and water-based muds the inclusion of the Batchelor expression for suspension viscosity improves agreement with the data at the higher volume fractions $v > 0.15$.

It is interesting to note that from the earlier measurements of $d\eta/dv$, the calculated viscosities for these water and oil-based muds were about 4 mPa s and 10 mPa s respectively, being close to the plastic viscosity values (see Table 5.1). In contrast, the measurements on the Newtonian liquids from both the ultrasonic parameters agreed within the error and so the discrepancy may be a result of the elastic properties of the muds. One might expect that the spheres would be subjected to the elastic properties because, as detailed earlier, ultrasonic amplitudes are small compared with particle size so that the yield strain

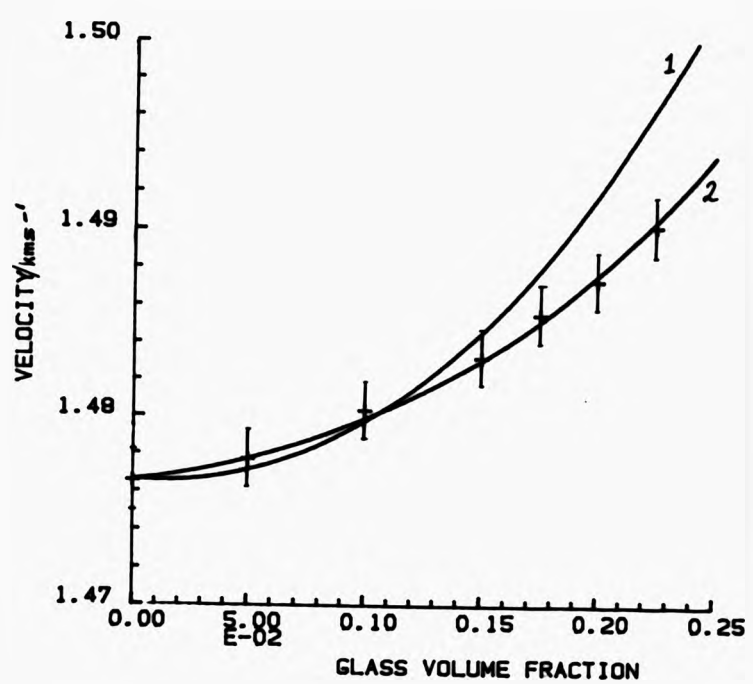


FIGURE 5.11 Velocity vs. Glass Volume Fraction

ballotini ($\bar{a} = 19.9\mu\text{m}$) in Bentopharm mud

$T = 22^\circ\text{C}$ $f = 5\text{MHz}$ $Ba \sim 6$ $\lambda/\bar{a} \sim 30$

KEY: 1. eqn.2.9, $\eta = 260\text{mPa s}$

2. eqn.2.9, $\eta = 0.188(1 + 2.5 v + 7.6v^2)$ Pa s

+, data

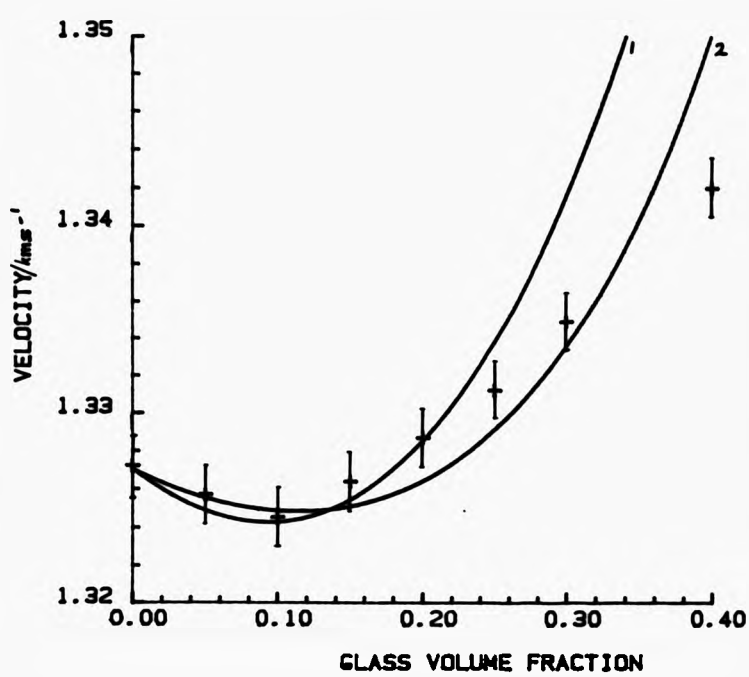


FIGURE 5.12 Velocity vs. Glass Volume Fraction

ballotini ($\bar{a} = 19.9\mu\text{m}$) in Carbogel mud

$T = 22^\circ\text{C}$ $f = 5\text{MHz}$ $Ba \sim 7$ $\lambda_a \sim 27$

KEY: 1. eqn.2.9, $\eta = 200\text{mPa s}$

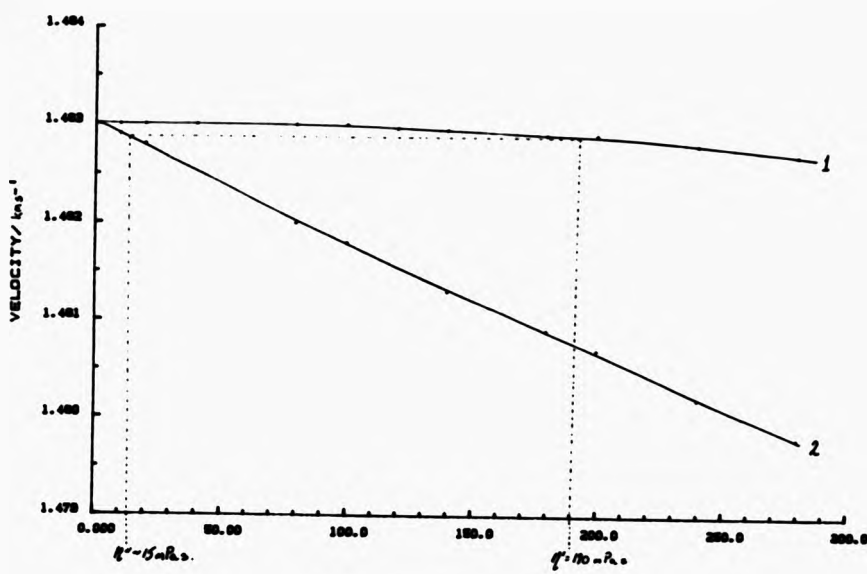
2. eqn.2.9, $\eta = 0.125(1 - 2.5v + 7.6v^2)$ Pa s

+, data

would not be reached. Further, Brillouin light scattering results provide a measure of Brownian and relaxation frequencies in materials, where the central Rayleigh line gives the structural relaxation frequency due to thermal effects and the Brillouin shift gives the propagation frequency of thermal phonons. Munch and Candau (1976) investigated polystyrene gels and found Rayleigh line widths in the range 20Hz to 20kHz also Bedborough and Jackson (1976) reported Brillouin shifts of about 5GHz in gelatin gels. This may suggest that at ultrasonic frequencies of about 5MHz the effects of Brownian motion and structural relaxation are not important, leaving the elasticity parameter to be explored. This can be done theoretically using the Gibson and Toksöz(1989) equation 2.5 when viscosity is assumed to be complex, as detailed in Chapter 2. Under the assumptions of a water-based Bentonite mud ($\nu=0.025$) containing glass spheres ($a=20\mu\text{m}$) at a volume fraction of 0.05, the resulting predictions for velocity and attenuation data are given in Figures 5.13 and 5.14 respectively. The curves marked 1 show the variation of the parameters as a function of suspension viscosity when no elasticity is included and those marked 2 show the variation with η'' (i.e. G/ω where G is the shear modulus) when η' (the simple viscosity) is fixed at 20mPa s (an approximation of the rheologically-measured value).

It can be seen that the attenuation is fairly flat as a function of η'' but is strongly effected by η' , whereas for velocity data the opposite appears to be the case. In terms of the viscous skin depth, one might expect the introduction of elasticity to increase the viscous coupling

between the phases as the spheres begin to get locked into the structure. For velocity this would mean that the spheres partake more in the ultrasonic wave motion, increasing the effective density and thus decreasing the velocity. In attenuation increased coupling means less relative motion and hence less viscous loss; so the theoretical predictions are consistent with expectations of the determining factors, i.e. viscous skin depth and effective density, in the phenomenological approach. This may explain the fair agreement between rheological and attenuation measurements and the disagreement with velocity data. In fitting the velocity data to the Ament equation it is assumed that the mud is purely viscous and this gives $\eta \sim 190 \text{ mPa s}$. From Figure 5.13 this viscosity can be used to predict a value for η'' when $\eta' = 20 \text{ mPa s}$ as shown. This results in a figure of $\eta'' \approx 15 \text{ mPa s}$ which occurs in a region where the predicted attenuation is almost indistinguishable from that with no elasticity present. This is consistent with the experimental results. Further as $\eta'' = G/\omega$ an estimate of G (the shear modulus) at 5MHz can be made i.e. $G = 15 \times 10^{-3} \times 2\pi \times 5 \times 10^6 \approx 0.5 \text{ MPa}$. Measurements of G at 0.1Hz for a sample of a Bentopharm, at a similar solid volume fraction as used here, have been made by Khandal and Tadros (1988). After over 15 hours a steady value of 500Pa was found for G. This is not too discouraging as the difference in measurement frequency is large, i.e. 0.1Hz vs. 5MHz, and the frequency dependence of G is not, ^{known} for the mud over this range. There is also the added factor of time dependence for G and some analysis of this in terms of gelation is presented in section 7.2.



$\eta' / \text{mPa}\cdot\text{s}$ (Curve 1) $\eta'' / \text{mPa}\cdot\text{s}$ (Curve 2)

FIGURE 5.13 Velocity vs. Complex Viscosity

glass spheres ($v = 0.05$) in bentonite mud $f = 5\text{MHz}$

KEY: using eqn.2.5, 1. x -axis gives η' , $\eta'' = 0$

2. x -axis gives η'' , $\eta' = 20\text{mPa}\cdot\text{s}$

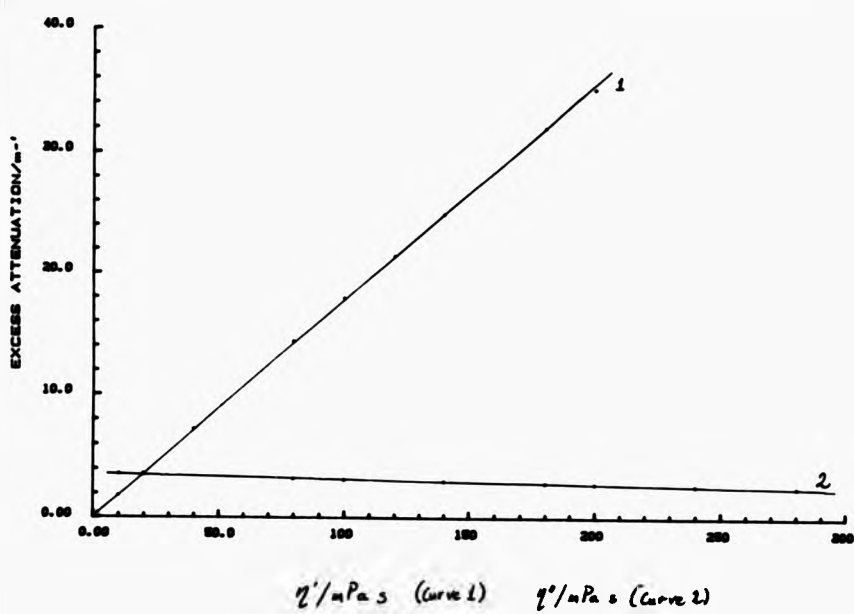


FIGURE 5.14 Excess Attenuation vs. Complex Viscosity

glass spheres ($v = 0.05$) in bentonite mud, $f = 2.25\text{MHz}$

KEY as figure 5.13

5.4 Summary

For the suspensions investigated it would appear that the assumption of non-interacting particles is valid up to 3% disperse phase volume concentration. In this range the Urick expression (eqn.2.2) for viscous attenuation is reliable when $Ba > 1$, $\lambda/a > 10$ and with any necessary correction for disperse phase polydispersity (e.g. using eqn.2.10). The Urick expression can then be used to calculate viscosities from experimental K measurements for Newtonian liquids and thixotropic muds, which correlate with rheologically measured values. For velocity, it has been shown that the simple Urick expression (eqn.2.6) begins to break down when $Ba > 1$ even if $\lambda/a > 10$. However the Ament theory (eqn.2.9) can be used successfully if a modified viscosity is assumed, which takes account of the presence of a disperse phase e.g. the Batchelor expression $\eta = \eta_0 (1 + 2.5\phi + 7.6\phi^2)$. This gives a suspending phase viscosity which agrees with the rheological data for Newtonian liquids but is higher than the plastic viscosity found for the muds. This can be modelled by the introduction of a shear modulus (i.e. viscosity becomes complex) into the propagation equation of Gibson and Toksöz (eqn.2.5) indicating that for water-based Bentopharm mud $G \sim 0.5 \text{MPa}$. Further, the difference can be explained in terms of increased viscous coupling between the phases, which means that the solid participates more in the fluid motion, increasing effective density and hence decreasing velocity. For attenuation, increased coupling means less relative motion and hence reduced viscous loss, however this effect has been shown to be not as strong a function of G as that on velocity.

6. EXPERIMENTAL RESULTS: Barite.

6.1 Attenuation

For suspensions of barite in both glycerol and PPG, α was found to be a linear function of solid volume fraction (up to 0.05) provided that the barite was added gradually to the liquid and time was allowed for any air bubbles to rise out. In the case of water-based mud, the entrapment of air was a problem owing to the finite yield stress of the mud and in Figure 6.1 curves 1 and 2 show the results for normal and de-gassed muds respectively. So, once the mud has been de-gassed a linear regime exists, as found for the Newtonian liquids and thus viscosity values could be calculated from $dv/d\alpha$ using eqn.2.10; this data is given in Table 6.1 overleaf. In the table, radii marked + are for the as received sample whereas the others were sieved and measured using the Microtrac. All data was obtained at 2.25MHz except that marked *, which was at 5MHz. The symbol # refers to viscometry values. For the Newtonian liquids, the agreement between calculated and measured viscosity is fair, but not as good as that found with the glass spheres. In the case of glycerol the calculated values are lower than expected. Due to the granular shape and fractured nature of the barite, there are two factors which may affect the attenuation results (i) stirring may break up the particles producing a radius distribution different to that measured by the Microtrac and (ii) it is conceivable that the effective ultrasonic radius is different to that found from light scattering, because some liquid becomes associated with the particle. In fact for the glycerol sample at 22°C

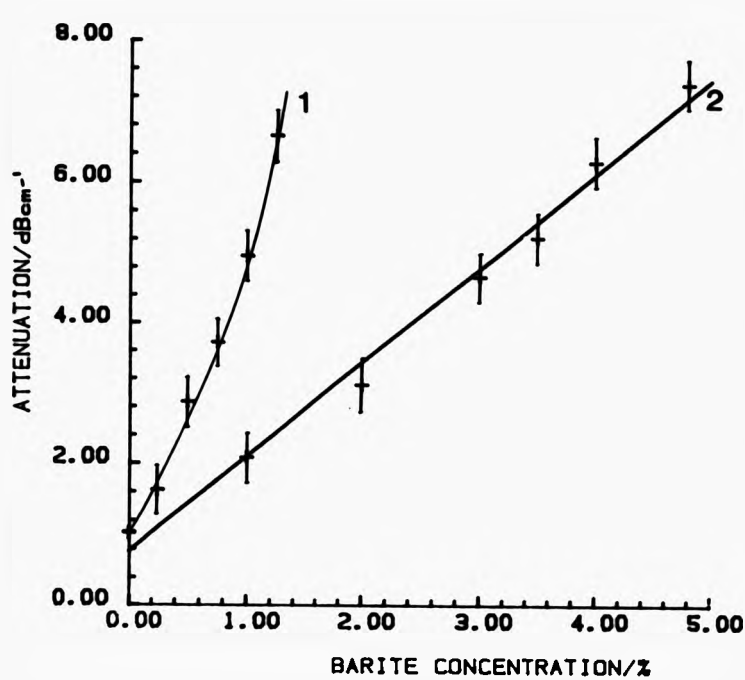


FIGURE 6.1 Attenuation vs. Barite Concentration

barite ($\bar{d} = 15.2\mu\text{m}$) in Milgel mud

$T = 22^\circ\text{C}$ $f = 5\text{MHz}$

KEY 1. mud not degassed

2. mud degassed

+, data

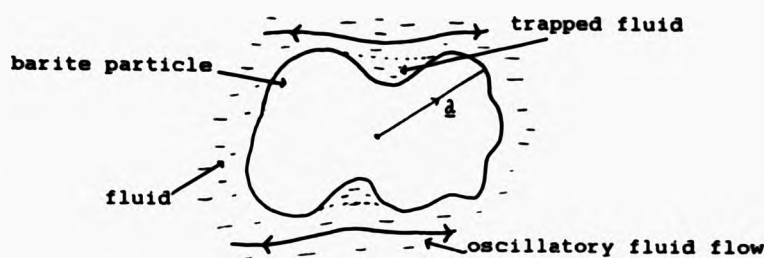
-, best fit

Continuous Phase	$a/\mu\text{m}$	σ	$T/^\circ\text{C}$	$(dV/dv)/\text{m}^{-1}$	$\eta/\text{mPa s}$	$\zeta/\text{mPa s}$
PPG 2025	15.2	0.5	23	3028+/-150	308+/-30	342
	+ 20	0.3	20	3478+/-100	370+/-30	415
Glycerol Analytical Reagent grade	15.2	0.5	22	2579+/-100	815+/-70	1210+/-10
	+ 20	0.3	20	1854+/-100	989+/-110	1330+/-30
Migjel in Water.	15.2	0.5	22	*1530+/-100	6+/-1	13.8
	+ 20	0.3	22	236+/-15	3+/-0.5	13.8

TABLE 6.1

if a is increased from $15.2\mu\text{m}$ to $19\mu\text{m}$ the viscosity becomes $(1258\pm 80)\text{mPa s}$ in good agreement with the viscometer value 1210mPa s . Similarly for the second sample if a is increased by $3.8\mu\text{m}$ to $23.8\mu\text{m}$ then one obtains $\eta = (1390\pm 110)\text{mPa s}$ compared with $(1330\pm 30)\text{mPa s}$ by viscometry. It would appear then that the effective particle radius in the ultrasound field is larger than that found from light scattering. The latter technique uses the diffractive effect of the particles measured over all orientations, and thus gives an area average for the radius vector a (see Figure 6.2).

FIGURE 6.2



In the ultrasound experiment the larger values of a will be more important as the oscillatory flow is unlikely to follow the particle contours exactly, leaving fluid associated with the particle. Thus the experimental observations may be explained by this effect.

For the PPG, the correlation between the calculated and measured viscosity is much closer. At 23°C there is agreement within the error and for the second sample the ultrasonically measured value is within about 10% of that from viscometry. Bearing in mind that the viscosity of PPG

is about 1/3rd that of glycerol, it may be that the former can wash more deeply into the surface irregularities during oscillatory motion, bringing the effective radius nearer to the light scattering value

In the case of the mud, ultrasonically measured viscosities are much lower than the viscometry values of plastic viscosity. Again one would not expect the mud to flow freely into the surface contours and trapped pockets of gel might occur associated with the particles. If, as found before for glycerol, the radius is increased by $3.8\mu\text{m}$ for the two samples listed in Table 6.1, the viscosities rise from 3 and 6mPa s to 5 and 10mPa s respectively. This is an improvement although the values are still low. However as before, when glass was used, it is possible to use eqn.2.5 with a complex viscosity in order to obtain a shear modulus for the mud. This has been done by finding the value of η'' needed, when η' is fixed at the viscometer value, to give attenuation the same as that calculated using the ultrasonic viscosity. Assuming a barite volume fraction of 0.05 and using the relevant mean radius from Table 6.1, for the mud where as received barite was used and measurement was made at 2.25MHz, $\eta'' \sim 1.6\text{Pa s}$ so $G \sim 22\text{MPa}$; when the sieved barite was used, at 5MHz, $\eta'' \sim 0.75\text{Pa s}$ so $G \sim 23\text{MPa}$. These figures for Milgel are much larger than the 0.5MPa found for Bentopharm mud when glass spheres were used. However results in section 7.2 indicate that G is strongly time dependent and measurements made on mature Milgel have been used to derive a value of $G \sim 18\text{MPa}$, which is closer to those found here.

6.2 Summary

It has been found that suspensions of granular particles can be modelled in the same way as the glass spheres, when an equivalent spherical radius and log-normal size distribution are assumed. So, from measurements of $d\kappa/dv$ it is possible to find an ultrasonic viscosity for Newtonian liquids, using eqn.2.10, which is at least within 20% of viscometry values. However it has been seen that this discrepancy may be due to a larger effective particle radius in the ultrasonic experiment compared with that measured by the light scattering method.

For the thixotropic mud, the fact that $d\kappa/dv$ is much greater for normal as opposed to de-gassed muds, indicates that the gel strength holds air bubbles in suspension. Using de-gassed samples it is possible to calculate an ultrasonic viscosity for the mud, which is lower than that found from viscometry at shear rates well above yield stress. This cannot be fully explained by the larger effective radius, but it can be interpreted in terms of elasticity where a shear modulus G exists. Calculations using the Gibson and Toksöz eqn.2.5 with a complex viscosity $\eta = \eta' + i\eta''$ indicate that at 5MHz $G \sim 23\text{MPa}$. This compares well with $G \sim 18\text{MPa}$ measured by studying the velocity changes as the mud gels with time. See section 7.2.

7. EXPERIMENTAL RESULTS: Clay Suspensions.

7.1 Kaolinite.

Figure 7.1 shows velocity (c) measured for a deflocculated aqueous kaolinite dispersion as a function of solid volume fraction (v); it should be noted that the range of v is no longer limited to the independent particle region noted earlier i.e. $0 < v < 0.03$. These measurements were made at 1MHz, where assuming an effective radius of $0.5\mu\text{m}$ (half the platelet length) and water viscosity = 1mPa s , then $Ba = 0.8$ and $\lambda/a \sim 1500$. The fitted curve can be obtained using both the Urick and Ament formulae (eqns. 2.6 and 2.9) when $\rho = 2600\text{kg/m}^3$, $\rho_f = 1000\text{kg/m}^3$ and $K = 4.45 \times 10^{-10} \text{Pa}^{-1}$ are fixed and K' is allowed to vary. For the sake of convenience, the data has been normalised to a water velocity value of $\sim 1500\text{m/s}$ in order that the published compressibility value (Kaye and Laby 1973) could be used. From the Urick expression the kaolinite compressibility is $K' = (3.8 \pm 0.1) \times 10^{-10} \text{Pa}^{-1}$ and using Ament's equation $K' = (10 \pm 2) \times 10^{-10} \text{Pa}^{-1}$. For comparison Urick (1947) found the ratio of compressibilities of kaolinite to water equal to 0.016, 0.028 and 0.023 giving an average value $K' \sim 10 \times 10^{-10} \text{Pa}^{-1}$. Thus it would appear again that once Ba approaches 1, Urick's equation begins to break down because viscous interaction between the continuous and disperse phase cannot be ignored.

In order to explore this further, measurements were also made at 5MHz where $Ba = 1.9$ and $\lambda/a = 300$, with the results being displayed in Figure 7.2. Having fixed the value of

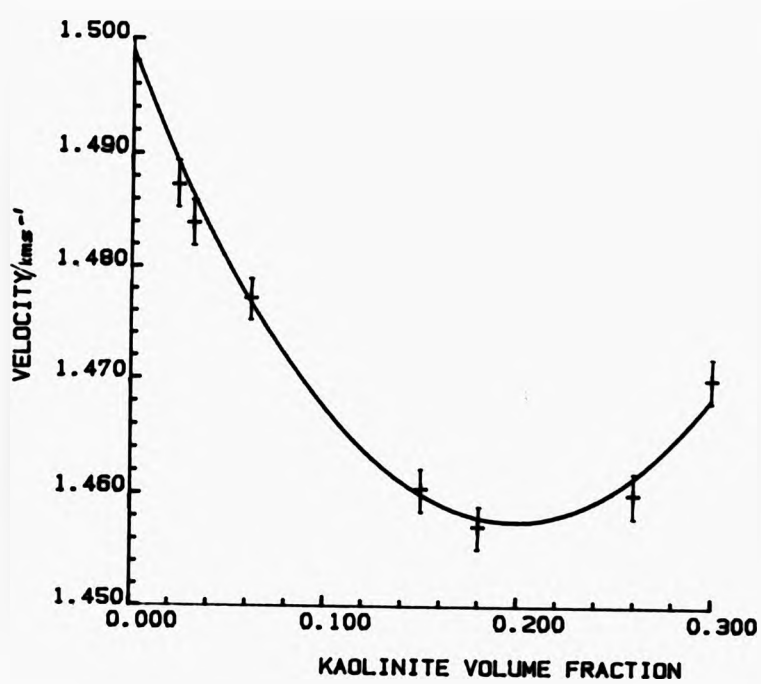


FIGURE 7.1 Velocity vs. kaolinite Volume Fraction

$T = 22^{\circ}\text{C}$ $f = 1\text{MHz}$ $B_a \sim 0.8$ $\lambda_a \sim 1500$

KEY +, data —, best fit (eqns. 2-6 and 2-9)

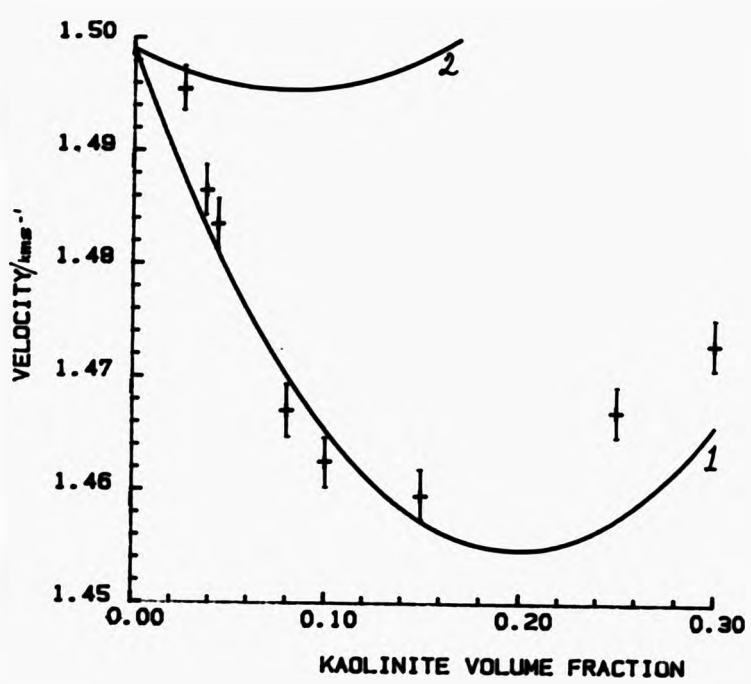


FIGURE 7.2 Velocity vs. Kaolinite Volume Fraction

$T = 22^{\circ}\text{C}$ $f = 5\text{MHz}$ $Ba \sim 1.9$ $\lambda/a \sim 300$

KEY: 1. eqn.2.6 2. eqn.2.9

+ , data

$K' = 10 \times 10^{-12} \text{ Pa}^{-1}$ curves 1 and 2 show the predictions of eqns. 2.6 and 2.9 respectively. Although the Urick curve does not give an excellent fit to the data, it is much closer than that found with the Ament formula. This can be explained in terms of the eccentricity of the kaolinite particles using the correction factors given by eqns. 2.11 and 2.12, due to Ahuja and Hendee (1978), in the Ament formula. In Figure 7.3 curves 1 and 2 are for edgewise and broadside particle orientation respectively, when an aspect ratio a/b of 100 is assumed; the radius a has been taken as $0.5 \mu\text{m}$. (The value $a/b \sim 100$ is used as an example from the work of Ahuja and Hendee: for kaolinite a/b is nearer 20). The distinction between the two orientations is not very great, as found by Ahuja and Hendee, but the effect on agreement with the data is remarkable as there is considerable improvement. This comes about because in the correction equations the factor B_b replaces B_a where appropriate and as $B_b = B_a/100$, viscous effects on the inertial density term are reduced. Hence the corrected Ament formula becomes closer to the Urick expression, where no viscous or inertial terms are used, and so the good agreement of the latter with the data in Figure 7.2 is not surprising. For comparison purposes curves 3 and 4 show the predictions of eqn. 2.5 when $a = 0.4 \mu\text{m}$ and $0.5 \mu\text{m}$ respectively; all other material values are unchanged from the above analysis. Again there is good agreement with the data and it can be seen that this is sensitive to the particle radius. The significance of the chosen values will be discussed in relation to interpretation of attenuation data in the following paragraph.

The expressions for complex wavenumber due to Hoven,

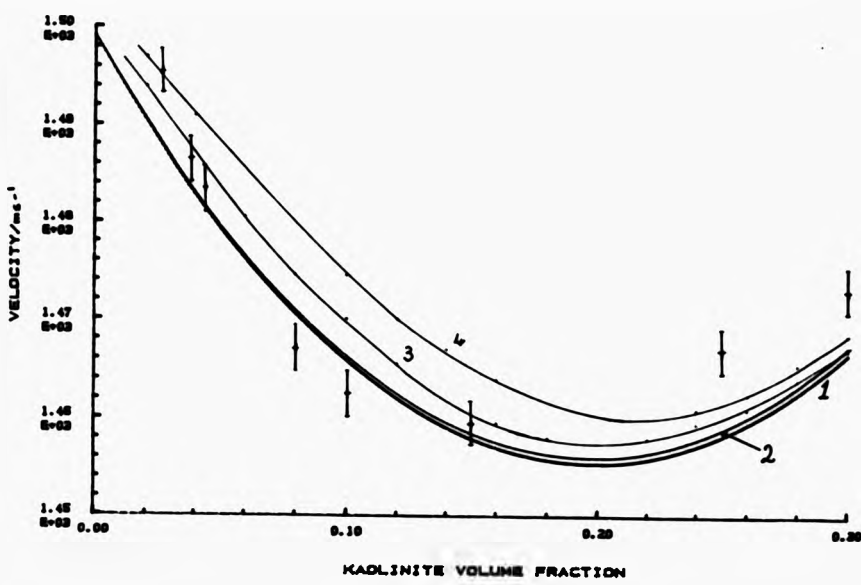


FIGURE 7.3 Velocity vs. Kaolinite Volume Fraction

$T = 22^\circ\text{C}$ $f = 5\text{MHz}$ $Ba \sim 1.9$ $\lambda/a \sim 300$

- KEY: 1. eqn.2.9 and broadside particle orientation
 2. eqn.2.9 and edgewise particle orientation
 3, 4. eqn.2.5 with $a = 0.4\mu\text{m}$ and $0.5\mu\text{m}$ respectively
 +, data

eqn.2.4, and Gibson and Toksöz, eqn.2.5, have been derived such that they should be applicable at disperse phase concentrations beyond the limit where contributions to attenuation are simply additive. In order to test this, attenuation at 5MHz as a function of volume fraction was measured for an aqueous kaolinite dispersion. The results are displayed in Figure 7.4 where the curves have been computed from $\text{Im}[k]$ in the wavenumber expressions. From before we have $\rho=1000\text{kg/m}^3$, $\rho'=2600\text{kg/m}^3$, $K=4.45 \times 10^{10} \text{Pa}^{-1}$, $K' \sim 1 \times 10^{-11} \text{Pa}^{-1}$ and $\eta=1\text{mPa s}$, leaving only radius as a variable and the choice of standard or frequency corrected forms of the equations. As the clay platelet length is about $1\mu\text{m}$ a reasonable assumption is $a=0.5\mu\text{m}$ and using this, curves 1 and 2 are produced from the standard forms of equations 2.4 and 2.5 respectively. Although both indicate that attenuation does not increase monotonically with v , neither provide an adequate description of what is observed in practice. However when the frequency corrected form of eqn.2.5 is used the situation is much improved, although the curve produced is still not a good fit to the data. Better agreement is found if radius is reduced from $0.5\mu\text{m}$ in curve 3 to $0.4\mu\text{m}$ in curve 4. An explanation for this lower radius may be found in that the correction term does not take into account the particle eccentricity. In the case of the velocity data, it was found that this reduced the viscous coupling effect when the term Bb was introduced to represent the thickness as well as the face of the platelet. Thus when a simple effective radius is assumed, one would expect this to be lower than the face radius, which is consistent with the results of Figure 7.4. As a final

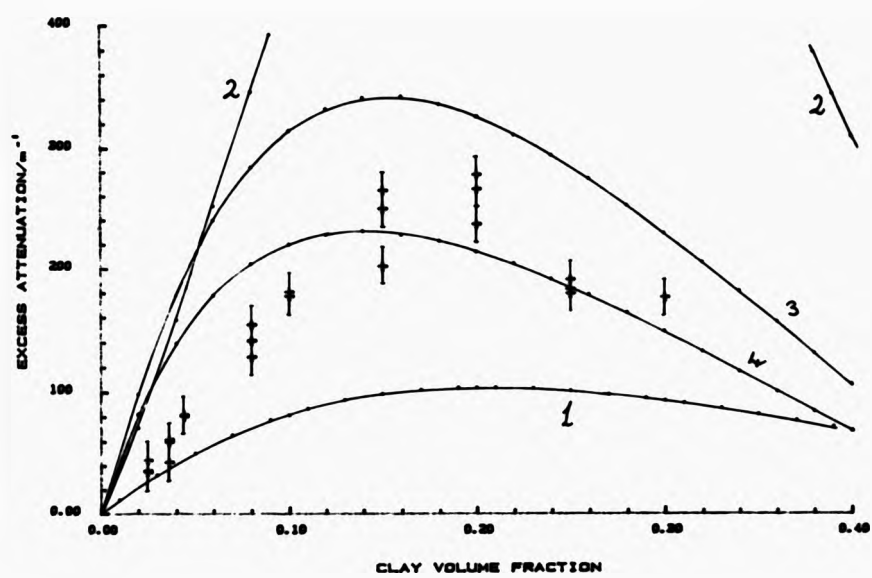


FIGURE 7.4 Excess Attenuation vs. Kaolinite Volume Fraction

$T = 22^{\circ}C$ $f = 5MHz$

KEY: 1. eqn.2.4, 2. eqn.2.5, 3,4. eqn.2.5 with frequency correction
and $a = 0.5\mu m$ and $0.4\mu m$ respectively

+ , data

check, eqn.2.5 was used to calculate velocity values, from $c = \omega/Re|k|$, for the kaolinite dispersion when $a=0.4\mu\text{m}$ and $a=0.5\mu\text{m}$, shown in curves 3 and 4 respectively in Figure 7.3. It is evident that the reduction in radius to $0.4\mu\text{m}$ also improves the agreement between data and theory for velocity.

7.2 Bentonite.

When contacted with water, bentonite behaves in a very different manner to kaolinite in that it is more likely to gel even at low concentrations (detail in Chapter 4). There is some evidence that the gel system does not quickly reach a stable condition when dispersed, and the gelation can be followed by the growth of a shear modulus with time. For example, Khandal and Tadros (1988) made measurements of the shear modulus G using a Rank pulse shearometer and found that at constant pH, the higher the dispersion concentration the longer the gelation time and the higher the final stable modulus. For this work, in order to get a measure of G , velocity at 5MHz was measured as a function of time for three different bentonites (which are used in drilling muds) at a standard concentration of $v \sim 0.025$. The results are shown in Figure 7.5. All samples show similar trends with an initial increase in velocity over the first day followed by a slight decrease to a settled value within about 4 days. Using eqn.2.6 we may write $c = \sqrt{M/\rho}$ where M is an effective bulk modulus and ρ an effective density. Assuming at time $t=0$ there is no elasticity ($G=0$) and that when the velocity is stable at c there is a stable elasticity G , then we can write;

$$\rho c_0^2 = M' \text{ and } \rho c_\infty^2 = M' + (4G_\infty)/3$$

where M' represents effective bulk modulus and therefore

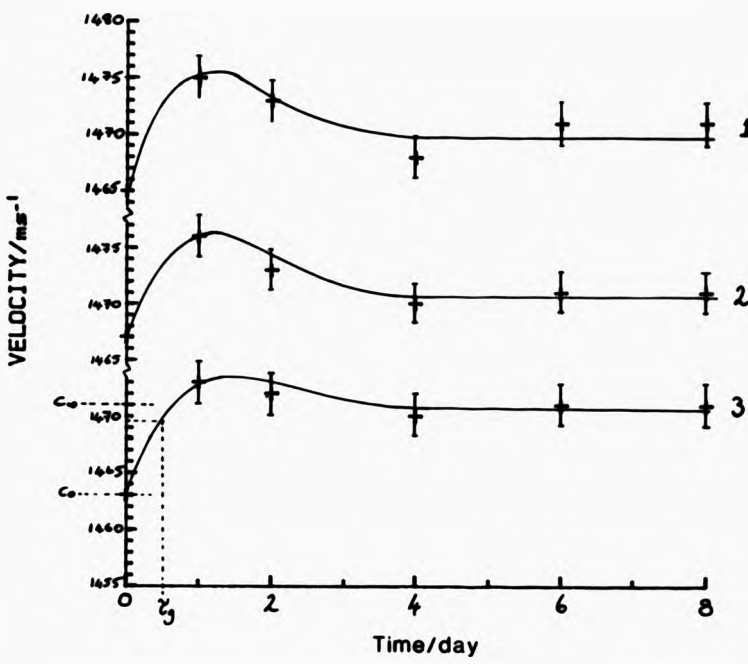


FIGURE 7.5 Velocity vs. Time

$T = 24^\circ\text{C}$ $f = 5\text{MHz}$

KEY: 1. Gelwhite 2. OCMA 3. Milgel

+, data

-, best fit

$$G_{\infty} = \frac{3}{4} \rho (c_{\infty}^2 - c_0^2) \quad (\text{eqn. 7.1})$$

Using the results for Milgel in Figure 7.5 $c_{\infty} \sim 1463 \text{ m/s}$ and $c_0 \sim 1471 \text{ m/s}$ and hence $G_{\infty} \sim (18 \pm 5) \text{ MPa}$.

This value compares well with the result $G \sim 23 \text{ MPa}$ found for Milgel in section 6.1, when a complex viscosity was assumed. In their experiments, Khandal and Tadros used Bentopharm, for which in this work a value $G \sim 0.5 \text{ MPa}$ at 5 MHz has been found (section 5.3). Even for acidic, strongly flocculated Bentopharm dispersions, Khandal and Tadros obtained shear modulus values that were less than half those obtained at SCR for Milgel, i.e. $G \sim 1 \text{ kPa}$, again using a pulse shearometer. Thus it is possible that the much lower shear modulus value calculated for Bentopharm compared with Milgel is due to their differing gelation properties. Certainly in practice it was found that the former could be dispersed at higher volume concentrations than the latter before stirring became impossible.

Attenuation was also measured as a function of time for the three suspensions. Figure 7.6 shows the results. Similarly to Figure 7.5, equilibrium values are reached within about 4 days. Defining a gelation time τ_g as the time taken for α to rise by $(1-1/e)(\alpha_{\infty} - \alpha_0)$ it can be seen that τ_g is about 1.5 to 2 days (~ 2000 to 4000 mins.). For velocity, although there is a lack of data in the initial region, in a similar manner one can infer a τ_g value of about 700-800 minutes which is less than half that obtained from attenuation. In their work on Bentopharm, Khandal and Tadros found that at $\text{pH} \sim 7.5$ and at a volume fraction close to that in the suspensions used here then $\tau_g \sim 900$ minutes, showing fair agreement with the velocity data. This not very

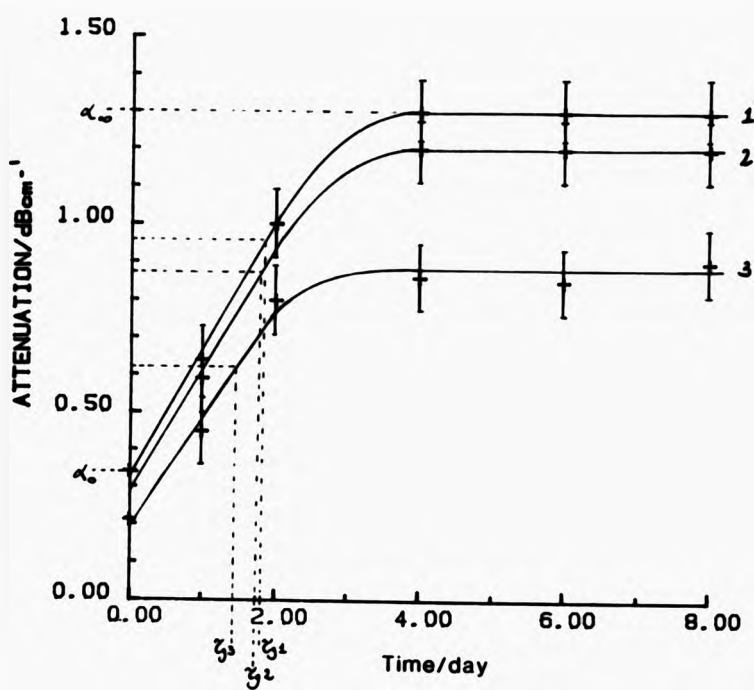


FIGURE 7.6 Attenuation vs. Time

$T = 24^\circ\text{C}$ $f = 5\text{MHz}$

KEY: 1. Milgel 2. OCMA 3. Gelwhite

+, data

-, test fit

surprising as in terms of experimental accuracy the velocity measurements from the PEO technique are very sensitive to change (e.g. changes <1m/s can be detected) whereas in the low attenuation range i.e. <1dB/cm, ultrasonic attenuation measurements are not very accurate.

Nevertheless there appears to be a real effect on attenuation and although c is expected to increase because the shear modulus grows, the expectations for attenuation are not obvious. Bourlion et al. (1986) found that for the barite-weighted drilling muds they investigated, α decreased with time reaching a steady value in about 3 to 5 hours. Again, these changes were relatively small ~2.5% and might be explained by the escape of air associated with the barite if the gel strength was not high enough to trap bubbles or simply sedimentation of the barite. There is also the possibility that the presence of barium sulphate (i.e. barite) initiates some chemical reaction not found in the unweighted muds. One way to interpret the data, is due to De Gennes (1976) where attenuation in a gelling system is given by:

$$\alpha = \frac{(2\pi f)^2}{[\rho_s + v\rho_s]c^3} \left(\eta_s + \frac{v^2 S_0 \rho_s E_s}{\rho_s F} \right) \quad (\text{eqn.7.2})$$

where F is a frictional coupling coefficient between fluid and gel network, S_0 is the gel fraction, ρ_s is the density of the network, η_s , ρ_s and E_s are the density viscosity and elastic constant of the solvent, v is the disperse phase concentration and c and f are ultrasonic velocity and frequency. Eqn.7.2 predicts that the attenuation should be related to the degree of gelation (in this case the square of the gel fraction) so the data in Figure 7.6 is consistent

with the formation of a more rigid gel matrix from an originally fluid dispersion. This is borne out by a visible decrease in the suspension fluidity with time.

Another useful means of comparison is the dependence of G' on clay volume fraction, generally of the form $G' \propto v^n$ where Khandal and Tadros found an index n of about 4-5 in the pH range 2.5 to 8.8 for G' measured at 0.1Hz. The samples used in this work were mixed in deionised water but the addition of the clay makes the dispersion slightly acidic, pH~6.5 to 7, so a reasonable comparison is possible. Values of G_{∞} can be inferred from c_{∞} using eqn.7.1 so measurements of this parameter were made as a function of solid volume fraction; results are given in Table 7.1.

TABLE 7.1 Sample: Bentopharm T=22°C f=5MHz

v	$(c_0+/-1)/ms^{-1}$	$(c_{\infty}+/-1)/ms^{-1}$	ρ/kgm^{-3}	G_{∞}/MPa
0.01	1482.1	1483.7	1016	3.6+/-2.2
0.02	1477.9	1480.5	1032	6.0+/-2.3
0.025	1475.9	1479.0	1040	7.1+/-2.3
0.03	1473.9	1476.6	1048	6.3+/-2.3
0.035	1472.0	1473.2	1056	2.8+/-2.4
0.04	1470.2	1473.0	1064	6.6+/-2.3
0.21	1442.8	1475.9	1336	97+/-3
0.25	1445.5	1478.6	1400	102+/-4
0.32	1458.5	1493.8	1512	118+/-4

As velocity values for no gelation, i.e. c_0 , are required to calculate G_{∞} , the Urick eqn.2.6 (assuming $K=4.5 \times 10^{-10} Pa^{-1}$ and $K'=1 \times 10^{-8} Pa^{-1}$) has been used to calculate c_0 , as this was found to be accurate for the non-gelling

kaolinite dispersions; then eqn.5.2 gives G_{∞} . Although the mid-range concentration G_{∞} values depart from the general upward trend, this may be explained by the difficulty of sample preparation. At these concentrations, it is hard to stir the mud in order to mix in the clay and air pockets can easily form. One might expect them to decrease the gel strength as they form discontinuities in the mud structure. The higher volume fraction samples were formed from low v suspensions which were de-watered by low pressure filtration and are thus less likely to contain air. From a linear regression for $\ln(G_{\infty})$ vs. $\ln(v)$ an index of $n=(1.5\pm 0.3)$ is obtained. This figure is much lower than that found by Khandal and Tadros (i.e. $n\sim 4-5$) and it does not compare well with predictions made using the fractal theory of colloidal flocs (Ball 1989) i.e.

$$G_{\infty} \propto v^{\frac{3-D}{3-D_0}} \quad (\text{eqn.7.3})$$

where D is the fractal dimension. D is the index relating the number of particles N in a flocculated structure to a linear dimension L , i.e. $N \propto L^D$. There are two regimes found for aggregation which are the diffusion limited or fast case, where flocculation occurs in the order of minutes, and the reaction limited or slow case, where the process takes hours or days. The corresponding fractal dimensions are about 1.86 and 2.1 respectively (Lin et al. 1989) and thus for a stable bentonite gel, one would expect $G_{\infty} \propto v^{4.9}$. However, further rheological experiments on swelling clay, in this case Gelwhite H, indicate that the index may be frequency dependent. Sohm and Tadros (1989) found that for Gelwhite the storage modulus measured at 1Hz was proportional to v^n where $n=3.7$, but for the modulus measured

using the pulse shearometer the index drops to $n \sim 3$. Although the shearometer measurement frequency is not specified by the authors, the manufacturer's manual indicates that it is approximately 200Hz. Thus there is evidence that n decreases with f and the value of $n \sim 1.45$ found at 5MHz is not unacceptable. Also it should be noted that eqn.7.3 has been derived assuming uniform strains applied to floc clusters. At 5MHz, the ultrasonic wavelength is around $300\mu\text{m}$ and so it is possible that strain gradients occur within the length of a floc.

Finally, measurements made using a Carrimed viscometer at BCR have shown that for bentonite muds G is also highly sensitive to the presence of certain ionic species in the dispersion (Meeten 1989). From an initial value for a mud made with deionised water, around 10Pa, τ_y (and hence G) increased as NaCl or CaCl₂ was added until a peak value was reached, followed by a fall in τ_y with salt concentration. The approximate values for the peaks were 30Pa at a NaCl concentration of 20g/L and 20Pa at a CaCl₂ concentration of 3 to 4g/L. It is thought that the differing concentrations required are due to different flocculation mechanisms being promoted by the ions in each case e.g. sodium ions may promote face to face aggregation and calcium ions edge to face. Having found that c was sensitive to G , it was hoped that these changes of a factor roughly 2 or 3 would be detected. Figure 7.7 shows the results obtained of ultrasonic velocity at 5MHz as a function of salt concentration for Milgel mud (bentonite volume fraction = 0.025). It can be seen that within the error no peak occurs in c for either case. For the addition of NaCl, any change

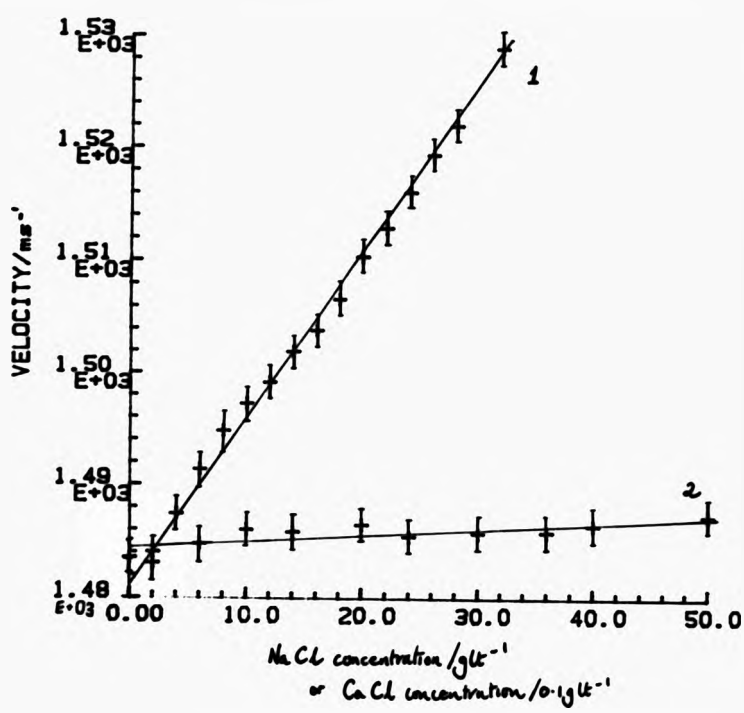


FIGURE 7.7 Velocity vs. Salt Concentration

T = 22°C f = 5MHz

KEY: 1. salt is NaCl 2. salt is CaCl

+, data

-, best fit

in G is masked by the decrease in compressibility of the liquid phase; $K_{\text{water}} \sim 4.5 \times 10^{-10} \text{ Pa}^{-1}$ $K_{\text{solution}} \sim 4.2 \times 10^{-10} \text{ Pa}^{-1}$ where the salt concentration is about 70g/L, corresponding to $c=1484\text{m/s}$ and $c=1514\text{m/s}$ respectively (Kaye and Laby 1973). In the case of the CaCl_2 , any masking effect from compressibility change is not so great as concentrations are a factor of ten down on the NaCl. However there is still no clear velocity maximum and so unfortunately the technique cannot be used in this manner to compare flocculation in the presence of sodium ions as opposed to calcium ions.

7.3 Summary

For aqueous kaolinite dispersions it has been found that as the product $Ba \rightarrow 1$, the Ament formula provides better agreement with velocity data than Urick's equation. However as Ba increases further, the Ament formula requires modification because the factor Bb , representing the platelet thickness which is about 10 times less than the length, becomes important and this can be done using inertial and shape correction factors derived by Ahuja and Hendee (1978). Consequently the Urick equation works remarkably well in this Ba region, even though no visco-inertial correction is made.

Further, the frequency-corrected Gibson and Toksöz eqn.2.5 gives better agreement when $a=0.4\mu\text{m}$ than when $a=0.5\mu\text{m}$ (the expected platelet radius) which is consistent with the findings above in that particle thickness cannot be ignored. There is therefore a problem in assigning an effective radius to an eccentric particle and when thickness $b \ll a$ it would appear that the effective radius is reduced

below a . However this only manifests itself when the Ba term becomes significant and then the Ahuja and Hendee correction factors are useful.

For predicting attenuation as a function of volume concentration when v exceeds around 0.05, both Hoven's expression (eqn.2.4) and the Gibson and Toksöz equation (eqn.2.5) are disappointing when the low frequency forms are used. However the latter is much improved when the frequency correction factor is included and further, better agreement is found when $a=0.4\mu\text{m}$ rather than $0.5\mu\text{m}$, consistent with observations in velocity measurements. Even though there is no provision for particle eccentricity, the theory gives a good qualitative model for the high volume fraction dispersions and is not a good quantitative fit to the data; Gibson and Toksöz also found this to be the case.

The velocity measured for bentonite suspensions has been found to be time-dependent, which can be interpreted in terms of the growth of a shear modulus G . For Milgel mud the steady state $G_s \sim 18\text{MPa}$ at 5MHz is compatible with values obtained from attenuation measurements when barite was used as a suspended phase. Further, a gelation time for Milgel, $\zeta_g \sim 800$ minutes, estimated from the velocity growth curve, is similar to a value found for Bentopharm $\zeta_g \sim 900$ minutes by Khandal and Tadros (1988) who measured G directly. Attenuation was also found to increase with time. This can be interpreted, using theory due to De Gennes (1976), in terms of an increasing gel fraction with time. Small changes in attenuation are measured (less than a few percent) and close to experimental resolvability, so more study of the phenomenon is required.

Using measurements of the equilibrium velocity c_{∞} as a function of v for the gelling bentonite clay, an estimate of the stable shear modulus G_{∞} can be calculated and its dependence on particle volume fraction observed. Measurements made at 5MHz on Bentopharm indicate that $G \propto v^{1.4}$, whereas at 0.1Hz Khandal and Tadros (1988) found an index of about 4-5, and fractal theory suggests that it should be 4.4. Further experimental evidence (Sohm and Tadros 1989) has shown that for a gelling clay suspension the index decreases from 3.7 at 1Hz to 3 at 200Hz, suggesting that a fall to 1.4 at 5MHz may not be unreasonable. Also, the fractal theory assumes a uniform strain applied to floc clusters and therefore at high frequencies where wavelength may be commensurate with or smaller than floc size, strain gradients would exist and the theory may not hold.

Finally, strong effects on G which can be measured rheologically, caused by the presence of sodium or calcium ions in the mud suspensions, cannot be detected by the ultrasonic velocity technique. This is because the effect of the ions on the effective bulk modulus dominates over the change in G .

8. EXPERIMENTAL RESULTS: Flowing Systems.

8.1 Velocity

A number of the colloids investigated in this work were also studied under conditions of flow using the apparatus shown in Figure 3.13. As a control experiment, a sample of glass spheres ($v=0.05$) in glycerol was chosen, as no orientation effects should occur. As expected with no particle anisotropy, ultrasonic velocity was found to be independent of shear rate up to $\dot{\gamma} \sim 100s^{-1}$, limited by the viscous nature of glycerol and the onset of detectable sample warming.

Similarly a deflocculated kaolinite dispersion, with $v=0.2$, was measured and again the ultrasonic velocity was the same under steady state or flow conditions up to $\dot{\gamma} \sim 200s^{-1}$.

At similar shear rates, optical flow orientation effects in kaolinite dispersions were detected (Molloy 1986) so it would appear that the ultrasonic velocity is fairly insensitive to particle orientation, at least when $\lambda \gg a$ as is the case here. In fact Ahuja and Hendee (1978) modelled ultrasonic propagation in suspensions of circular disk-shaped particles in water and they predicted that for $v=0.1$, differences in velocity for edgewise verses broadside particle orientation to the sound field, were of the order 0.1% at 5MHz. In the experimental case we might expect similar changes as although $v=0.2$, which might double the effect, the non-flow orientation would be random and so movement would not be between the two extremes of complete broadside to complete edgewise orientation. Thus, although some flow orientation must take place, the levels of change

in velocity cannot be detected by this technique.

In order to obtain results for bentonite muds, samples were introduced to the cell and left overnight to equilibrate. Then the steady state c_{∞} could be measured followed by monitoring of c as flow took place. Assuming that all structure was destroyed by the flow field, a value of G could be calculated from $c_{\infty}^2 - c^2$ using eqn.7.1; the results are given in Table 8.1.

TABLE 8.1 Sample: Milgel $T=(22\pm 0.1)^{\circ}\text{C}$ $f=5\text{MHz}$ $\dot{\gamma}=50\text{s}^{-1}$

v	$(c_{\infty} \pm 1)/\text{ms}^{-1}$	$(c \pm 1)/\text{ms}^{-1}$	ρ/kgm^{-3}	G/MPa
0.01	1483	1483	1016	—
0.02	1481.8	1481.7	1032	0.2 \pm 0.4
0.03	1478	1477.8	1048	0.5 \pm 0.5
0.04	1488.5	1487.9	1064	1.4 \pm 0.6

In the above table, the calculated G values rely on the change in velocity and not the absolute values. Hence the errors quoted for G come from the velocity change resolution found for the PEO technique i.e. $\pm 0.1\text{m/s}$ and not the quoted absolute error for c . The values of G are low when compared with those found from time dependent velocity and complex viscosity measurements (see section 7.2) i.e. $\sim 20\text{MPa}$. This is not due to the relatively low shear rate, a limitation introduced by the higher volume fraction samples which are difficult to pump, because no change was found in the $v=0.01$ and 0.02 results when shear rate was raised to 300s^{-1} . This indicates that the detectable level of structure breakdown has occurred as soon as the gel starts to flow; in

order to obtain a true c_0 , all individual flocs would have to be broken up to reproduce the initial dispersion, a process that may require even higher shear rates. Further, the changes found in velocity are at the resolution limit of the PEO apparatus, making the calculated G values subject to relatively high uncertainties. However the decrease in velocity during flow appears to be real because although the main experimental problem is temperature control, flow would be expected to increase the sample temperature and hence increase the velocity, as dc/dT is positive for water at 22°C.

Thus the flow experiments give an indication that some structure breakdown does occur but that ultrasonic velocity is fairly insensitive to it, at least when the wavelength (i.e. $\sim 300\mu\text{m}$) is much larger than the fundamental structure length (i.e. for bentonite $\sim 1\mu\text{m}$). Unfortunately, an increase in f to reduce the wavelength will also increase the attenuation, roughly as a function of frequency squared, making resolution of pulses more difficult.

8.2 Attenuation

Finally, the effect of flow on attenuation was examined for the Milgel bentonite mud. Measurements at 2.25MHz and 5MHz over the volume fraction range 0.01 to 0.04 with shear rates up to 300s^{-1} failed to produce any detectable change. This is consistent with the observations of Blue and McLeroy (1968) who found that in suspensions of gelling clay platelets, attenuation was the same for the sol or gel state. They suggested that the gel was broken down by the passage of the acoustic wave, but this is unlikely unless very high amplitudes were used, as mentioned earlier. In Figure 5.14 it was shown that at 2.25MHz the attenuation

of a suspension of glass particles in mud was insensitive to elasticity of the order expected for bentonite. So, in this work we would not expect attenuation to be very sensitive to flow effects when, *ceteris paribus*, all that may occur is a decrease in G . The frequencies used by Blue and McLeroy were lower (range 150 to 1500kHz) and so if G is proportional to frequency, one would expect the clay suspensions to appear predominantly as viscous liquids to the sound wave because G is lower. Unfortunately, the above evidence is contrary to the time-dependent growth observed in attenuation, as described in section 7.2, which was interpreted in terms of an increasing gel fraction. There are problems with this data as the changes were monitored at the low attenuation resolution limit (i.e. $\sim 1\text{dB/cm}$). Here small changes in an initially large output voltage are measured, which are highly sensitive to temperature instability. A further investigation of time-dependent attenuation and flow effects using equipment specifically designed for accuracy at around 1dB/cm would be necessary to resolve this problem.

8.3 Summary

Orientation effects on velocity at 5MHz during flow of suspensions of non-spherical clay platelets appear to be small, at least when the wavelength \gg particle dimensions. This has been predicted by Ahuja and Hendee (1978) who computed a change of $\sim 0.1\%$ in c (at around 5MHz) for a complete re-orientation from edgewise to broadside motion in the sound field.

For kaolinite there was no resolvable velocity change, even for shear rates of 200s^{-1} , but for the gelling Milgel

mud changes of 0.1 to 0.6m/s were detected, allowing estimates of the shear modulus to be made. Assuming all elastic structure was destroyed by flow, the values found i.e. ~1MPa were much lower than those from time-dependence measurements i.e. ~18MPa, even at shear rates up to $300s^{-1}$. This suggests that some structure may still exist in the flowing mud.

Finally, attenuation for Milgel at 2.25MHz and 5MHz was found to be unaffected by flow consistent with observations elsewhere (Blue and McLeroy 1968). It is also consistent with data for glass suspensions in gelling clay where attenuation was found to be weakly dependent on gel elasticity. However the time-dependent growth observed in attenuation suggests that it is sensitive to the state of gelation and hence if flow breaks up the long range gel structure, one might expect a change in attenuation.

9. CONCLUSION.

Three near-field techniques for measuring ultrasonic attenuation (α) and longitudinal velocity (c), namely continuous wave interferometry, tone burst transmission and broadband pulse analysis have been intercompared. For measurements on Dow Corning 710 silicone oil standard deviations of $\pm 3\%$ in α and $\pm 0.5\%$ in c were found. Excellent agreement for α and c of this oil has been obtained with those measured for the same sample by the NPL (Zeqiri 1987) using a far-field method. Also, measurements made in the frequency range 1-10MHz on silicone fluids give good agreement with data in the literature e.g. Dunn and Breyer (1962). Using the tone burst and PEO techniques to measure α and c respectively, results obtained for colloidal dispersions have been intercompared with relevant theory. In general, excellent agreement has been found for suspensions where the solid volume fraction does not exceed 0.05 and for higher concentrations some successful correlation has been achieved.

Measurement of attenuation as a function of solid volume fraction for dispersions where particle radius is much smaller than the sound wavelength have shown that spherical glass particles are non-interacting up to $v=0.05$. This has also been found to be true for granular shaped barite particles provided that their surface is wetted by the continuous phase and that air is not trapped in suspension. Under these conditions, for dispersions where visco-inertial losses are expected to dominate over thermal losses (i.e. when $aB_v \sim 1$ and $aB_p \ll 1$) and scattering of

Rayleigh type, the attenuation expression due to Urick (1948) provides excellent agreement with experimental data when $aB_v \gg 1$, $\lambda/a \gg 10$ and if disperse phase polydispersity is accounted for. The latter condition has been satisfied by measuring equivalent spherical radius using a light scattering technique and assuming a log-normal particle size distribution. Hence from measurements of attenuation as a function of solid volume fraction, the continuous-phase viscosity values can be calculated using Urick's equation and these have been found to correlate with rheological measurements of viscosity for Newtonian liquids and thixotropic muds. However it appears that when barite is used, some of the continuous phase remains associated to the particle, within surface irregularities, as it moves in the sound field. Consequently a larger effective radius is found compared with light scattering measurements.

Using deflocculated, platelet-like particle kaolinite dispersions, volume fractions above 0.05 can be achieved and hence attenuation measurements made when particles are not acting independently. The behaviour of α with v can be modelled qualitatively using the theory of Gibson and Toksöz (1989) when a frequency correction term, which scales with the product Ba , is introduced into the viscous drag force. However a good quantitative fit to the data is not achieved as it is difficult to assign an effective radius to the eccentric particle.

Measurements of velocity as a function of solid volume fraction for suspensions of glass spheres in Newtonian liquids have shown that the simple effective medium velocity equation due to Urick (1947) begins to fail

when $Ba \gg 1$, even if $\lambda/a \gg 10$. The Ament (1953) theory, which introduces viscous drag effects in the effective suspension density expression, has been found to give good agreement with the data over the Ba range investigated, provided that the effect of non-independent particles at higher volume concentrations was accounted for. This was done by assuming an effective viscosity for the suspension, taking account of the disperse phase, using the expression derived by Batchelor (1974) i.e. $\eta_{eff} = \eta_0 (1 + 2.5v + 7.6v^2)$ where η_0 is the continuous phase viscosity. When measurements were made using the gelling bentonite clay Bentopharm, best agreement between theory and data was obtained when $\eta_0 \approx 190 \text{ mPa}\cdot\text{s}$, much higher than the rheologically measured plastic viscosity $\eta_p \approx 20 \text{ mPa}\cdot\text{s}$. This discrepancy has been accounted for in terms of a complex viscosity of the continuous phase (i.e. the introduction of a shear modulus) encountered by the particles. The Gibson and Toksöz (1989) equation has been modified to model this and a value for the shear modulus i.e. $G \approx 0.5 \text{ MPa}$ at 5 MHz has been calculated.

This analysis predicts that for a given dispersion at frequencies $\sim 2.25\text{--}5 \text{ MHz}$, the effect of increasing elasticity (i.e. G) is to decrease α and increase c . This is consistent with the concepts of effective density and viscous skin depth used in this work, as the elasticity would increase the coupling between the continuous and disperse phase. Thus for α , increased viscous coupling means less relative motion and less viscous dissipation and for c , increased viscous coupling means that the particles partake more in the fluid motion so that effective density is increased (as $\rho' > \rho$) and so velocity must decrease. The theory also indicates

that the introduction of a shear elasticity (G) has a stronger effect on c than on κ . This is consistent with the experimental data, as viscosities calculated from attenuation are close to the directly-measured rheological values.

For suspensions of kaolinite, as the product Ba approaches 1 (where a is taken as the platelet face radius) the Ament formula again gives better agreement with the data than Urick's equation. As the visco-inertial term becomes more significant, i.e. as Ba increases, the Ament theory requires modification to include the effect of platelet thickness. This can be done using shape and inertial correction factors due to Ahuja and Hendee (1978) and the result is a moderation of the effect of the Ba term. Hence the Urick expression which contains no visco-inertial term provides fair agreement with the data in this case. Further evidence of the effect of particle eccentricity has been found in that velocity calculated from the Gibson and Toksöz (1989) expression gives better agreement with data when particle radius is taken as $0.4\mu\text{m}$ rather than the face radius $0.5\mu\text{m}$. This is consistent with a reduction in the visco-inertial effect, represented by Ba , caused by the particle thickness.

Both the attenuation and velocity for bentonite suspensions have been found to increase with time up to a steady state value after about 3-4 days. The velocity data has been interpreted in terms of the growth of a shear modulus as gelation takes place, making calculations of G possible. For Milgel a steady state $G_{\omega} \sim 18\text{MPa}$ at 5MHz was found which is compatible with a value derived from

attenuation measurements using barite as the disperse phase i.e. $G_0 \sim 23\text{MPa}$. Also the estimated gelation time $\tau_g \sim 700$ to 800 minutes is commensurate with that found for Bentopharm by Khandal and Tadros (1988) i.e. $\tau_g \sim 900$ minutes. This attenuation data has been interpreted in terms of an increasing gel fraction as the mud structure forms, using a theory due to De Gennes (1976). A more precise and in depth study of the muds is required to resolve this.

Orientation effects on the ultrasonic velocity at 5MHz for non-spherical kaolinite clay suspensions, caused by shear flow, have been found to be undetectable, even for shear rates $\sim 200\text{s}^{-1}$. For Milgel bentonite mud small changes have been found, $< 0.1\%$, when $\lambda \gg$ particle dimensions, consistent with appropriate calculations made by Ahuja and Hendee (1978). The flow appears to partially break down the structure, as c is reduced, however the changes are lower than those found for time-dependent measurements suggesting that some structure remains in the flowing mud.

Attenuation for Milgel has been found to be unaffected by flow even when glass spheres are present. This is consistent with observations that attenuation originating from the spheres is weakly dependent on gel elasticity.

Finally measurements of the steady state velocity c can be used to find the modulus G_0 of a fully-gelled mud at 5MHz as a function of volume fraction of the clay. Measurements for Bentopharm show that $G_0 \propto v^n$, where $n=1.45$. This compares with $n=3.3-4.4$ expected from fractal floc theory, and suggests a decreasing index n with frequency. This is also found in the results of Sohm and Tadros (1989) where G was measured directly for Gelwhite



bentonite. The decrease is not understood, but it may suggest that the small wavelengths i.e. $\sim 300\mu\text{m}$ produce strain gradients within the length of the flocs.

10. REFERENCES

- Ahuja, A.S. and Hendee, W.R., (1978). *J. Acoust. Soc. Am.*, 63, 1074-1080.
- Alderman, N., (1989). SCR, Madingley Rd., Cambridge, Personal Communication.
- Ali, A.V. and Langton, C.M.L., (1989). Dept. of Physics, City of London Polytechnic, Personal Communication.
- Allegra, J.R. and Hawley, S.A., (1972). *J. Acoust. Soc. Am.*, 51(5), 1545.
- Ament, W.S., (1953). *J. Acoust. Soc. Am.*, 25, 638-641.
- Avery, R.G. and Ramsey, J.D.F., (1985). *J. Colloid and Interface Sci.*, 109, 441-454.
- Bacri, J.C., Courdille, J.M., Dumas, J. and Rajaonarison, R., (1980). *J. De Phys. Lettres*, 41, 369.
- Batchelor, G.K., (1974). *Annual Review of Fluid Mechanics*, 6, 227-255.
- Bedborough, D.S. and Jackson, D.A., (1976). *Polymer*, 17, 573-576.
- Ball, R.C., (1989). Fractal Structure of Colloidal Flocs. Paper presented to Society of Chemical Industry Meeting, Belgrave Square, London. 21st February 1989.
- Biot, M.A., (1956a). *J. Acoust. Soc. Am.*, 28(2), 168-178.
- Biot, M.A., (1956b). *J. Acoust. Soc. Am.*, 28(2), 179-191.
- Blitz, J., (1967). *Fundamentals of Ultrasonics*, pp49, Butterworths, London.
- Blue, J.E. and McLeroy, E.G., (1968). *J. Acoust. Soc. Am.*, 44(4), 1145-1148.
- Bouillon, M., Denis, J. and Soucemerianadin, A., (1986). Paper presented at Congres du Groupe Francais de Rheologie, Strasbourg.
- Breazeale, M.A., Cantrell, J.H. and Heyman, J.S., (1981). *Methods of Experimental Physics*, 19, Ultrasonics Ed. P.D. Edmunds, pp97-99, Academic Press, London.
- Carman, P.C., (1956). *Flow of Gases Through Porous Media*, Academic Press, New York.
- Casson, N. (1959). *Rheology of Disperse Systems*, Pergamon, London.
- Chow, J.C.F., (1964). *J. Acoust. Soc. Am.*, 36(12), 2395-2401.
- Davis, M.C., (1979). *J. Acoust. Soc. Am.*, 65, 387-390.

- DeGennes, P.G., (1976). *Macromolecules*, 9, 587.
- Dimitrov, D.P. and Radcev, B.P., (1989). *J. Colloid and Interface Science*, 131(2), 596-597.
- Dumas, G.A., Thiry, P.S. and Drouin, G., (1983). *IEEE Transactions On Sonics and Ultrasonics*, 30(2), 59.
- Dunn, G. and Breyer, J.E., (1962). *J. Acoust. Soc. Am.*, 34(6), 775.
- Duykers, L.R.B., (1970). *J. Acoust. Soc. Am.*, 47(1), 396-398.
- Einstein, A. (1906). *Ann. Phys.*, 19, 289.
- Epstein P.S. and Carhart, R.R., (1953). *J. Acoust. Soc. Am.*, 25, 553.
- Franklin, J.G. and Javanand, C., (1985). *Physics Letters*. 109A(3), 127-132.
- Gibson, R.L. and Toksöz, M.N., (1989). *J. Acoust. Soc. Am.*, 85(5), 1925-1934.
- Goberman, G.L., (1968). *Ultrasonics Theory and Application*, pp29-34, English Universities Press.
- Goodwin, J.W., Pekenc, E., Pand, B. and Smith, R.W., (1980). *J.C.S. Faraday I.*, 16, 225-235.
- Hampton, L.D., (1967). *J. Acoust. Soc. Am.*, 42, 882-890.
- Harker, A.H. and Temple, J.A.G., (1988). *J. Phys. D: Applied Phys.* 21, 1576-1588.
- Hasimoto, H., (1959). *J. Fluid Mech.*, 5, 317-328.
- Hay, A.E. and Mercer, D.G., (1989). *J. Acoust. Soc. Am.*, 85(5), 2215-2216.
- Hertzfeld, K.F. and Litovitz, T.A., (1965). *Absorption and Dispersion of Ultrasonic Waves.*, pp428-516., Academic Press, New York.
- Holliday, D.V., (1987). *Coastal Sediments '87 Conf. Proc.*, 260-272.
- Hoven, J.H., (1980a). *J. Acoust. Soc. Am.*, 67(5), 1559-1563.
- Hoven, J.H., (1980b). *J. Acoust. Soc. Am.*, 66, 1513.
- Hubbard, J.C., (1940). *Am. J. Phys.*, 8, 207.

- Hussia, A.B.B.H. and Povey, M.J.W., (1984). J. Am. Oil Chem. Soc., 61, 560-564.
- Javanaud, C., (1988). Ultrasonics, 26, 117-123.
- Kaye, G.W.C. and Laby, T.H., (1973). Tables of Physical and Chemical Constants, 14th Ed., Longmans Press.
- Kessler, L.W., Hawley, S.A., and Dunn, F., (1971). Acustica, 24, 105.
- Khandal, R.K. and Tadros, Th. F., (1988). J. Colloid and Interface Science, 125(1), 122-128.
- Kinsler, L.E. and Frey, P., (1962). Fundamentals of Acoustics, pp166-177, J. Wiley, New York.
- Lamb, H., (1945). Hydrodynamics, pp361-363, Dover Publications, New York.
- Langton, C.M., Palmer, S.B. and Porter, R.W. (1984). Eng. In. Med., 13, 89.
- Lin, M.Y., Lindsay, H.M., Weitz, D.A., Bail, R.C., Klein, R. and Meakin, P., (1989). Nature, 339, 360-362.
- McClements, D.J. and Povey, M.J.W., (1987a). Ultrasonics International '87 Conc. Proc., 43-47.
- McClements, D.J. and Povey, M.J.W., (1987b). Adv. in Colloid and Interface Sci., 27, 285-316.
- McMillan, D.R. and Langermann, R.J., (1947). J. Acoust. Soc. Am., 19, 956.
- Mason, W.P., (1950a). Piezoelectric Crystals and their Application to Ultrasonics, pp313-320, D. Van Nostrand, New York.
- Mason, W.P., (1950b). Piezoelectric Crystals and their Application to Ultrasonics, pp335, D. Van Nostrand, New York.
- Matsuzawa, K., Inoue, N. and Hasegawa, T., (1987). J. Acoust. Soc. Am., 81(4), 947.
- Meeten, G.M., (1989). SCR, Cambridge, Personal Communication.
- Mitchell, J.K., (1976). Fundamentals of Soil Behaviour, pp112-133, J. Wiley, New York.
- Molloy, P.J., (1986). Ph.D. Thesis, City of London Polytechnic, CNAA.
- Munch, J.P. and Candau, S., (1976). Polymer, 14, 1097-1109.
- Musa, R.S., (1958). J. Acoust. Soc. Am., 30(3), 215.

- Nandi, A.K., (1987). Dept. of Electrical Engineering, Imperial College, London. Personal Communication.
- Papadakis, E.P., (1972). J. Acoust. Soc. Am., 52(3), 843.
- Perdigao, J.M., Gazalet, N., Frohly, J. and Bruneel, C., (1987). Ultrasonics, 25, 209-213.
- Povey, M.J.W., (1983). J. Coll. Int. Sci., 93(2), 565-567.
- Povey, M.J.W., (1984). J. Am. Oil Chem. Soc., 61, 560-564.
- Rahalkar, R.R., Gladwell, N., Javanaud, C., and Richmond, P., (1986). J. Acoust. Soc. Am., 80(1), 33.
- Roussel, J-F., (1988). Universite de Provence, France: Personal Communication.
- Salin, D. and Schon, W. (1981). J. Physique - Lettres, 42, 477-480.
- Schwartz, L.M. and Johnson, D.L., (1984). Am. Phys. Soc. Phys. Rev. B., 30(8), 4302-4313.
- Sherwood, J.D., (1988). Internal Research Note, SCR, Cambridge.
- Sohn, R. and Tadros, Th. F., (1989). J. Colloid and Interface Science, 132(1), 62-71.
- Urick, R.J., (1947). J. App. Phys., 18, 983.
- Urick, R.J., (1948). J. Acoust. Soc. Am., 20(3), 283.
- Van Olphen, H., (1963). Clay Colloid Chemistry, J. Wiley, New York.
- Vincent, A., (1987). Ultrasonics, 25, 237.
- Waterman, P.C. and Truell, R., (1961). J. Math. Phys., 2, 512.
- Wells, P.N.T., (1969). Physical Principles of Ultrasonic Diagnosis, pp53-55, Academic Press, London.
- Wood, A.B., (1941). A Textbook of Sound, G. Bell and Sons, London.
- Zeqiri, B. (Sept.1987). National Physical Laboratory, Teddington, Middx. Personal Communication.

APPENDIX A

```
2KEM
10REM Thurlby DVM Interface for BBC Micro
20REM Ultra Sonic Interferometry
30REM City of London Polytechnic
40REM 27th January, 1987
50
60
70MODE 0
80DIMY(639)
90PROCassemble
100REPEAT
110PROCmenu
120ON C% GOSUB 140,150,160,170,180
130UNTIL FALSE
140PROCscaling:RETURN
150PROCshako:PROCacquiredata:X%*GET:RETURN
160PROCreplot:X%*GET:RETURN
170PROCfile:RETURN
180PROCtransducer:RETURN
190
200DEFPROCmenu
210CLS
220PRINT"##### Ultra Sonic Interferometry #####"
230PRINT""
240PRINTTAB(32)"----- MenuPage-----"
250PRINT""
260PRINTTAB(29)"Set Parameters (1)"
270PRINTTAB(29)"Scan (2)"
280PRINTTAB(29)"Replot Old Data (3)"
290PRINTTAB(29)"Save Data (4)"
300PRINTTAB(29)"Set Transducer Position (5)"
310PRINT""
320INPUT" CHOICE(1-5) "C%
330CLS
340ENDPROC
350
360DEFPROCloop
370REPEAT
380CALL Thurlby
390PRINT Sstring;:PRINT LEN(Sstring)
400UNTIL FALSE
410ENDPROC
420
430DEFPROCscaling
440CLS
450INPUT"VOLT(max)/mV="VMAX
460INPUT"VOLT(min)/mV="VMIN
470INPUT"STEP SIZE ="stepsize%
480INPUT"DIRECTION(U/D)"DIR%
490INPUT"DELAY/centisecs."delay%
500k=1/(VMAX-VMIN)
510IFPE62=LF:REM set user port all output lines
520IF DIR%="U" THEN ?PE60=LA0 ELSE ?PE60=680
530A%=?PE60
540ENDPROC
550
560DEFPROCassemble
570DIM code% 100,string 10,v(640)
580osbyte=FFFF:counter=70
590REM enable RS423 port
600*FX2,2
610REM 9600 baud receive
620*FX 7,7
630FOR X%=0 TO 2 STEP 2
640?%=code%
650OPT X%
```

```

660.Thurlyby
670\ Reset string counter
680LDA#0:STA counter
690\ Flush RS423 input buffer *PX21,1
700LDA#21:LDX#1:LDY#0:JSR osbyte
710
720\ Check the RS423 input for "R", i.e. a measurement reading
730.search JSR getchr
740COPY#ASC"R":DNR search
750
760\ Read in DVM string output
770.DVMstring JSR getchr
780LDX counter:TYA:STA string,X:INC counter
790CMP#&0D:BNR DVMstring:RTS
800
810\ Routine to get character from RS423 port
820.getchr LDA #145:LDX #1:LDY#0:JSR osbyte:BCS getchr:RTS
830J
840NEXT
850ENDPROC
860
870DEFPROCacquiredata
880PROCframe
890X=0
900CALL Thurlyby
910V=VAL(Sstring):v(0)=V:Y%=k*1023*(V-VMIN)
920PLOT 69,X%,Y%
930FOR A%=2 TO 1279 STEP 2*stepsize%
940PROCstepmove(stepsize%,delay%)
950CALL Thurlyby
960V=VAL(Sstring):v(X%/2)=V:Y%=k*1023*(V-VMIN)
970PLOT 69,X%,Y%
980NEXT
990ENDPROC
1000
1010DEFPROCstepmove(S%,D%)
1020REM stepper motor move by stepsize S%
1030FOR I=1 TO S%
1040A%=7&FE60
1050FOR I%=1 TO 2
1060A%=A% EOR &80
1070%&FE60=A%
1080NEXT
1090TIME=0:REPEAT UNTIL TIME=D%
1100NEXT
1110ENDPROC
1120
1130DEFPROCshake
1140 PROCupdown
1150 PROCstepmove(50,10)
1160 PROCupdown
1170 PROCstepmove(50,10)
1180ENDPROC
1190
1200DEFPROCupdown
1210A%=A% EOR &20
1220%&FE60=A%
1230ENDPROC
1240
1250DEFPROCframe
1260MOVE 0,0:DRAW 1279,0:DRAW 1279,1023:DRAW 0,1023:DRAW 0,0
1270ENDPROC
1280
1290DEFPROCreplot
1300CLS
1310PROCdata
1320CLS

```

```

1330PROCframe
1340FOR I=0 TO 638
1350PLOT 69,2*I,Y(I)
1360NEXT I
1370ENDPROC
1380
1390PROCfile
1400DEFPROCfile
1410INPUT"NAME OF DATAFILE ? "AS
1420X=OPENOUTAS
1430
1440FOR X%=0 TO 1279 STEP 2
1450Y%=k+1023*(v(X%/2)-VMIN)
1460PRINT#X,X%/2,Y%
1470NEXT X
1480CLOSE#X
1490ENDPROC
1500
1510DEFPROCdata
1520INPUT"NAME OF DATAFILE ? "BS
1530X=OPENINBS
1540INPUT#X,C
1550FOR I=0 TO 639
1560INPUT#X,Y(I),I
1570NEXT I
1580CLOSE#X
1590ENDPROC
1600
1610DEFPROCtransducer
1620INPUT"NUMBER OF STEPS-"S%
1630INPUT"DIRECTION(U/D)"DIRS
1640INPUT"DELAY/centisec."D%
1650?LFE62=LFF
1660IF DIRS="U" THEN ?LFE60=L6A0 ELSE ?LFE60=L680
1670A%=?LFE60
1680PROCshake
1690PROCstepmovo(S%,D%)
1700ENDPROC

```


$$R + R(1-R)^2 e^{-2\alpha t} + R^3(1-R)^2 e^{-4\alpha t} + R^5(1-R)^2 e^{-6\alpha t} + \dots$$

hence

$$R_{tot.} = R + (1-R)^2 / R \{ (R^2 e^{-2\alpha t}) / (1-R^2 e^{-2\alpha t}) \} \quad \text{eqn.(1)}$$

This analysis assumes the same liquid both sides of the reflector whereas in the experimental case, the liquid at the second interface is water and at the first a sample for test. However this is not an unreasonable assumption as most liquids have acoustic impedances of similar order which are much lower than that of a steel reflector, for example:-

TABLE 1. - Acoustic Impedances Of Various Materials.

Material	(Z±0.1) × 10 ⁶ / kg m ⁻² s ⁻¹
*Water	1.5
*Castor Oil	1.4
+Drilling Fluid	1-2.5
*Steel	40

*values calculated using values of ρ and c at 20°C from *Kaye and Laby (1973)* + estimates from experimental measurement of ρ and c in this work.

Thus, using eqn.(1), an estimate of the contribution to total reflected intensity from multiple reflections can be made. Taking as an example a castor oil/steel system at 5MHz where:-

$$R \approx 0.87 ; \alpha_{oil} \approx 2.3 \text{ m}^{-1} ; t = 2.5 \text{ cm} ; \text{ then } R_{tot.} \approx 0.874$$

This represents a contribution of approximately 0.5% which appears acceptable within the few percent accuracy constraint required for α and c in this work.

THE BRITISH LIBRARY DOCUMENT SUPPLY CENTRE

TITLE

ULTRASOUND PROPAGATION IN COLLOIDAL DISPERSIONS

AUTHOR

(Nigel B. Sherman

INSTITUTION
and DATE

CITY OF LONDON POLYTECHNIC
1989 C.N.A.A.

Attention is drawn to the fact that the copyright of this thesis rests with its author.

This copy of the thesis has been supplied on condition that anyone who consults it is understood to recognise that its copyright rests with its author and that no information derived from it may be published without the author's prior written consent.

THE BRITISH LIBRARY
DOCUMENT SUPPLY CENTRE
Boston Spa, Wetherby
West Yorkshire
United Kingdom



CAM. 9

REDUCTION X

21



DX

89699